Insights into the regulatory networks and RNA processes governed by the *Escherichia coli* ribosome associated protein ProQ, and the *Saccharomyces cerevisiae* kinase Ksp1p

by

Daniel T. Sheidy

A dissertation submitted in partial fulfillment
of the requirements for the degree of
Doctor of Philosophy
(Molecular, Cellular, and Developmental Biology)
in the University of Michigan
2015

Doctoral Committee:

Associate Professor Anuj Kumar, Chair
Associate Professor Matthew R. Chapman
Assistant Professor Aaron C. Goldstrohm
Associate Professor Lyle A. Simmons

Dedication

To my wife, without whose unyielding support, this accomplishment would mean nothing.

To my children, who always bring a smile to my face, and remind me to *play* as hard and as often as I can.

To my parents, who taught me the value of asking, “Why?” and instilled in me an insatiable curiosity.

Acknowledgments

I would be remiss if I did not extend a sincere “thank you” to those who have helped me pursue my scientific career for the last decade. I have had the pleasure of working for great mentors both before and during my Ph. D. In chronological order, I thank Dr. Karen Arndt and Dr. Andrew VanDemark. For three great years, an interesting project, and for allowing me to “find myself” scientifically, I thank Dr. Janine Maddock. Lastly, I thank Dr. Anuj Kumar for providing a smooth transition and solid guidance for the last years of my doctoral training, as well as for helping me to transition into the next stage of my career. A also extend my sincere appreciation to the members of my labs for helpful discussion and feedback on my projects.

On a lighter note, I thank Ashley’s Ann Arbor (Michigan’s Premier Multi-tap) for providing beer at a price cheaper than therapy, and all of my colleagues with whom I shared a pint and discussion, either scientific or philosophical.

Table of Contents

Dedication ii

Acknowledgements iii

List of Figures ix

List of Tables xi

Chapter

I. General translation and its control in prokaryotes 1

1.1. The central dogma 1

1.2. The structure and assembly of the ribosome 2

1.3. Translation in three stages 3

1.3.1. Translation initiation and initiation factors 4

1.3.2. Translation elongation and elongation factors 6

1.3.3. Translation termination and termination factors 8

1.4. Examples of mRNA specific translational control 9

1.4.1. Hfq, small RNAs, and translational control 9

1.4.2. FinO, *finP*, and *traJ* 11

1.4.3. sRNA independent regulation by TRAP 11

1.5. Summary 11

II. Analysis and expansion of the role of the *Escherichia coli* protein ProQ 25

2.1. Introduction 25

2.2. Materials and methods 27

2.2.1. Bacterial strains and growth conditions 27

2.2.2. Preparation of cell lysates for ribosomal fractionation 28

2.2.3. MNase digestion of ribosomes 28

2.2.4. *In vitro* binding of ProQ and 70S ribosomes 29

2.2.5. Ribosomal fractionation 29

2.2.6. Mutant His-ProQ constructs 30

2.2.7. ProQ purification and antibody production 30
2.2.8. Western-blot analysis of ribosomal fractionations 31
2.2.9. Copy number calculation 32
2.2.10. *In vitro* transcription 32
2.2.11. Tryptophan fluorescence 33
2.2.12. Biofilm assays 34
2.3. Results 34
2.3.1 ProQ associates with translating ribosomes 34
2.3.2. The N-terminus and linker regions are necessary for ribosome association 35
2.3.3. ProQ interacts with the mRNA being translated 37
2.3.4. ProQ does not bind selectively to *proP* mRNA 38
2.3.5. Ribosome association of ProQ is not dependent on *prop* or *proU* 39
2.3.6. ProQ is necessary for biofilm formation, independent of ProP 40
2.4. Discussion 41
2.5. Update 45
2.6. Acknowledgements 47
III. Coordinating the sensing of and response to nutrient availability in *Saccharomyces cerevisiae* 65
3.1. Consequences of nitrogen and glucose stresses 65
3.1.1. Pseudohyphal growth 65
3.1.2 Formation of cytoplasmic mRNP granules 66
3.2. Nutrient responsive pathways in PHG and mRNP formation 67
3.2.1. The cAMP/PKA pathway 68
3.2.1.1 The cAMP/PKA pathway in pseudohyphal growth 69
3.2.1.2. The cAMP/PKA pathway in mRNP regulation 69
3.2.2. The MAPK pathways 70
3.2.2.1. The MAPK pathways in pseudohyphal growth 70
3.2.2.2. The MAPK pathways in mRNP regulation 71

3.2.3. The SNF1 pathway 71
3.2.3.1. The SNF1 pathway in pseudohyphal growth 72
3.2.3.2. The SNF1 pathway in mRNP regulation 73
3.2.4. The TOR pathway 73
3.2.4.1. The TOR pathway in pseudohyphal growth 74
3.2.4.2. The TOR pathway in mRNP regulation 75
3.3. Summary 75
IV. Proteomic analysis of the signaling network of the *Saccharomyces cerevisiae* kinase Ksp1p and discovery of a novel role in mRNP regulation 90
4.1. Introduction 90
4.2. Materials and methods 93
4.2.1. Strains, media, and growth conditions 93
4.2.2. Construction of chromosomal mutants and fusions 94
4.2.3. Peptide sample preparation and phosphopeptide enrichment 95
4.2.4. Mass spectrometric analysis and SILAC quantification 96
4.2.5. Surface spread filamentation and invasion assays 97
4.2.6. B-galactosidase assays of *FLO11* transcription activity 98
4.2.7. Induction and visualization of mRNP granules 98
4.3. Results 98
4.3.1. Analysis of the Ksp1p signaling network 98
4.3.2. Mutation of SILAC-identified residues affects pseudohyphal growth and invasion 100
4.3.3. Mutants are defective for PKA control of *FLO11* transcription 101
4.3.4. Ksp1p affects mRNP granules formed during high-OD stress 102
4.3.5. Pbp1p and Ste20p point mutants have aberrant mRNP phenotypes 103
4.4. Discussion 105
V. Future directions 149
5.1. ProQ 149
5.1.1. Exploring the ProQ-mRNA-Ribosome interaction 149

5.1.2. Identifying the ProQ regulatome 150
5.1.3. RNase III and ProQ 151
5.2. Ksp1p 152
5.2.1. Probing of Ksp1p structural domains 152
5.2.2. Finding direct targets of Ksp1p phosphorylation 154
5.2.3. Understanding the purpose of Ksp1p granule localization 155
5.3. Conclusion 156

List of Figures

Figure 1.1. The central dogma of molecular biology 13
Figure 1.2. Organization of the 7 rRNA operons in *Escherichia coli* 14
Figure 1.3. Base modifications of ribosomal RNAs 15
Figure 1.4. Initiation of translation 16
Figure 1.5. Cartoon of tRNA occupied sites on the *E. coli* ribosome 17
Figure 1.6. The translocation cycle 18
Figure 1.7. Termination of translation 19
Figure 1.8. Control of *rpoS* translation by a small RNA (sRNA) and Hfq 20
Figure 2.1. Ribosome association of ProQ under native and dissociating conditions 48
Figure 2.2. Ribosome association of plasmid encoded *proQ* mutant constructs in polysome profiles 49
Figure 2.3. Robust 70S ribosome association of ProQ requires intact mRNA 50
Figure 2.4. mRNA binding kinetics monitored by native tryptophan fluorescence 51
Figure 2.5. Ribosome association of ProQ in various strain backgrounds 52
Figure 2.6. Biofilm formation defects in a Δ*proQ* strain 53
Figure 2.7. Changes in *proP* mRNA and protein levels in response to RNase III 54
Figure 2.8. Location of the RNase III cleavage site with respect to P1 and P2 55
Figure 2.9. Δ*proQ* cells lack appreciable FliC protein 56
Figure 2.10. Attempted complementation of the Δ*proQ* dependent loss of FliC 57
Figure 3.1. Haploid and diploid *Saccharomyces cerevisiae* growth forms 77
Figure 3.2. Pseudohyphal growth causes changes in colony morphology 78
Figure 3.3. The cAMP/PKA/Ras pathways in filamentous growth and mRNP regulation 79

Figure 3.4. 5 MAPK pathways and MAPK signaling in filamentous growth and mRNP regulation 80
Figure 3.5. The SNF1 pathway in filamentous growth and mRNP regulation 81
Figure 3.6. Invasion of a solid surface by haploid filamentous strains 82
Figure 3.7. The TOR pathway in filamentous growth and mRNP regulation 83
Figure 3.8. Summary of *FLO11* regulation by four different signaling pathways 84
Figure 4.1. Experimental design for discovery of differentially phosphorylated peptides 111
Figure 4.2. Overview of genes with altered phosphorylation in a *ksp1*^{K47D} strain 112
Figure 4.3. Analysis of Gene Ontology (GO) Terms 113
Figure 4.4. Diploid pseudohyphal growth phenotypes 114
Figure 4.5. Diploid agar invasion phenotypes 115
Figure 4.6. Quantification of PKA-dependent *FLO11* transcription 116
Figure 4.7. Dynamics of PGK mRNA-containing mRNP granules in various *KSP1* backgrounds 117
Figure 4.8. Dynamics of Pbp1p-GFP and MS implicated mutant *pbp1*p-GFP foci 118
Figure 4.9. Quantification of Pbp1p-GFP and MS implicated mutant *pbp1*p-GFP foci dynamics 119
Figure 4.10. Dynamics of Ste20p-GFP and MS implicated mutant *ste20*p-GFP foci 120
Figure 4.11. Quantification of Ste20p-GFP and MS implicated mutant *ste20*p-GFP foci dynamics 121
Figure 4.12. A partial Ksp1p signaling network 122
Figure 4.13.Ksp1p in mRNP formation 123

List of Tables

Table 2.1. Strains and plasmids 58
Table 2.2. Oligonucleotide sequences 59
Table 4.1. Yeast strains used in this study 124
Table 4.2. Plasmids used in this study 126
Table 4.3. Oligonucleotides used in this study 127
Table 4.4. Table of hyperphosphorylated peptides 130
Table 4.5. Table of hypophosphorylated peptides 132
Table 4.6. Table of novel phosphorylation sites 137
Table 4.7. Table of differentially phosphorylated peptides 139

Chapter I
General translation and its control in prokaryotes

1.1. The central dogma

Almost every biological phenomenon, of which scientists are aware, is a consequence of the interplay among three macromolecular polymers: DNA, RNA, and Protein. So essential is this to our understanding of the microscopic world that we have dubbed the process of transitioning from one type of polymer to another the “Central Dogma”. To over-simply restate the tenet: the hereditary material, DNA, can be faithfully replicated to make a perfect copy of itself for the next generation, or it can be transcribed into RNA. Once transcribed, RNA may act as the final product, capable of performing some vital function, be reverse-transcribed back into a DNA molecule, or, in the case of messenger RNA (mRNA), it may be translated into a protein product (Figure 1.1). It is this process of translation which will be the focus of the first half of the discussion to follow, specifically, the general process of faithful translation, the accessory factors involved, and the targeted regulation of specific mRNAs in the bacterium *Escherichia coli*. Though the process of translation is generally well conserved *up* the evolutionary ladder, there are some key differences between prokaryotes and eukaryotes which will not be discussed here (For review see [1, 2]), and this document will focus on the mechanisms of translation in prokaryotes.

1.2. The structure and assembly of the ribosome

The ribosome is a large complex of ribosomal RNAs (rRNAs) and proteins which come together to form a structure with a sedimentation coefficient of 70S. Further, the translating unit is a complex of a large and a small subunit of sizes 50S and 30S respectively [3, 4]. Though the exact numbers depend upon the isolation conditions used during purification, the large subunit contains about 33 proteins and two rRNAs. These rRNAs themselves have sedimentation coefficients of 23S and 5S. The small subunit contains about 22 proteins and one 16S rRNA.

Because of the importance of the ribosome, many resources are dedicated to its assembly. In total, it is estimated that rRNA comprises over 90% of the total RNA present at any given time in the *E. coli* cytosol [5]. The three rRNAs are transcribed polycistronically from seven different operons [6] (Figure 1.2 [7]). The multiple loci allow high levels of expression of rRNA genes during logarithmic growth, and the polycistronic nature of the genes helps to maintain the proper stoichiometry. Once transcribed, these rRNAs undergo processing which includes cleavage into pre-rRNAs, as well as subsequent trimming into mature rRNAs (For review see [7]), and post-transcriptional modifications such as pseudouridylation and methylation (Figure 1.3 [8]).

As mentioned, the ribosome is a large ribonuclear protein complex which, in addition to 3 rRNAs, contains over 50 proteins (r-proteins). Like the rRNAs, many of these proteins are located within operons across the *E. coli* genome. Though the mRNAs encoding r-proteins themselves are not processed, expression of r-proteins is also highly regulated, in order to maintain stoichiometry. Cleverly, r-proteins use feedback mechanisms to regulate their own expression, often decreasing the

translational efficiency of their own mRNAs or attenuating the transcription of their operons (For review see [9]).

Even with all of the parts present at the proper ratios, the ribosome still needs assistance in order to properly assemble. *In vitro,* the ribosome can be assembled from all of its individual components, and complex maps have been constructed based on the information obtained from the interdependency of r-proteins for assembly into the finished ribosomes [10]. Unfortunately, this *in vitro* assembly requires non-physiological temperatures, magnesium concentrations, and timescales. *In vivo* efficient assembly is facilitated by ribosome associated factors (RAFs) which catalyze assembly [11]. In some cases, deletion of these factors leads to inviability. In other cases, perturbation of ribosomal structure is observed, usually manifested as a change in the sedimentation coefficient of one of the subunits. This may or may not lead to an accumulation of the other ribosomal subunit and a concurrent decrease in 70S ribosomes and polysomes (more than one ribosome bound to a single mRNA) [12, 13].

1.3. Translation in three stages

As with any “heavy machinery”, there are considerations for starting, operating, and shutting down the engine. Analogously, translation can be broken down into its three main phases: initiation, elongation, and termination. Initiation of translation involves binding of the small (30S) subunit to the mRNA, recruitment of the first charged tRNA, and coupling of the large (50S) subunit to form the complete 70S ribosome. Elongation starts with the arrival of the second charged tRNA, formation of a peptide bond between the growing polypeptide chain and the newly recruited amino acid, and

movement of the ribosome along the mRNA. This stage of translation continues until a signal is reached in the mRNA which triggers the final step: termination. During termination, three things must occur. The nascent protein must dissociate from the ribosome. The subunits must separate, and the mRNA must be released. These individual stages of translation, as well as the factors which facilitate the accurate and timely completion of the same, have been exhaustively studied. Here I will describe each stage in more detail, as well as discuss the canonical factors involved at each step. This background will help to place the hypothesized mRNA-specific regulation of translation by the *E. coli* protein ProQ into the context of the entire process.

1.3.1. Translation initiation and initiation factors

In eukaryotes, initiation of translation, with some exceptions, involves the recognition of a 5’ methylguanosine “cap” structure on the mRNA. Once located, the ribosome is able to scan for the start site for translation and begin synthesizing protein [14]. In prokaryotes, mRNA processing is less common, and this 5’ cap structure is not present. Instead, a sequence within the mRNA called the Shine-Dalgarno sequence is recognized by a complementary sequence in the 16S rRNA of the 30S subunit. Base pairing between these sequences positions the small ribosomal subunit over the start site for translation. An analogous sequence, called the Kozak sequence, exists in eukaryotes, but the sequence is more degenerate than that of the Shine-Dalgarno sequence [15, 16]. Once the 30S subunit is positioned, the rest of the translating complex must be assembled on the mRNA. This includes recruitment of the initiator

tRNA to the mRNA at the first codon and coupling of the 50S to the 30S/mRNA complex (Figure 1.4 [17]).

There are three core initiation factors in *E. coli*, appropriately named IF1, IF2, and IF3. In addition, the first transfer RNA (tRNA), which brings with it the first amino acid, in slightly different than the “normal” tRNAs which bring the subsequent amino acids necessary for peptide synthesis during the elongation phase. These factors help to ensure that initiation occurs with speed and accuracy. IF3 is the first factor to interact with the 30S ribosome during initiation. Binding of IF3 to the 30S subunit precludes 50S binding and premature formation of the 70S complex [6]. This ensures that the mRNA, as well as the other initiation factors can bind to the 30S and form a competent initiation complex.

It is important, here to note that amino acid-carrying tRNAs (also called charged tRNAs) can be found in one of three locations in the ribosome, at the interface between the 30S and 50S subunits. The first site is the peptidyl transferase site (P-site). Here, the newly arriving amino acids are added to the growing protein. It is also the site of binding of the initiator tRNA, which will be discussed in detail later. The other two sites are the acceptor site (A-site), and the exit site (E-site). The A-site is the location of initial binding for the charged tRNAs as they bring the amino acids to the ribosome, and the E-site allows the uncharged tRNA to dissociate from the ribosome (Figure 1.5, For review see [18]).

After binding of IF3 to the 30S subunit, mRNA can bind to the 30S subunit via base pairing between the Shine-Dalgarno sequence in the mRNA and the 16S rRNA, as previously mentioned. Once the mRNA is positioned, the initiator tRNA can be brought

to the P-site by IF2. The initiator tRNA carries a specially modified methionine residue which is formylated. This formylmethionine (fmet) is what is recognized by IF2 [19]. Other regions of the $tRNA^{fmet}$ are also altered slightly when compared to non-initiator tRNAs. Presumably, these alterations facilitate initiation complex formation [20, 21]. For its part, IF1 helps to stabilize the formation of the completed 30S preinitiation complex by assisting in the positioning of the initiator tRNA by IF2 and the blocking of 50S association by IF3 [22].

In the final stages of initiation, the 50S must be joined to the 30S subunit, and the initiation factors must leave the ribosome. After IF3 dissociates, the 50S can bind. IF1 then leaves the ribosome. IF2 has GTPase activity, and hydrolysis to GDP by IF2 provides the energy to lock the initiator tRNA into its final position and prime the ribosome to begin translation. At this point, IF2 leaves the initiated ribosome, and the A-site is available for new charged tRNAs to bind [23].

1.3.2. Translation elongation and elongation factors

The elongation phase of translation requires the coordination of several processes. First, the correct charged tRNA must be brought to the A-site of the ribosome. The amino acid on that tRNA must be transferred to the nascent protein, and the ribosome must move along the mRNA. The catalysis of the addition of the new amino acid to the growing chain is carried out by the enzymatic activity of the ribosome. Specifically, the 23S rRNA possesses peptidyl transferase activity [24]. The other steps are facilitated by another suite of factors called elongation factors. Again, I will discuss the action of three factors: EF-Tu, EF-Ts, and EF-G.

EF-Tu is responsible for assisting with the first step of elongation, where the charged elongator tRNA is brought to the A-site of the ribosome, positioning it for incorporation into the growing polypeptide chain. In this way, EF-Tu is analogous to IF2, in that it binds to the charged tRNA and brings it to the ribosome [25, 26]. Additionally, like IF2, EF-Tu is a GTPase. Once EF-Tu positions the tRNA in the A-site, and a match is made between the codon in the mRNA and the anticodon of the tRNA, GTP is hydrolyzed to GDP by EF-Tu. GDP-bound EF-Tu has decreased affinity for the ribosome and tRNA, and it dissociates [27]. Transfer of the growing polypeptide and formation of a peptide bond between the elongating peptide and the A-site tRNA-bound amino acid is catalyzed by the ribosome [24]. Simultaneously, it is necessary for the P-site and A-site tRNAs to shift to the E-site and P-site respectively in a process called translocation.

Translocation is often described as a “ratcheting” motion. Because of this ratchet, tRNAs often exist in hybrid states, occupying different positions in the 50S subunit relative to the 30S subunit. These states are often referred to as the P/E and A/P states. The elongation factor EF-G helps to facilitate this ratchet by binding near the A-site of the ribosome. Like EF-Tu, EF-G is a GTPase. Hydrolysis of GTP to GDP by EF-G moves the translocation process through the P/E and A/P intermediate states, culminating in the P-site tRNA moving to the E-site and the A-site tRNA moving to the P-site [28, 29]. Finally, EF-G leaves the ribosome and the A-site is available for binding of the next charged tRNA (Figure 1.6 [30]).

Again, EF-Tu is responsible for bringing the next charged tRNA to the ribosome, but it has lowered affinity for charged tRNA in its GDP bound state. The last elongation

factor, EF-Ts is a nucleotide exchange factor. It helps to dissociate “spent” guanine nucleotides from EF-Tu. Once EF-Ts facilitates the release of GDP from EF-Tu, EF-Tu is able to bind to GTP, and the cycle continues [31].

1.3.3. Translation termination and termination factors

Elongation of translation continues until the ribosome reaches a signal in the mRNA which causes translation to cease: a stop codon. Like other amino acid-determining codons, it is a triplet of bases in the mRNA, but it does not code for the incorporation of an amino acid, rather it causes the ribosome to pause, allowing termination to occur. Three unique stop codons exist, though all contain a uracil at the first position: UAA, UAG, and UGA [32, 33].

Upon encountering a stop codon, several steps occur. First, the protein is released from the P-site tRNA. The subunits dissociate from each other and the mRNA is released. The first step is facilitated by release factors 1, 2, and 3 (RF1/2/3) (Figure 1.7 [30]). Dissociation of the subunits and the mRNA is stimulated by ribosome recycling factor (RRF) as well as IF3 and EF-G [34].

To recognize a stop codon, *E. coli* use RF1 and RF2 to function semi-redundantly. Both RF1 and RF2 recognize the UAA codon. RF1 alone recognizes UAG, and RF2 recognizes UGA [35, 36]. Structurally, RF1 and RF2 resemble the anticodon loop of tRNA. This is not surprising as the RFs bind at the A-site of the ribosome. Once the stop codon is recognized by one of the RFs, hydrolysis of the peptide bond between the P-site tRNA and the protein is catalyzed. Three conserved amino acids in the RFs,

termed the GGQ motif, facilitate this hydrolysis in the peptidyl transferase center of the ribosome, and the peptide is released [37].

Release of RF1 or 2 occurs after RF3 binds to the ribosome (Figure 1.7 [30]). RF3 is also a GTPase, and GTP hydrolysis is important for its dissociation from the ribosome, but the current literature seems unclear as to whether RF3 binds to the ribosome in its GDP or GTP bound state and whether or not it requires a GEF [38, 39]. Once RF1/2 has been released, the subunits are dissociated by the actions of RF3 and EF-G. There are conflicting reports as to whether the tRNA and mRNA are dissociated at this time as well or if the action of IF3 is required for removing the remaining tRNA and mRNA [34, 40]. In either case, the three factors: RF3, EF-G, and IF3, work together to stabilize the dissociated subunits, freeing them for another round of initiation.

1.4. Examples of mRNA specific translational control

The factors described above are often termed “general translation factors”, as they exert their control over the process as a whole, rather than specific mRNAs. In addition to these factors, there are a suite of RNA-RNA and Protein-RNA interactions which regulate the translation of a subset of messages. In the following sections, I will discuss three such cases of Protein-RNA (and in some cases Protein-RNA-RNA) interactions which work in this manner. This will serve as a primer for Chapter II of this document, as my work in the Maddock Lab examined the *E. coli* protein ProQ, a factor hypothesized to regulate the translation of a subset of mRNAs.

1.4.1. Hfq, small RNAs, and translational control

Hfq is a well conserved protein which appears in the genomes of many different bacteria. It is relatively small (102 AA in *E. coli*), but it has a large effect on gene expression, especially under cellular stress conditions [41]. Hfq is said to possess RNA chaperone activity, defined as the ability to alter the shape of an RNA in such a way as to functionalize it [42]. The main role of Hfq is to facilitate binding between small RNAs (sRNAs) and their target mRNAs. In some cases, this pairing leads to the degradation of the mRNA and decreased expression [43, 44]. In other cases, this interaction can amplify the expression of a gene by increasing the mRNA half-life or facilitating more efficient translation [45, 46].

An example of Hfq negatively regulating translation is in the target recognition of the sRNA RhyB. RhyB is transcribed to high levels when iron levels are low. Once transcribed, RhyB helps to target iron-binding and storage protein mRNAs for degradation [44, 47]. It was later found that, in the absence of Hfq, RhyB sRNA is unstable. In this way, Hfq regulates translation of specific messages by binding to a sRNA and increasing its stability, as well as helping it to find its targets and direct RNase cleavage by RNaseE [43].

Hfq can have a stimulatory effect on translation as well. The stationary sigma factor RpoS contains a hairpin structure within its 5’ UTR. This hairpin structure blocks binding of the ribosome to the Shine-Dalgarno sequence by keeping it in a double stranded moiety. The sRNA DsrA can base pair with the 5’ UTR of RpoS and make the message competent for translation. This interaction is stabilized by Hfq, and RpoS protein levels are decreased in an *hfq* mutant strain (Figure 1.8 [45, 46]).

1.4.2. FinO, *finP*, and *traJ*

The protein product encoded by the *traJ* gene is a transcription factor involved in the transfer of DNA between bacteria, a process called conjugation. The *finP* gene encodes for a sRNA which has inhibitory effects on *traJ* expression. Analogous to the RhyB and DsrA/RpoS systems, this effect is mediated by a physical interaction between complementary sequences on the two RNAs which blocks the Shine-Dalgarno sequence of *traJ* [48]. For its part FinO stabilizes this interaction [49, 50].

FinOP repression of *traJ* expression is also dependent upon RNaseE and RNase III. The evidence suggests that binding of FinO to *finP* RNA prevents degradation by RNaseE, a single stranded ribonuclease. Additionally, *finP-traJ* duplexed DNA can be digested by RNase III, a double stranded ribonuclease [48, 51].

1.4.3. sRNA independent regulation by TRAP

The two previous examples discussed the importance of small RNAs, proteins, and nucleases in the regulation of translation. Other mechanisms exist which are more direct. One such example from *Bacillus subtilis* is the attenuation of tryptophan metabolism genes by direct binding of the protein TRAP at or near the ribosome binding site [52, 53]. Other studies have shown that TRAP does not need to physically block the RBS itself, but it can bind and influence the secondary structure of the mRNA to block the RBS from a distance [54]. TRAP is regulated by an anti-TRAP protein which is expressed when levels of tryptophan are low. This protein binds to TRAP and prevents it from binding to the mRNA [55].

1.5. Summary

Translation is a regulated process which requires the allocation of much of the cell's time and energy. Additionally, tight controls are in place at all steps, from assembly to termination, to ensure that the process is completed in a highly faithful manner. Much effort and many resources have been employed in the study of "just" the canonical factors which facilitate all stages.

In addition to the traditional factors and mechanisms, translation of specific mRNAs can be tightly regulated by other factors. In general, these factors serve one of two over-simplified functions. They change the stability of an RNA, or they modify the ability of the mRNA to interact with the ribosome itself.

In the next chapter, I will discuss the *E. coli* protein ProQ, its association with the ribosome, and its potential role as a messenger specific translation factor.

Figure 1.1. The Central Dogma of Molecular Biology. The central dogma describes the flow of important genetic/cellular information through the indicated biological processes to affect cell function.

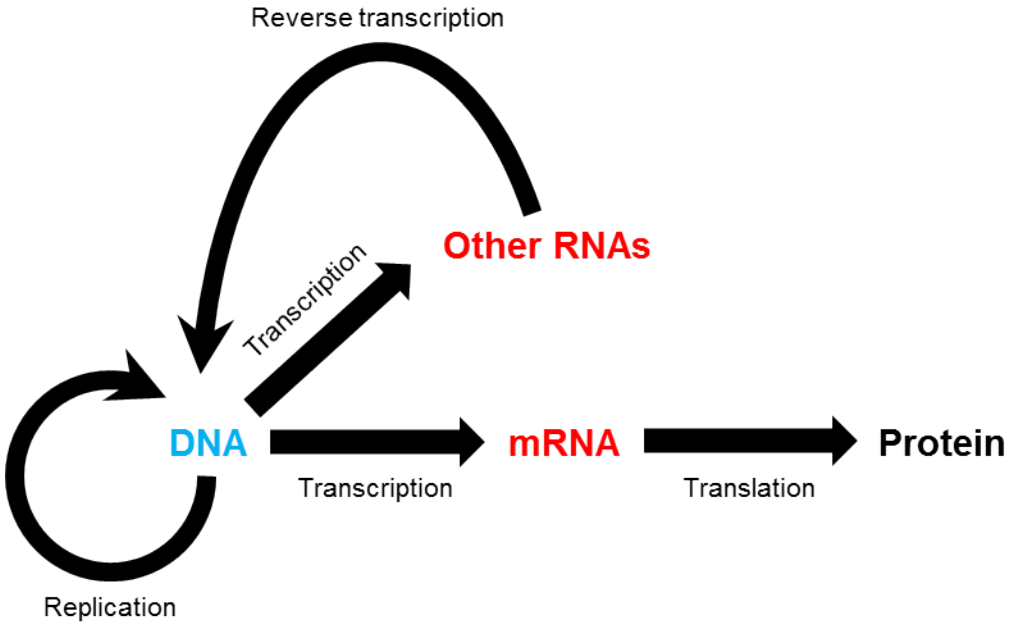

Figure 1.2. Organization of the 7 rRNA operons in *Escherichia coli*. The genes encoding the 3 ribosomal RNAs (rRNA) and some transfer RNA (tRNA) genes are transcribed from seven operons. All operons contain at least one copy of all three rRNA genes and at least one additional tRNA gene. Shown are the operon names, the rRNA genes (red boxes) and the tRNA genes (colored boxes). The tRNA genes are shown in the key below the operon diagrams. (Adapted from [7]).

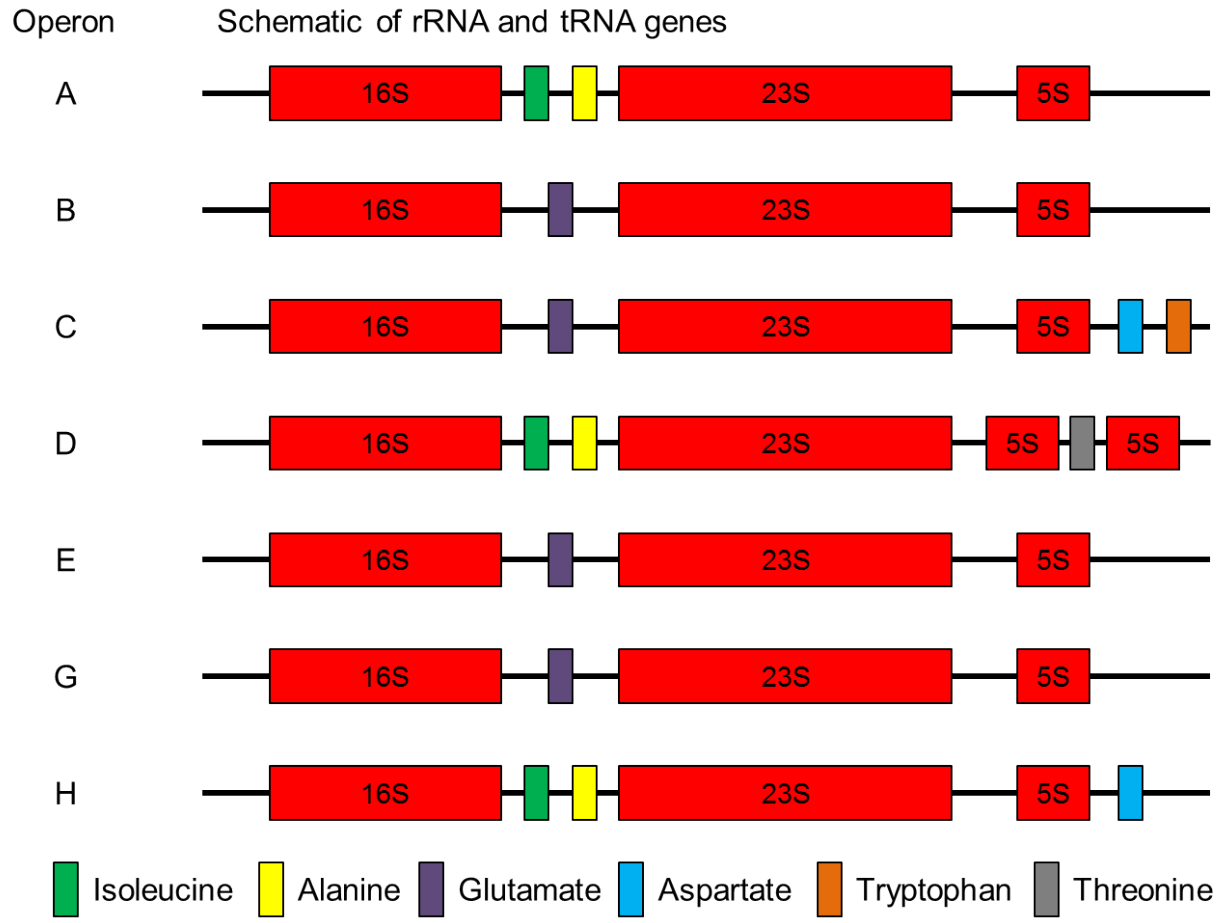

Figure 1.3. Base modifications of ribosomal RNAs. Proper assembly and function of the ribosome is dependent upon modifications of the ribosomal rRNAs. Uridine bases can be isomerized to form pseudouridines by pseudouridine synthases [56, 57]. Additionally, the 2' oxygen can be methylated by uridine methyltransferases [58].

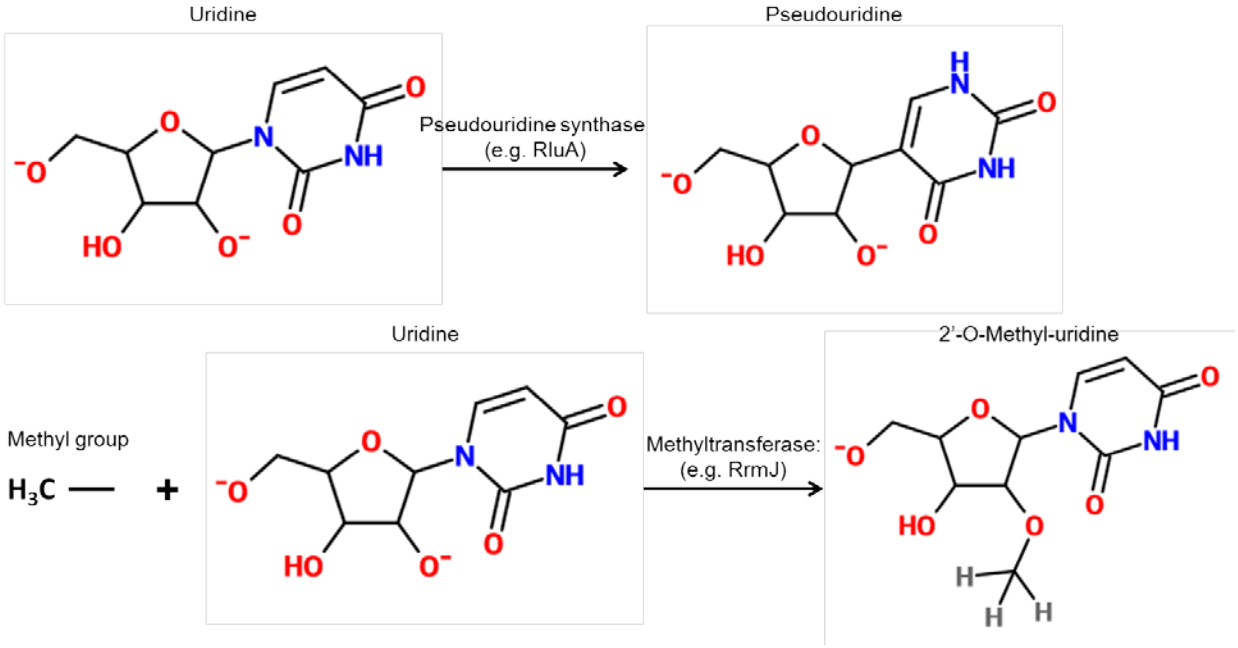

Figure 1.4. Initiation of translation. Proper formation of the 70S initiation complex is facilitated by three initiation factors and the intiator tRNA. First, Interaction between IF3 and the 30S subunit blocks the binding of the 50S. Then, the Shine-Dalgarno sequence in the 5' end of the mRNA is recognized by a complementary sequence in 16S rRNA of the 30S subunit. The initiator tRNA is then brought to the ribosome by IF2, and IF1 helps to position the tRNA and stabilize the 30S preinitiation complex. After IF3 dissociates, the 50S subunit can bind. Subsequently, IF1 and IF2 leave the 70S initiation complex, leaving only the initiator tRNA in the P-site of the ribsome. Elongation can then proceed. Adapted from [17].

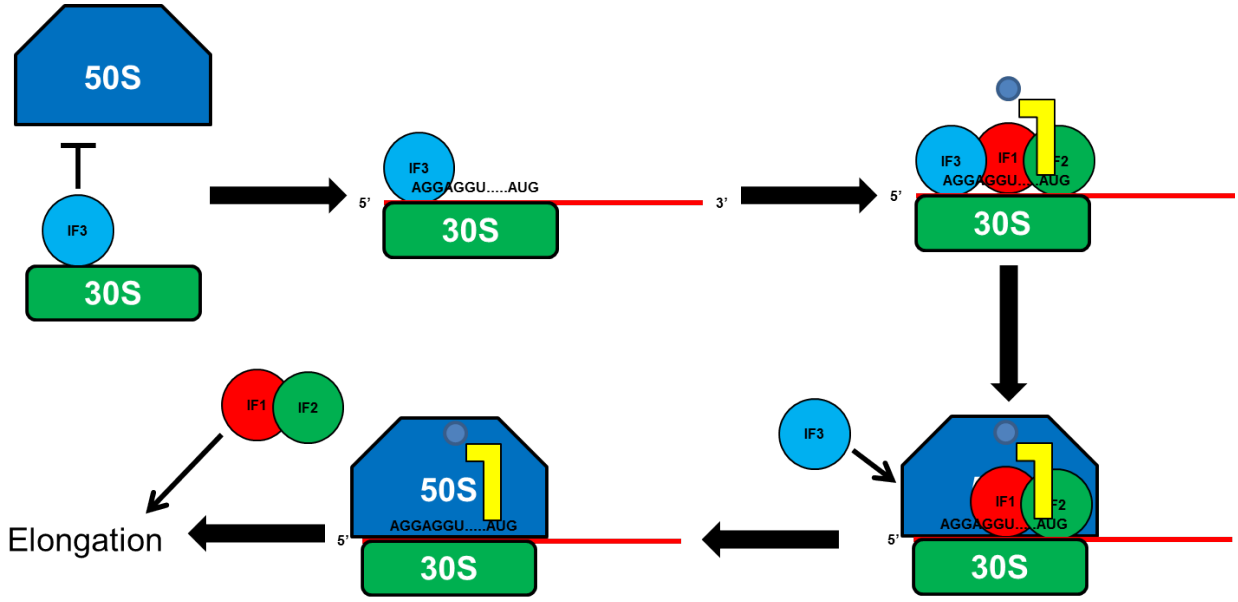

Figure 1.5. Cartoon of tRNA occupied sites on the *E. coli* ribosome. The interface of the 30S and 50S subunits forms three distinct sites which are occupied by different tRNA species.

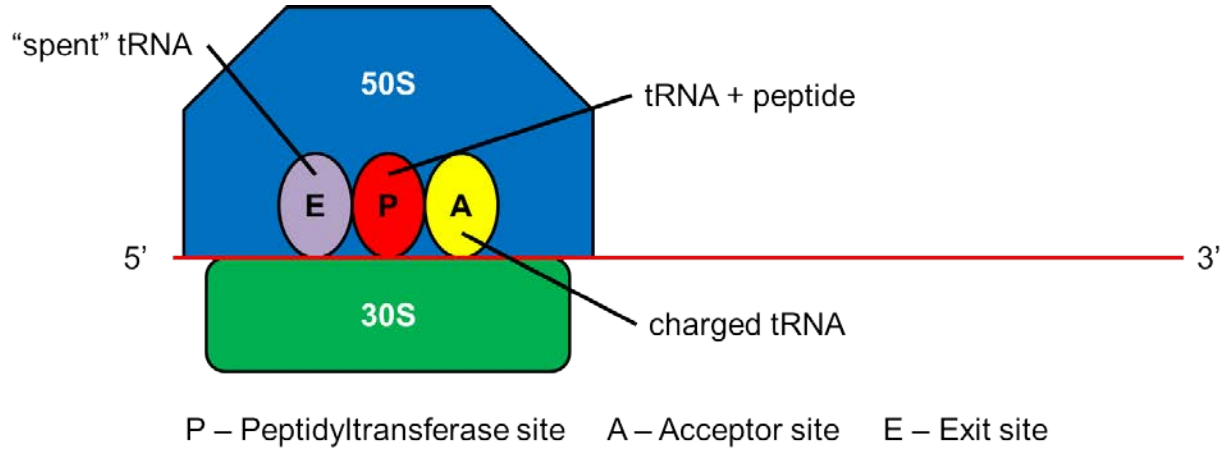

Figure 1.6. The translocation cycle. During elongation, tRNAs simultaneously occupy different ribosome sites in the small and large subunit. Movement of tRNAs through various hybrid states is facilitated by EF-G and its GTP hydrolysis activity. Adapted from [30].

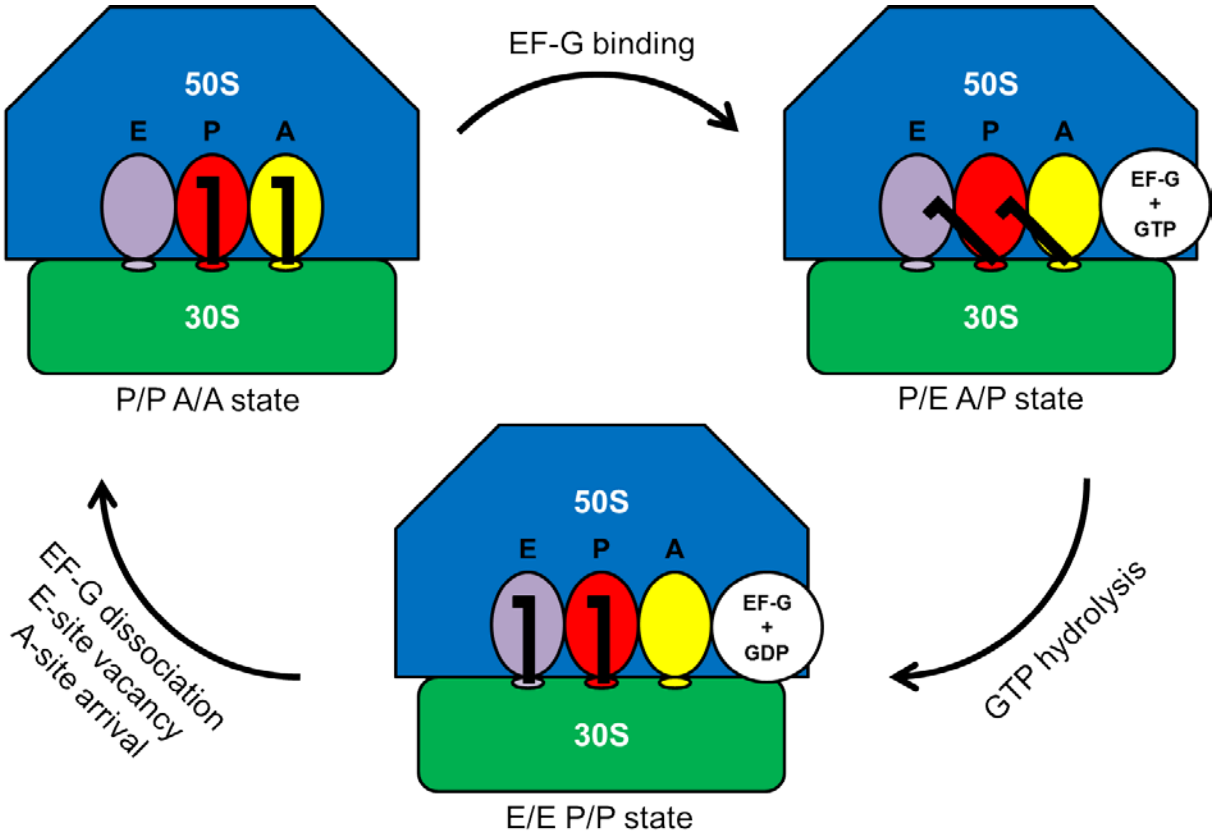

Figure 1.7. Termination of translation. At termination, either RF1 or RF2 recognizes a stop codon toward the 3' end of an mRNA. Hydrolysis causes liberation of the peptide, and RF3 binds to help promote termination via its GTP hydrolysis activity. Once RF1/2/3 leave, dissociation of the subunits and mRNA is facilitated by Ribosome Release Factor (RRF). Additionally, IF3, as mentioned previously, as well as EF-G maintain the ribosome as dissociated subunits and prevents reformation of 70S complexes. Adapted from [30].

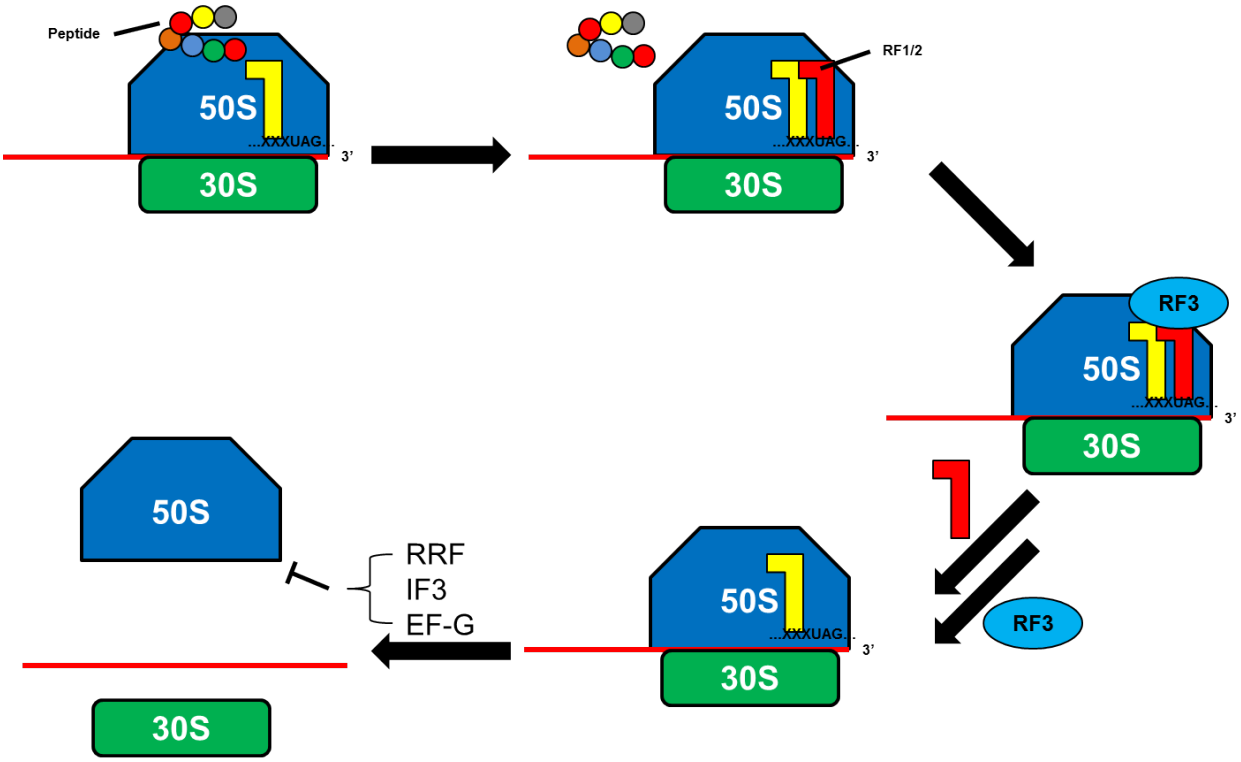

Figure 1.8. Control of *rpoS* translation by a small RNA (sRNA) and Hfq. The 5' end of the *rpoS* mRNA contains secondary structure such that the Shine-Dalgarno (SD) sequence is base paired with a complementary sequence (anti-SD). This prevents association of the 30S subunit. An sRNA containing an anti-anti-SD sequence, with the help of the RNA chaperone Hfq, can help to dissolve this secondary structure, exposing the SD-sequence and allowing the 30S to bind. Adapted from [46].

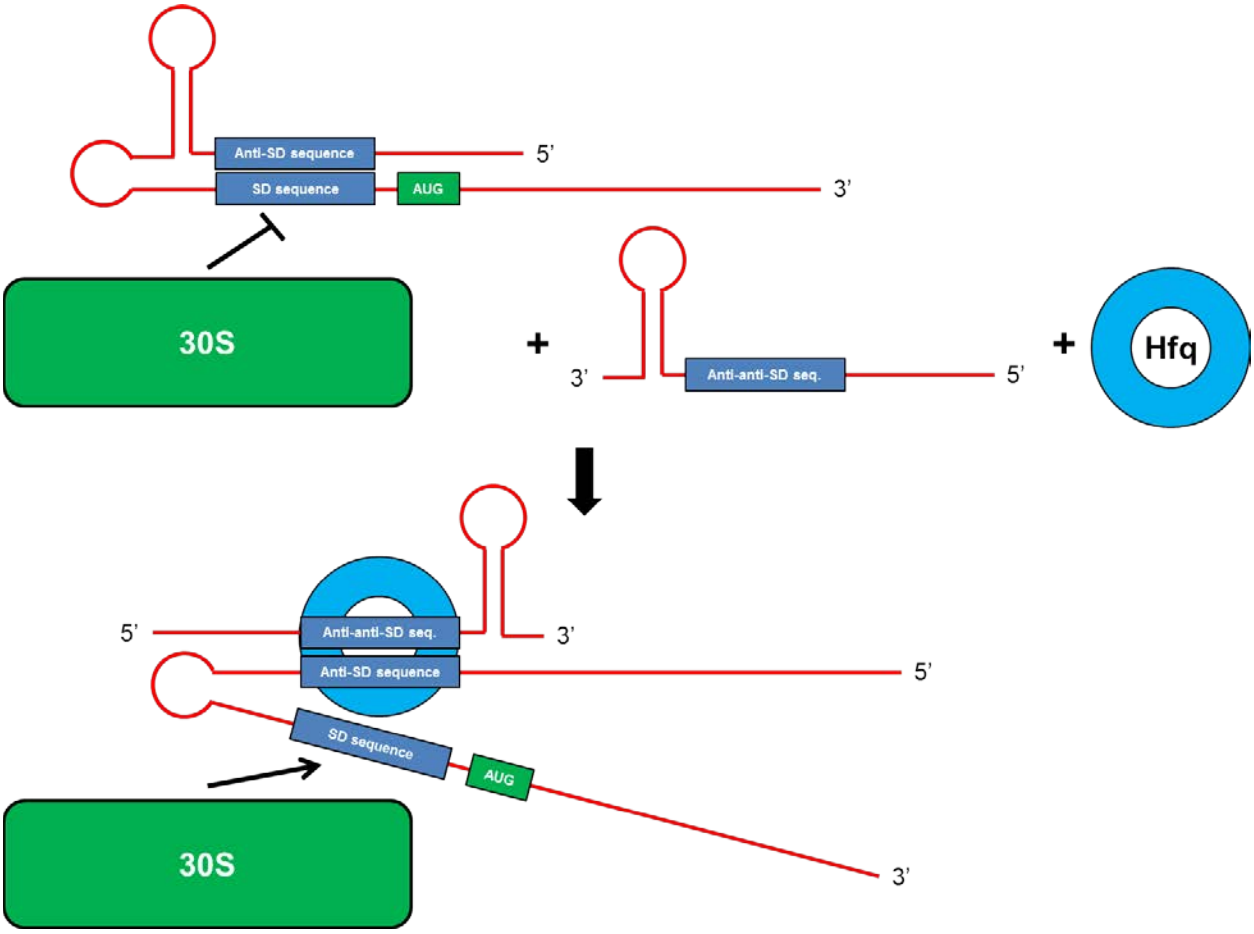

References

1. Jackson, R.J., C.U. Hellen, and T.V. Pestova, *The mechanism of eukaryotic translation initiation and principles of its regulation.* Nat Rev Mol Cell Biol, 2010. **11**(2): p. 113-27.
2. Laursen, B.S., et al., *Initiation of protein synthesis in bacteria.* Microbiol Mol Biol Rev, 2005. **69**(1): p. 101-23.
3. Vila-Sanjurjo, A., et al., *X-ray crystal structures of the WT and a hyper-accurate ribosome from Escherichia coli.* Proc Natl Acad Sci U S A, 2003. **100**(15): p. 8682-7.
4. Borovinskaya, M.A., et al., *Structural basis for hygromycin B inhibition of protein biosynthesis.* Rna, 2008. **14**(8): p. 1590-9.
5. Haas, B.J., et al., *How deep is deep enough for RNA-Seq profiling of bacterial transcriptomes?* BMC Genomics, 2012. **13**: p. 734.
6. Neidhardt, F.C., ed. *Escherichia coli and Salmonella typhimurium Cellular and Molecular Biology*. Vol. 2. 1987, American Society for Microbiology: Washington, D.C. 1654.
7. Srivastava, A.K. and D. Schlessinger, *Mechanism and regulation of bacterial ribosomal RNA processing.* Annu Rev Microbiol, 1990. **44**: p. 105-29.
8. Decatur, W.A. and M.J. Fournier, *rRNA modifications and ribosome function.* Trends Biochem Sci, 2002. **27**(7): p. 344-51.
9. Nomura, M., R. Gourse, and G. Baughman, *Regulation of the synthesis of ribosomes and ribosomal components.* Annu Rev Biochem, 1984. **53**: p. 75-117.
10. Nierhaus, K.H., *The assembly of the prokaryotic ribosome.* Biosystems, 1980. **12**(3-4): p. 273-82.
11. Shajani, Z., M.T. Sykes, and J.R. Williamson, *Assembly of bacterial ribosomes.* Annu Rev Biochem. **80**: p. 501-26.
12. Jiang, M., et al., *The Escherichia coli GTPase CgtAE is involved in late steps of large ribosome assembly.* J Bacteriol, 2006. **188**(19): p. 6757-70.
13. Jiang, M., et al., *Identification of novel Escherichia coli ribosome-associated proteins using isobaric tags and multidimensional protein identification techniques.* J Bacteriol, 2007. **189**(9): p. 3434-44.
14. Kozak, M., *Initiation of translation in prokaryotes and eukaryotes.* Gene, 1999. **234**(2): p. 187-208.
15. Kozak, M., *An analysis of 5'-noncoding sequences from 699 vertebrate messenger RNAs.* Nucleic Acids Res, 1987. **15**(20): p. 8125-48.
16. Kozak, M., *At least six nucleotides preceding the AUG initiator codon enhance translation in mammalian cells.* J Mol Biol, 1987. **196**(4): p. 947-50.

17. Simonetti, A., et al., *A structural view of translation initiation in bacteria.* Cell Mol Life Sci, 2009. **66**(3): p. 423-36.

18. Lafontaine, D.L. and D. Tollervey, *The function and synthesis of ribosomes.* Nat Rev Mol Cell Biol, 2001. **2**(7): p. 514-20.

19. Hartz, D., et al., *Domains of initiator tRNA and initiation codon crucial for initiator tRNA selection by Escherichia coli IF3.* Genes Dev, 1990. **4**(10): p. 1790-800.

20. Wrede, P. and A. Rich, *Stability of the unique anticodon loop conformation of E.coli tRNAfMet.* Nucleic Acids Res, 1979. **7**(6): p. 1457-67.

21. Lancaster, L. and H.F. Noller, *Involvement of 16S rRNA nucleotides G1338 and A1339 in discrimination of initiator tRNA.* Mol Cell, 2005. **20**(4): p. 623-32.

22. Pon, C.L. and C.O. Gualerzi, *Mechanism of protein biosynthesis in prokaryotic cells. Effect of initiation factor IF1 on the initial rate of 30 S initiation complex formation.* FEBS Lett, 1984. **175**(2): p. 203-7.

23. Allen, G.S., et al., *The cryo-EM structure of a translation initiation complex from Escherichia coli.* Cell, 2005. **121**(5): p. 703-12.

24. Cech, T.R., *Structural biology. The ribosome is a ribozyme.* Science, 2000. **289**(5481): p. 878-9.

25. Parlato, G., et al., *The GTPase activity of elongation factor Tu and the 3'-terminal end of aminoacyl-tRNA.* FEBS Lett, 1981. **125**(2): p. 257-60.

26. Wikman, F.P., et al., *The site of interaction of aminoacyl-tRNA with elongation factor Tu.* Embo J, 1982. **1**(9): p. 1095-100.

27. Krab, I.M. and A. Parmeggiani, *Mechanisms of EF-Tu, a pioneer GTPase.* Prog Nucleic Acid Res Mol Biol, 2002. **71**: p. 513-51.

28. Agrawal, R.K., et al., *EF-G-dependent GTP hydrolysis induces translocation accompanied by large conformational changes in the 70S ribosome.* Nat Struct Biol, 1999. **6**(7): p. 643-7.

29. Stark, H., et al., *Large-scale movement of elongation factor G and extensive conformational change of the ribosome during translocation.* Cell, 2000. **100**(3): p. 301-9.

30. Dunkle, J.A. and J.H. Cate, *Ribosome structure and dynamics during translocation and termination.* Annu Rev Biophys, 2010. **39**: p. 227-44.

31. Kawashima, T., et al., *The structure of the Escherichia coli EF-Tu.EF-Ts complex at 2.5 A resolution.* Nature, 1996. **379**(6565): p. 511-8.

32. Brenner, S., A.O. Stretton, and S. Kaplan, *Genetic code: the 'nonsense' triplets for chain termination and their suppression.* Nature, 1965. **206**(988): p. 994-8.

33. Brenner, S., et al., *UGA: a third nonsense triplet in the genetic code.* Nature, 1967. **213**(5075): p. 449-50.

34. Hirokawa, G., et al., *The role of ribosome recycling factor in dissociation of 70S ribosomes into subunits.* Rna, 2005. **11**(8): p. 1317-28.

35. Brown, C.M. and W.P. Tate, *Direct recognition of mRNA stop signals by Escherichia coli polypeptide chain release factor two.* J Biol Chem, 1994. **269**(52): p. 33164-70.

36. Weixlbaumer, A., et al., *Insights into translational termination from the structure of RF2 bound to the ribosome.* Science, 2008. **322**(5903): p. 953-6.

37. Mora, L., et al., *The essential role of the invariant GGQ motif in the function and stability in vivo of bacterial release factors RF1 and RF2.* Mol Microbiol, 2003. **47**(1): p. 267-75.

38. Koutmou, K.S., et al., *RF3:GTP promotes rapid dissociation of the class 1 termination factor.* Rna, 2014. **20**(5): p. 609-20.

39. Zavialov, A.V., R.H. Buckingham, and M. Ehrenberg, *A posttermination ribosomal complex is the guanine nucleotide exchange factor for peptide release factor RF3.* Cell, 2001. **107**(1): p. 115-24.

40. Karimi, R., et al., *Novel roles for classical factors at the interface between translation termination and initiation.* Mol Cell, 1999. **3**(5): p. 601-9.

41. Gottesman, S., et al., *Small RNA regulators and the bacterial response to stress.* Cold Spring Harb Symp Quant Biol, 2006. **71**: p. 1-11.

42. Rajkowitsch, L., et al., *RNA chaperones, RNA annealers and RNA helicases.* RNA Biol, 2007. **4**(3): p. 118-30.

43. Masse, E., F.E. Escorcia, and S. Gottesman, *Coupled degradation of a small regulatory RNA and its mRNA targets in Escherichia coli.* Genes Dev, 2003. **17**(19): p. 2374-83.

44. Masse, E., C.K. Vanderpool, and S. Gottesman, *Effect of RyhB small RNA on global iron use in Escherichia coli.* J Bacteriol, 2005. **187**(20): p. 6962-71.

45. Brown, L. and T. Elliott, *Efficient translation of the RpoS sigma factor in Salmonella typhimurium requires host factor I, an RNA-binding protein encoded by the hfq gene.* J Bacteriol, 1996. **178**(13): p. 3763-70.

46. Soper, T., et al., *Positive regulation by small RNAs and the role of Hfq.* Proc Natl Acad Sci U S A, 2010. **107**(21): p. 9602-7.

47. Masse, E. and S. Gottesman, *A small RNA regulates the expression of genes involved in iron metabolism in Escherichia coli.* Proc Natl Acad Sci U S A, 2002. **99**(7): p. 4620-5.

48. van Biesen, T., et al., *Structural and functional analyses of the FinP antisense RNA regulatory system of the F conjugative plasmid.* Mol Microbiol, 1993. **10**(1): p. 35-43.

49. Koraimann, G., et al., *The FinOP repressor system of plasmid R1: analysis of the antisense RNA control of traJ expression and conjugative DNA transfer.* Mol Microbiol, 1996. **21**(4): p. 811-21.

50. van Biesen, T. and L.S. Frost, *The FinO protein of IncF plasmids binds FinP antisense RNA and its target, traJ mRNA, and promotes duplex formation.* Mol Microbiol, 1994. **14**(3): p. 427-36.

51. Jerome, L.J., T. van Biesen, and L.S. Frost, *Degradation of FinP antisense RNA from F-like plasmids: the RNA-binding protein, FinO, protects FinP from ribonuclease E.* J Mol Biol, 1999. **285**(4): p. 1457-73.

52. Babitzke, P., D.G. Bear, and C. Yanofsky, *TRAP, the trp RNA-binding attenuation protein of Bacillus subtilis, is a toroid-shaped molecule that binds transcripts containing GAG or UAG repeats separated by two nucleotides.* Proc Natl Acad Sci U S A, 1995. **92**(17): p. 7916-20.

53. Yang, M., et al., *Translation of trpG in Bacillus subtilis is regulated by the trp RNA-binding attenuation protein (TRAP).* J Bacteriol, 1995. **177**(15): p. 4272-8.

54. Du, H. and P. Babitzke, *trp RNA-binding attenuation protein-mediated long distance RNA refolding regulates translation of trpE in Bacillus subtilis.* J Biol Chem, 1998. **273**(32): p. 20494-503.

55. Snyder, D., et al., *Interaction of the trp RNA-binding attenuation protein (TRAP) with anti-TRAP.* J Mol Biol, 2004. **338**(4): p. 669-82.

56. Hamma, T. and A.R. Ferre-D'Amare, *Pseudouridine synthases.* Chem Biol, 2006. **13**(11): p. 1125-35.

57. Raychaudhuri, S., et al., *Functional effect of deletion and mutation of the Escherichia coli ribosomal RNA and tRNA pseudouridine synthase RluA.* J Biol Chem, 1999. **274**(27): p. 18880-6.

58. Hager, J., B.L. Staker, and U. Jakob, *Substrate binding analysis of the 23S rRNA methyltransferase RrmJ.* J Bacteriol, 2004. **186**(19): p. 6634-42.

Chapter II
Analysis and expansion of the role of the *Escherichia coli* protein ProQ

This chapter has been published as, and modified from:
Sheidy DT, Zielke RA (2013) Analyss and Expansion of the Role of the*Escherichia coli* Protein ProQ. PLoS ONE 8(10): e79656.

2.1 Introduction

The maintenance of osmotic balance is essential for the fitness and survival of bacteria. One mechanism used by prokaryotes to achieve this balance in hyperosmotic environments is the import of osmoprotectant molecules which balance internal and external osmolarity and prevent the flow of water out of the cell [for review see [1]]. Several membrane bound transporters exist with a variety of specificities for different molecules. One such transporter, ProP, senses hyperosmotic stress, and responds by importing proline and glycine betaine [2-4]. Examination of the transcriptional regulation of *proP* has revealed a complex network of both growth-phase and osmolarity dependent control. Briefly, *proP* transcription can occur from a proximal (P2) or distal (P1) promoter [5]. Transcription from the P2 promoter occurs as cells transition from the logarithmic-growth phase into stationary phase and is dependent upon the stationary-phase sigma factor RpoS. Transcription from the P2 promoter is further enhanced by the nucleoid-associated factor Fis [6,7] and cyclic AMP receptor protein (CRP) [6]. The binding of Fis and CRP inhibit transcription from the P1 promoter [7, 8]. The P1 promoter is activated after subculture into fresh media, and is responsible for responding to upshifts in media osmolarity [5, 8, 9].

Beyond transcription, ProP activity is modulated by the cytoplasmic effector ProQ [10]. ProQ is a 232-residue protein, predicted to contain two structural domains, tethered by an unstructured linker [11, 12]. The N-terminal domain has been modeled on the structure of the RNA-binding, translational regulator FinO [11, 13], and the C-terminal domain has been modeled on the RNA chaperone Hfq [14]. Biochemical studies have been performed to support the structural predictions. The FinO-like domain, as well as the full length protein, are capable of binding to a model dsRNA template. The FinO-like domain also facilitates strand exchange, and both domains promote duplexing between complimentary strands of RNA [14]. Thus, ProQ behaves as an RNA chaperone. The mechanism behind ProQ regulation of ProP activity, however, remains largely unknown. Disruption of the *proQ* locus has no effect on the transcription of *proP*, but the proline uptake activity of ProP is significantly decreased in a Δ*proQ* strain [10, 15]. A post-translational mechanism was initially proposed after ProP protein levels appeared unchanged in a Δ*proQ* strain [15]; however, a direct physical interaction between ProP and ProQ has not been found. Most recently it was shown that, at osmolalities lower than those previously examined, ProP levels are decreased in a *proQ* mutant [14]. Additionally, as cells enter stationary phase, there is a modest decrease in the level of ProP in a *proQ* mutant compared to wild type [14]. In light of these findings, and the homology models comparing the ProQ domains to known RNA-binding proteins, a post-transcriptional mode of regulation is likely.

It had been reported in a high throughput study that ProQ was associated with ribosomes [16]. This led to the hypothesis that ProQ regulates ProP activity at the level

of translation. In this study, we verify that ProQ is associated with ribosomes *in vivo*, and we characterize this association under various conditions. We also determine which domains of ProQ are important for association. We demonstrate that ProQ binds tightly, but non-selectively to *in vitro* transcribed *proP* mRNA, and we report the K_D values for P1, P2, and an mRNA whose translation is not predicted to be dependent upon ProQ. Though we demonstrate that mRNA integrity is important for the association of ProQ with translating ribosomes, disruption of the *proP* locus, as well as the closely related *proU* operon, does not affect ProQ localization in polysome profiles. It had also been reported in a high throughput study that a *proQ* mutant exhibits decreased biofilm formation. Here we verify that result by complementing the phenotype and show that a *proP* mutant strain is not defective in biofilm formation. It follows that ProQ may act as a translation factor for a broader subset of mRNAs.

2.2. Materials and methods

2.2.1. Bacterial strains and growth conditions

E. coli strains used in this study are listed in Table 1. Strains were grown at 37^{o}C in Luria-Bertani (LB) broth (10 g tryptone, 5 g yeast extract, 10 g NaCl per liter). Cultures of JM6733 containing plasmids were supplemented with 20 µg/mL chloramphenicol (BioExpress). JM6733 (Δ*proQ::KAN*), JM6753 (Δ*proP::KAN*), JM6754 (Δ*proV::KAN*), JM6755 (Δ*proW::KAN*), and JM6877 (Δ*proX::KAN*) were constructed by P1 transduction [17] of KEIO-collection mutants, JW5300, JW4072, JW2652, JW2653, and JW2654 respectively, into a clean BW25113 background [18]. JM6881 (Δ*proVWX::KAN*) was made using the λ_{red} recombination system [19]. JM6906

(Δ*proP::FRT*) was constructed by transformation of JM6753 (Δ*proP::KAN*) with pCP20, and subsequently, screening for sensitivity to kanamycin [20]. JM6926 (Δ*proP::FRT*, Δ*proVWX::KAN*) was constructed by P1 transduction of JM6906 by phage grown on JM6881. Genotypes were verified using primers flanking the genomic regions of interest (Table 2). Culture growth was monitored by measuring the absorbance at 600 nm.

2.2.2. Preparation of cell lysates for ribosomal fractionation

Isolation of ribosomal species was performed as previously described [21] with the following exceptions. Cultures of LB broth were inoculated with 1/200th volume of a stationary overnight culture. For strain JM6733 (Δ*proQ::KAN*) containing the indicated plasmids, Isopropyl β-D-1-thiogalactopyranoside (IPTG) was added to a final concentration of 15 µM after the first 30 min of incubation to induce the expression from the *lac* promoter. Cell pellets were resuspended in 700 µL of lysis buffer containing 10 mM Tris pH 7.5, 10 mM $MgCl_2$, and 60 mM NH_4Cl per 100 mL of starting culture, flash frozen in liquid nitrogen, and stored at -80^{o}C. 300 µm glass beads were added to frozen cells as they thawed. Cells were lysed by repeated vortexing for 1 min followed by 1 min on ice for a total time of 10 min. The lysate was cleared by centrifugation at 21,000 x g for 10 min at 4^{o}C. For subunit dissociation experiments, cells were lysed without addition of chloramphenicol, in buffer containing 10 mM Tris pH 7.5, 1 mM $MgCl_2$, and 60 mM NH_4Cl and clarified as described. The absorbances of clarified lysates were measured at 260 nm.

2.2.3 MNase digestion of ribosomes

Lysates were prepared as previously described. 13 OD_{260} units of lysate were transferred to a clean, 1.5 mL microcentrifuge tube. $CaCl_2$ was added to a final concentration of 5 mM. BSA (NEB) was added to a final concentration of 0.1 mg/mL. 4 µL of MNase (NEB) were added and the final reaction volume was brought up to 400 µL with lysis buffer. Digests were carried out at room temperature for 30 min. Mock digests were set up as controls, containing all reagents except MNase.

2.2.4. *In vitro* binding of ProQ and 70S ribosomes

70S ribosomes (NEB) were incubated with an equimolar ratio of purified ProQ in polysome lysis buffer, with or without equimolar P2 mRNA. Reactions were loaded onto sucrose gradients and separated as described.

2.2.5. Ribosomal fractionation

Ribosomal species were separated on sucrose gradients ranging from 10% to 47% sucrose in pollyalomar ultracentrifuge tubes (Beckman). Sucrose was dissolved in the following buffer: 100 mM NH4Cl, 10 mM Tris pH 7.5, 10 mM $MgCl_2$. 550 µL of 47% sucrose was added into the bottom of the tube and placed at -80^{o}C until frozen. Next, 42% sucrose was added and the tube was placed back at -80^{o}C until frozen. This method was repeated until the gradient was complete, using the following concentrations of sucrose: 47%, 42%, 37%, 32%, 27%, 22%, 17%, 12%, 10%. Gradients were stored at -80^{o}C. Gradients were allowed to thaw completely at room temperature. 13 OD_{260} units of lysate were applied to the top of each gradient. Gradients were balanced and submitted to ultracentrifugation in an SW50.1 (Beckman)

rotor at 41K RPM for 1.5 h at 4^{o}C. After ultracentrifugation, fractionation was performed as previously described [21]. Separation of dissociated subunits was done by ultracentrifugation on 20% sucrose cushions in an SW40TI (Beckman) rotor at 23 K RPM for 15 h at 4^{o}C. Fractionation was performed as previously described.

2.2.6. Mutant His-ProQ constructs

Mutant constructs were made using pCA24N-ProQ from the ASKA collection [22] as a template for inside-out PCR. A *Sac*I restriction endonuclease site was added to both primers (Table 2), allowing linear products from PCR amplification to be digested and self-ligated in frame to create pDS1-pDS5 (Table 1).

2.2.7. ProQ purification and antibody production

A culture of JM6733 (Δ*proQ::KAN*), transformed with pCA24N-ProQ, was grown to late-logarithmic growth phase (OD_{600} ≈ 0.8) at 37^{o}C in LB media. Production of a 6 histidine epitope-tagged ProQ was induced by addition of IPTG to a final concentration of 1mM, and the culture was shifted to ambient temperature with shaking. Cells were harvested 18 h post induction. Cells were resuspended in 8 mL of lysis buffer (10% glycerol, 20 mM Tris pH 8.0, 500 mM NaCl, 10 mM Imidazole, and 1 mM β-Mercaptoethanol) and complete EDTA-free protease inhibitors (Roche) per 1 g of wet pellet weight and disrupted by 5 passes through a french press. Insoluble debris was cleared via centrifugation at 15,000 RPM for 30 min at 4^{o}C in an SA-600 rotor (Sorvall). Nickel affinity chromatography was performed using Ni-NTA Superflow resin (Qiagen) as per manufacturer's directions with the following exceptions. After batch binding of

6His-ProQ the column was washed with 5 column volumes (CVs) of lysis buffer. Additional 5 CV washes were done with lysis buffer containing 1 M NaCl, as well as lysis buffer containing 20 mM and 30 mM Imidazole. 6His-ProQ was eluted from the column using 5 CVs of lysis buffer containing 500 mM Imidazole. Protein purity was monitored via SDS-PAGE, and the eluent was dialyzed overnight at 4^{o}C in a low-salt buffer (10% glycerol, 20 mM Tris pH 8.0, 100 mM NaCl, 1 mM β-Mercaptoethanol). Cation exchange chromatography was performed using SP Sepharose Fast Flow resin (GE Healthcare). Cation exchange resin was equilibrated with 5 CVs of low salt buffer. Dialyzed 6His-ProQ was incubated with equilibrated resin for 30 min at room temperature with occasional agitation. After batch binding, the column was washed with 5 CVs of low salt buffer. 6His-ProQ was eluted from the column using a gradient of NaCl (100 mM to 1 M). 6His-ProQ purity was monitored via SDS-PAGE, and purified 6His-ProQ was again dialyzed against a low-salt buffer. After dialysis, 6His-ProQ was concentrated using a centrifugal filter with a 3 kDa molecular weight cutoff (Amicon), as per manufacturer's directions. Purified 6His-ProQ was quantified using an ND-1000 spectrophotometer (NanoDrop Technologies, Inc.) and 600 µg was sent for antibody production in a rabbit host (Cocalico Biologicals, Inc).

2.2.8. Western-blot analysis of ribosomal fractionations

Denaturing SDS-PAGE loading buffer (50 mM Tris pH 6.8, 2% Sodium dodecyl sulfate (SDS), 10% glycerol, 1% β-Mercaptoethanol, 13 mM EDTA, 0.02% Bromophenol blue) was added to trichloroacetic acid (TCA) precipitated ribosomal fractions. Briefly, TCA was added to polysome gradient fractions to a final concentration

of 15% and incubated at 4^{o}C for 30 min. The precipitant was pelleted in a microcentrifuge at maximum speed for 10 min. The supernatant was removed and the pellet was washed twice with ice cold 100% acetone. Proteins were separated via SDS-PAGE and transferred to nitrocellulose (GE Water & Process Technologies). Protein detection was carried out using antibodies against ProQ (1:5000 in 5% dry milk in PBS + 0.1% Tween20) and ribosomal proteins L3 (1:5000 in same) and S2 (1:5000 in same). Antibodies to L3 and S2 were a generous gift from Catherine Squires.

2.2.9. Copy number calculation

proQ was cloned into vector pMCSG7 as described [23] using DS046 and DS047 (Table 2) to make pDS6 (Table 1), which adds an N-terminal 6-Histidine epitope tag, followed by a TEV cleavage site. ProQ was purified as previously described with the following exceptions. After the first nickel affinity column, elution fractions were pooled and dialyzed overnight in the presence of 6His-TEV protease. A second nickel affinity column was used to remove TEV protease and the flow through was collected. Fractions were analyzed via SDS-PAGE and pooled for cation-exchange chromatography. Purified ProQ was quantified using a Bradford assay (Biorad). Known amounts of ProQ, as well as whole cell lysate from a known number of wild type BW25113 *E. coli* cells were loaded onto SDS-PAGE and transferred to nitrocellulose for western-blot analysis using anti-ProQ antibodies. Band intensities were quantified using ImageJ and cellular concentration was calculated.

2.2.10. *In vitro* transcription

The *proP* genomic region was cloned into pBluescriptKS+ in two forms, starting at either -182 (*proP* P1, DS037, DS039) or -95 (*proP* P2, DS038, DS039). The *rpoS* genomic region was cloned into pBluescriptKS+ (rpoS-T7-forw_SacII, rpoS-T7-rev-PstI). PCR was performed to amplify the plasmid DNA for use as an *in vitro* transcription template. The forward primer maintained the integrity of the T7 polymerase dependent promoter (pBSIVTforward), and the reverse primer added a stop codon after glycine 245 for *proP* P1and P2 (DS076) and after tyrosine 147 for *rpoS* (rposIVTreverse), yielding mRNAs with sizes of 927 bp, 840 bp, and 1041 bp respectively. *In vitro* transcription was carried out as described previously [24], and the mRNAs were checked for quality using urea-acrylamide gel electrophoresis and TAE-agarose electrophoresis. The mRNA concentrations were determined by electrophoresis on a TAE-agarose gel and quantitative comparison to the RiboRuler High Range RNA Ladder (Thermo Scientific).

2.2.11. Tryptophan fluorescence

Purified ProQ was dialyzed into 10% glycerol, 20 mM HEPES pH 7.5, and 100 mM NaCl. The concentration was determined using Bradford assay. For binding experiments, ProQ was diluted to a final concentration of 20 nM in the same buffer plus 0.005% BRIJ35. Temperature was held constant at 20^{o}C and tryptophan was excited at 295 nm and fluorescence was monitored at 355 nm using a QuantaMaster4 (Photon Technology International). The excitation wavelength was chosen to avoid any possible inner-filter effect stemming from the use of nucleic acids as ligands [25]. Increasing

amounts of *in vitro* transcribed mRNAs were added to the reaction and the change in fluorescence was observed.

2.2.12. Biofilm assays

Plasmid pMR20-ProQ was constructed by cloning the amplicon from primers DS083 and DS084 into pMR20 [26] cut with *Kpn*I and *Sac*I (Table 2). Biofilm assays were performed with modifications of previous protocols [27, 28] as follows. Strains were grown overnight in LB + 12.5 µg/mL tetracycline. 30 µL of the saturated overnight was inoculated into 1 mL of LB without salt (10 g tryptone, 5 g yeast extract) plus 12.5 µg/mL tetracycline, in a previously unused borosilicate test tube. Tubes were incubated at 25^{o}C without shaking for 6 d. After 6 d, the media and loose cells were removed and the OD_{600} was measured. Tubes were gently rinsed by submerging in deionized water 5 times and allowed to air dry. Biofilms were stained using 1% crystal violet for 20 min. Tubes were again rinsed by submerging in deionized water to reduce background staining. Biofilms were resuspended completely in 0.5% SDS and the OD_{600} was measured. Relative biofilm formation was calculated as described previously [27].

2.3. Results

2.3.1. ProQ associates with translating ribosomes

In order to verify the localization of ProQ on ribosomes, the soluble lysates from wild type *E. coli* (strain BW25113) were separated on sucrose density gradients (Figure 2.1A). Western-blot analysis of the resulting fractions revealed that ProQ predominantly associates with 70S and translating ribosomes, and to a lesser extent, at the top of the

gradient and in fractions corresponding to the 30S ribosomal subunit. Antibodies against small and large ribosomal subunit proteins validated the assignment of the peaks in the UV-absorbance trace. Deletion of some ribosome-associated factors can lead to ribosomal defects and perturbation of the polysome profile [21]. Profiles from a Δ*proQ* strain were indistinguishable from wild type (data not shown), and therefore, ProQ is not likely a ribosome assembly factor, nor is it required for the translation of the majority of mRNAs in the cell.

Since the 30S and 50S ribosomal subunits work in tandem, but with separate roles during translation, identifying the subunit with which ProQ associates provides a clue as to the function of ProQ during translation. When isolated at lower concentrations of Mg^{2+}, 70S ribosomes dissociate into 30S and 50S subunits [29]. At 1 mM Mg^{2+}, the 70S and polysome species were predominantly dissociated, as revealed by the UV-absorbance trace and localization of S2 and L3 (Figure 2.1B). A large proportion of ProQ was found at the top of the gradient, but ProQ that did migrate into the gradient peaked with the 30S subunit but not with the 50S subunit. These data are consistent with the localization under non-dissociating conditions (Figure 2.1A). Thus, ProQ appears to preferentially associate with the 30S subunit.

2.3.2. The N-terminus and linker regions are necessary for ribosome association

ProQ is predicted to contain two structural domains, tethered by a positively charged linker region. The N- and C-termini have been modeled on the RNA binding proteins FinO and Hfq respectively [11, 14]. Using available bioinformatic tools to predict secondary structure, disordered regions, and nucleic acid binding propensity

[30-32], we assigned the boundaries of the linker region as amino acids E116-V180. Assignment of the lower bound was the most difficult. The nucleic acid binding predictor, BindN, indicated the presence of an unstructured positively charged domain starting at E116. The secondary structure predictor, PSIPRED, indicated the presence of an alpha helix until A124. Domain constructs were made using the 6HIS-ProQ plasmid from the ASKA collection [22] as a template. A schematic of each construct is provided (Figure 2.2A). To determine the regions of ProQ that are necessary for its association with the ribosome, each ProQ construct was expressed in a Δ*proQ* background, such that it was the only copy of ProQ in the cell. We could not detect a ProQ variant expressing only the C-terminal domain (*proQ181-232*). The distribution of ectopically expressed 6HIS-ProQ (Figure 2.2B) was similar to that of ProQ from wild type cells (Figure 2.1A); although, in addition to an association with 70S, polysome, and 30S fractions, there was a general increase in ProQ throughout the gradient. This broader distribution may reflect a higher than normal cellular concentration caused by exogenous expression or a decrease in affinity for translating ribosomes due to the N-terminal 6HIS-epitope tag. The high rate of speed and high G-forces produced during polysome fractionation can physically disrupt binding interactions, so addition of the epitope tag may cause dissociation of 6HIS-ProQ from ribosomes as it progresses through the gradient. Deletion of the C-terminal Hfq domain (*proQΔ181C*) did not affect association with the ribosomes (Figure 2.2B), and therefore, this part of the protein is not required for ribosome localization. In contrast, both the N-terminus and linker regions are required for ribosome association, as the majority of *proQΔ115N* and *proQΔ124-180* were found at the top of the gradient. Consistently, removal of the C-

terminus and linker domains together (*proQ2-123*) caused ProQ to be found at the top of the gradient. Moreover, the linker domain (*proQ116-180*) was not sufficient for ribosome association. These data suggest that both the N-terminal FinO domain and the linker regions are required for ribosome association of ProQ.

2.3.3. ProQ interacts with the mRNA being translated

The comigration of ProQ into sucrose gradients with translating ribosomes could occur because of a physical interaction with the ribosome directly or because of an interaction with the mRNA bound by a 30S particle and/or 70S particle. To determine the nature of the ProQ association with ribosomes, we partially hydrolyzed the mRNA in cell lysates with micrococcal nuclease (MNase) under conditions that did not perturb the integrity of the highly structured, and relatively RNase insensitive, ribosome. As expected, the small ribosomal protein S2 was found associated with the remaining 70S and 2-mers, and no appreciable amount of S2 was found at the top of the gradient. This supports the claim that the integrity of these ribosomes was maintained. In mock treatments, mRNAs with up to 4 ribosomes are seen in sucrose gradients, and ProQ associates with all translating ribosomes (both the 70S and polysome forms) (Figure 2.3A). After treatment with MNase, the level of total polysomes was decreased concomitant with a large increase in free 70S ribosomes (Figure 2.3A) and consistent with cleavage of intra-ribosome mRNA. Strikingly, in contrast to a robust association of ProQ with 2-mer and 3-mer polysomes in untreated samples, ProQ was almost absent from these particles in the MNase treated samples. Additionally, a significant amount of ProQ was found at the top of the gradient, consistent with dissociation of ProQ from the

ribosomes after disruption of mRNA. Thus, ribosome association of ProQ appears to be partially dependent on the mRNA being translated. In order to support this finding, we also performed *in vitro* binding experiments with mRNA-free 70S ribosomes. 70S ribosomes were incubated with equimolar purified ProQ, with or without *proP* P2 mRNA. After incubation, the reactions were applied to sucrose gradients and separated as before (Figure 2.3B). Though some ProQ is found in the gradient under the 70S peak, indicating a weak interaction with 70S ribosomes, the bulk of the ProQ is located in the fractions not corresponding to the 70S ribosomes. It is also worth noting that when *proP* mRNA was added, we consistently observed the concentration of ProQ in the gradient peaking around fraction 5. The best explanation for this result is that ProQ is binding to the *proP* mRNA and migrating to this region of the gradient.

2.3.4. ProQ does not bind selectively to *proP* mRNA

It has been demonstrated that ProQ can bind to a model RNA substrate *in vitro* [14]. However, the model double-stranded substrate used previously was relatively small (39 bp in duplex form) compared to the size of an mRNA. To further understand the RNA binding properties of ProQ, binding experiments were performed using purified ProQ and *in vitro* transcribed mRNA substrates (Figure 2.4A). One possibility is that ProQ acts as a *proP* mRNA-specific translation factor. If true, we would predict that ProQ should interact preferentially with *proP* mRNA *in vitro*. We tested the ability of ProQ to bind to mRNA made from the *proP* P1 and P2 promoters, as well as an unrelated mRNA, *rpoS* (see methods). Under the conditions tested, ProQ showed no preference for *proP* mRNA transcribed from promoter P1 or P2, and the binding affinity

for *proP* P1 and P2 were similar (17.0 ± 6.1 nM and 11.6 ± 2.7 nM, respectively; Figure 2.4). Interestingly, ProQ also bound tightly to *rpoS* mRNA (19.5 ± 7.8 nM; Figure 2.4). These slight differences among the K_D values are not sufficient to confer selectivity *in vivo.* Comparisons of our values to those previously reported for the model substrate are in agreement [14], though we report consistently lower K_D values. ProQ binds non-selectively to all mRNAs tested, but it does not bind to DNA, and we include the results as a negative control. To complement the determination of the K_D values for specific mRNAs we sought to determine the cellular abundance of ProQ. Using quantitative western-blot analysis, we estimate the cellular copy number of ProQ to be $1.90 \times 10^3 \pm 324$ (95% confidence interval, data not shown). Assuming a cellular volume of 1.3 μm^3 [33], the cellular concentration of ProQ is 2.43 ± 0.414 µM. This number is comparable to another estimate for the ProQ copy number obtained by high-throughput proteomic analysis of *E. coli* cytosolic proteins [34], and at approximately 2,000 copies/cell, ProQ is in the top 25% in terms of protein abundance.

2.3.5. Ribosome association of ProQ is not dependent on *proP* or *proU*

We have shown that ProQ is found on translating ribosomes and this association appears to be mediated through mRNA. Because the only well characterized phenotype for a *proQ* mutant is a decrease in proline uptake, we posit that ProQ is involved in the translation of a subset of mRNAs in the cell, including one or more of the proline transporter mRNAs. We therefore asked whether the ribosome association of ProQ was dependent on these mRNA transcripts. We first examined the localization of ProQ in a Δ*proP* mutant, as *proP* mRNA is the predicted target of ProQ. We found, however, that

the ribosome association of ProQ was similar in a Δ*proP* strain to that seen in the wild type strain (Figures 2.1 and 2.5). A genetic interaction has been reported between *proQ* and the *proW* and *proX* loci within the *proU* operon [35] and therefore, these genes may be regulated by ProQ. For this reason, we examined ProQ localization in strain backgrounds deleted for each member of the *proU* operon, as well as a deletion of the entire *proU* operon (*proVWX*), and deletion of both *proVWX* and *proP* together. In all backgrounds tested, ProQ is repeatedly found associated with 70S particles and polysomes (Figure 2.5). Thus, ProQ ribosome association is not absolutely dependent on any of these genes, and the ribosome association of ProQ may be due to one or more additional cellular mRNAs.

2.3.6. ProQ is necessary for biofilm formation, independent of ProP

Having shown that ProQ localization to the ribosome is independent of all known potential interactions involved in proline transport, we sought to expand the ProQ target list by looking for new Δ*proQ* phenotypes. A high throughput study implicated ProQ in biofilm formation; though, it only reported it as a hit and did not verify the result through plasmid-based complementation [27]. Under the conditions tested, a *proQ* mutant strain was found to be about 50% deficient in biofilm formation compared to wild type cells (Figure 2.6). This phenotype was complemented by transforming Δ*proQ* cells with a low-copy plasmid containing the *proQ* gene, plus 500 bp of sequence upstream of the translation start site. To test if this phenotype was independent of the role of ProQ in ProP regulation, we examined biofilm formation in a *proP* mutant strain. This strain was able to form biofilms as well as wild type. As a result, we conclude that the decrease in

biofilm formation is unique to a *proQ* mutant and is independent of the ProQ-ProP interaction, though the reason for this deficiency remains unclear.

2.4. Discussion

It has been proposed that ProQ is a translational regulator of *proP* mRNA [14]. This hypothesis has evolved and emerged out of a sort of “process of elimination”, whereby it has been shown that i) *proP* transcript levels are unchanged in a *proQ* mutant [10] ii) no physical interaction can be detected between ProQ and ProP [35], and recently iii) ProP expression levels are affected by deletion of *proQ* [14]. In this study, we present the first *direct* evidence of a ProQ-translation link by demonstrating the association of ProQ with 70S particles, translating ribosomes, and 30S particles (Figure 2.1), but we have not detected a specific interaction between ProQ and *proP* mRNA at the ribosome. Some proteins that associate with the ribosome are involved in ribosome maturation and assembly [21, 36]. Deletion of these factors can result in defects in polysome profiles and decreased growth rates [for reviews see [37]]. These phenotypes are not observed in a *proQ* mutant (data not shown), and because of the relative dearth of phenotypes associated with a *proQ* deletion, it is unlikely that ProQ is an assembly factor. Thus far, ProQ has only been implicated in proline uptake [10] and stimulation of biofilm formation [[27] and this study]. For these reasons, we propose that ProQ has a very narrowly defined role in the translation of only a subset of mRNAs. This hypothesis is bolstered by the fact that the N-terminus of ProQ has been modeled on FinO, a highly specified translational regulator, which acts to specifically represses the translation of *traJ* mRNA by facilitating the interaction between *traJ* and the anti-sense RNA *finP* [38,

39]. As for the identities of the specific mRNA targets of ProQ, *proP* remains a favored target, but it is unknown if this effect is direct or indirect. Additionally, one or more additional targets are predicted to exist, based on the ProP-independent biofilm defect in a *proQ* mutant.

It had previously been shown that ProQ could bind to a model RNA, and that ProQ exhibits RNA chaperone-like activity [14]. Here we sought to explore the interaction between ProQ and RNA in three distinct ways. First, we examined the consequences of nuclease treatment on the association of ProQ with the ribosome (Figure 2.3A). Limited treatment of lysates with MNase caused a decrease in the number of polysomes observed after centrifugation. Specifically, the number of 3-mers and higher molecular weight species were significantly decreased. The loss of 3-mers is consistent with the increase in the number of 70S ribosomes observed. Though 3-mers were almost completely missing, a significant amount of ribosomes were still found to exist as 2-mers. MNase treatment had a large effect on the localization of ProQ, however, causing it to almost completely delocalize from 2-mers and 70S ribosomes. To further explore the requirement of mRNA for ProQ-ribosome association, we examined the ability of ProQ to bind to mRNA-free ribosomes *in vitro.* Not surprisingly, ProQ did not robustly associate with these ribosomes, and instead, seemed to prefer to bind to mRNA when present in the reactions (Figure 2.3B). For these reasons, we conclude that the mRNA being translated is very important for the comigration of ProQ with 70S and polysome species. Next, we used a quantitative *in vitro* binding assay to determine the affinity of ProQ for its predicted mRNA target, *proP* (Figure 2.5). The hypothesis that ProQ enhances *proP* translation, to the exclusion of other mRNAs, leads to the

prediction that ProQ should selectively recognize *proP*. Under the conditions tested, ProQ binds tightly to *proP* mRNAs, but this binding is not selective, as ProQ binds with similar affinity to *rpoS* mRNA (Figure 2.4). Though we cannot rule out the possibility that *rpoS* is also a target of ProQ regulation we believe this is unlikely since RpoS is a known regulator of *proP* transcription [7, 40], *proP* transcript levels are unchanged in a ProQ mutant [10], and a *proQ* deletion strain does not have the same lack of thermotolerance seen in an *rpoS* deletion strain [14]. If *proP* is a direct target of ProQ, some other factor must confer specificity *in vivo*.

Little is known about ProQ, mechanistically. Previous studies have shown that exogenous expression of the N-terminal, FinO-like domain (residues 1-130) can partially complement the proline uptake deficiency of a *proQ* chromosomal deletion, and the N-terminus (1-130) is necessary and sufficient for binding to RNA [12, 14]. Our study of the domains of ProQ involved in ribosome association is not entirely consistent with these previous results. For example, even though the first 130 residues could bind to a model RNA, we do not observe ribosome association of a similar construct to any appreciable degree (Figure 2.2B). In this study, we expand the linker by seven residues to include amino acids 124-180, thus shortening the N-terminal domain from 1-130 to 1-123 (Figure 2.2A). This difference could account for the lack of ribosome association if residues 124-130 are necessary for RNA binding. Another inconsistency is observed with the C-terminus. In this study we find that a construct lacking residues 181-232 is associated with the ribosome in a manner comparable to plasmid-expressed wild type ProQ (Figure 2.2B). However, in previous studies, this construct did not suppress the proline uptake deficiency as well as a construct containing the C-terminal domain [12]. It

must be noted that our present study sought only to identify the domains of ProQ which are important for ribosome association, independent of *proQ-proP* genetic interactions. Based on our results, we conclude that only the C-terminus is dispensable for ribosome association. Though we would predict that ribosome association is necessary for suppression of the proline uptake phenotype, we do not observe a direct dependence. This further complicates the mechanism by which ProQ enhances proline uptake.

A deeper exploration of the mechanism of ProQ action will be predicated on the discovery of *direct* mRNA targets. To date, finding these targets has been challenging. To begin the process, here we verified that ProQ is involved in promoting biofilm formation [27]. More importantly, we show that this phenotype is independent of ProP, yielding the first ProP-independent ProQ phenotype (Figure 2.6). Further independence of ProQ from ProP is demonstrated by the fact that ProQ is still associated with ribosomes in the absence of *proP* and *proU* mRNAs (Figure 2.5).

Though further studies are needed to definitively determine the function of the ribosomal association of ProQ, it is not unreasonable to propose a role for ProQ in translation initiation. Under non-dissociating conditions, we observe the highest concentration of ProQ in fractions corresponding to 70S and polysome species, but there is a modest, yet consistent, increase in signal under the peak corresponding to 30S particles, the first particle to bind during initiation (Figure 2.1A). This 30S localization is confirmed under dissociating conditions (Figure 2.1B). We present data showing that ProQ can bind tightly to mRNA *in vitro* (Figure 2.4), and mRNA integrity is necessary for robust ribosome association (Figure 2.3). Thus, ProQ is ideally positioned

to function in translation initiation of its mRNA targets, perhaps by facilitating the interaction between 30S particles and these as-yet unidentified mRNAs.

2.5. Update

Since publication of this chapter, a paper has been published which demonstrates that the stability of *proP* mRNA and the level of ProP protein in the cell is controlled by the riboendonuclease RNase III [41]. In RNase III deficient cells, the half-life of *proP* is increased, and the protein levels, likewise, increase (Figure 2.7). As noted, *proP* mRNA is transcribed from two different promoters, a distal promoter called P1 and a proximal promoter, P2. Because the effects of ProQ deletion on ProP protein levels were reported to be dependent upon growth phase and osmolarity of the media, I had originally predicted that ProQ might affect the translation of one *proP* mRNA, while having little effect on the other. As P1 is the osmotically responsive promoter, I hypothesized that ProQ might bind more tightly to, and therefore regulate the translation of, *proP* P1 mRNA. Interestingly, the paper referenced above finds that only the P1 transcript is affected by RNase III. This arises from the RNase III recognition and cleavage site being positioned upstream of the P2 promoter (Figure 2.8).

Discovery of this fact made it necessary to reexamine whether choosing *rpoS* mRNA as a negative control for my *in vitro* ProQ-mRNA binding experiments was valid, as *rpoS* levels are regulated by RNase III [42]. Even though it was reported that *proQ* mutant strains do not exhibit phenotypes similar to that of *rpoS*-deficient cells, it is possible that, like its reported control of *proP* translation, the effects of ProQ on *rpoS* translation might be subtle and nuanced. This experiment should be replicated using an

mRNA not regulated by RNase III; though, the ability of ProQ to bind to *proP* P2 mRNA in this assay still suggests that binding to mRNA is not selective under the conditions tested.

In light of both of these data, I examined the RNase III regulatome more closely. In this chapter, I show that deletions of *proQ* have an effect on biofilm formation, causing about a 50% decrease in formation (Figure 2.6). Formation of robust biofilms is dependent upon many factors, but one factor which is positively correlated with biofilm formation is the *E. coli* flagella. The main protein component of the flagella is FliC, and preliminary data I obtained shows that FliC expression is almost completely abolished in Δ*proQ* strain (Figure 2.9). More evidence of a ProQ-RNase III link comes from the fact that *fliC* mRNA levels are also regulated by RNase III. Again, *fliC* mRNA levels are much higher in an RNase III mutant than they are in wild type. Oddly, attempts to complement the loss of FliC expression in Δ*proQ* strains by expression of ProQ from a plasmid were unsuccessful (Figure 2.10). It is unclear what consequence this has on the hypothesis that *fliC* might be a target for regulation by ProQ. However, personal communications with labs studying the mRNAs associated with ProQ strengthen the connection between FliC and ProQ.

Taken together, there is a “preponderance of evidence” linking RNase III and ProQ. In the cases of *proP* P1 and *fliC* mRNAs, loss of RNase III stabilizes the mRNAs, while loss of ProQ results in a decrease in protein levels. The effects of ProQ on *rpoS* are not currently known, but should be examined. It seems that ProQ and RNase III are functioning semi-redundantly to upregulate translation, RNase III by increasing messenger stability, and ProQ by enhancing translation through some unknown

mechanism. It is possible that deletion of *proQ* might abolish the increase in proline uptake by ProP observed in an RNase III mutant strain. To extend it further, an RNase III mutant might suppress the biofilm defect in a *proQ* mutant and restore FliC levels to that of wild type cells. Further discussion is presented in Chapter V of this document.

2.6. Acknowledgements

The authors wish to thank Dr. Titus Franzmann for training and technical assistance with tryptophan fluorescence experiments and Dr. Stefan Walter for assistance with ProQ-mRNA binding data analysis.

Figure 2.1. Ribosome association of ProQ under native and dissociating conditions. Polysome profiles (254 nm) from wild type cell extracts in (A) associating conditions (10 mM Mg^{2+}) and (B) dissociating conditions (1 mM Mg^{2+}) are shown. Western-blot analysis of TCA-precipitated fractions using antibodies to ProQ, small ribosomal subunit protein 2 (S2), and large ribosomal subunit protein 3 (L3) are shown and aligned to the UV-absorbance trace. Whole cell extracts from wild type (BW25113) and Δ*proQ* (JM6733) are included, as is the soluble lysate (Load). UV-absorbance peaks correspond to (L to R): Free RNA/protein, 30S, 50S, 70S, and polysomes.

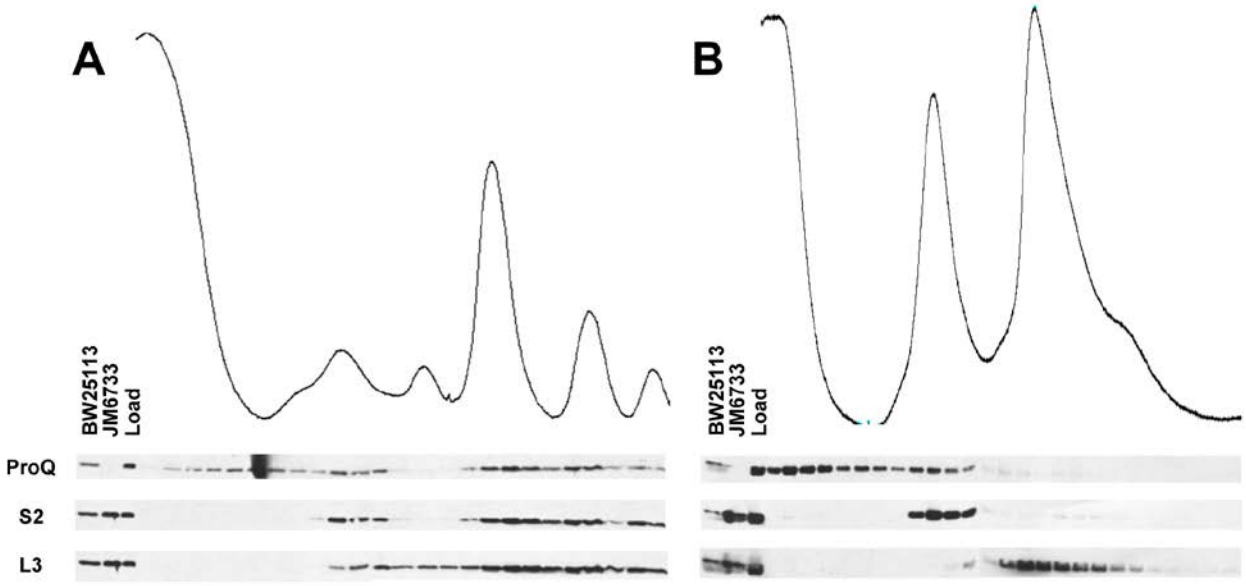

Figure 2.2. Ribosome association of plasmid encoded *proQ* mutant constructs in polysome profiles. (A) Schematic representation of *proQ* mutant constructs expressed from the IPTG inducible plasmid pCA24N. The predicted RNA binding region is colored in black, and amino-acid boundaries of each construct are labeled. (B) Mutant constructs were expressed as the lone copy of *proQ.* Western-blot analysis of TCA-precipitated fractions from the separation of ribosomal moieties on sucrose density gradients was performed. Whole cell extracts of cells after induction were included (Induced) along with soluble lysate (Load). Position of the 30S, 50S, 70S, and Polysome species are indicated based on western-blot localization of S2 (data not shown).

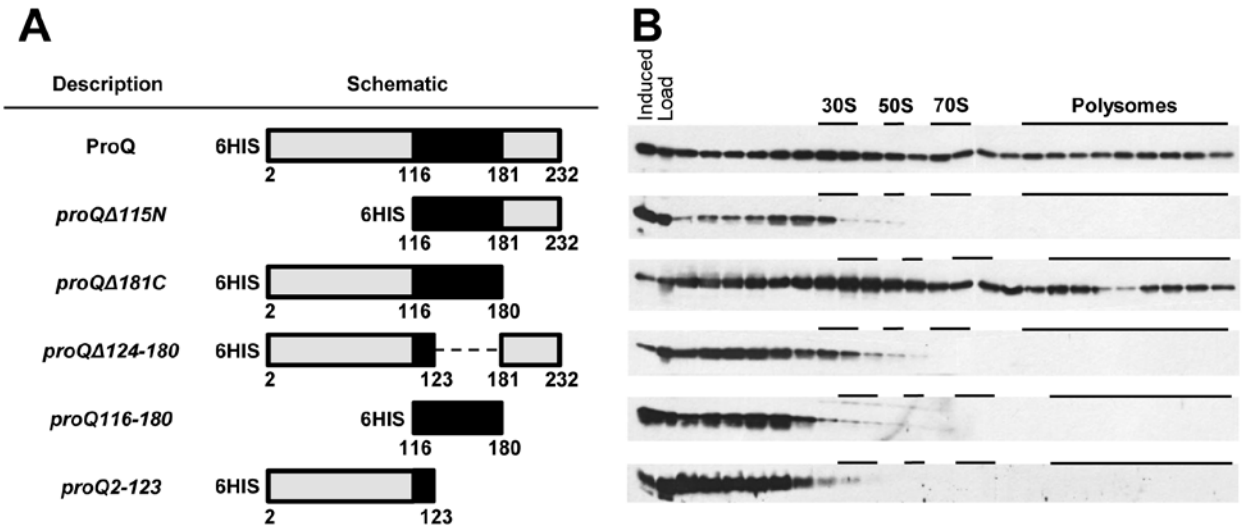

Figure 2.3. Robust 70S ribosome association of ProQ requires intact mRNA. (A) Cell lysates were left untreated (solid line) or treated with limited MNase (dashed line) and ribosomal species separated on sucrose gradients. The positions of ProQ and ribosomal protein S2 in the resulting TCA-precipitated fractions is determined by western-blot analysis. (B) mRNA free 70S ribosomes were mixed with equimolar amounts of purified ProQ without (foreground) or with (background) the addition of equimolar P2 mRNA before application to sucrose gradients. The position of ProQ and ribosomal protein S2 in the resulting TCA-precipitated fraction is determined by western-blot analysis.

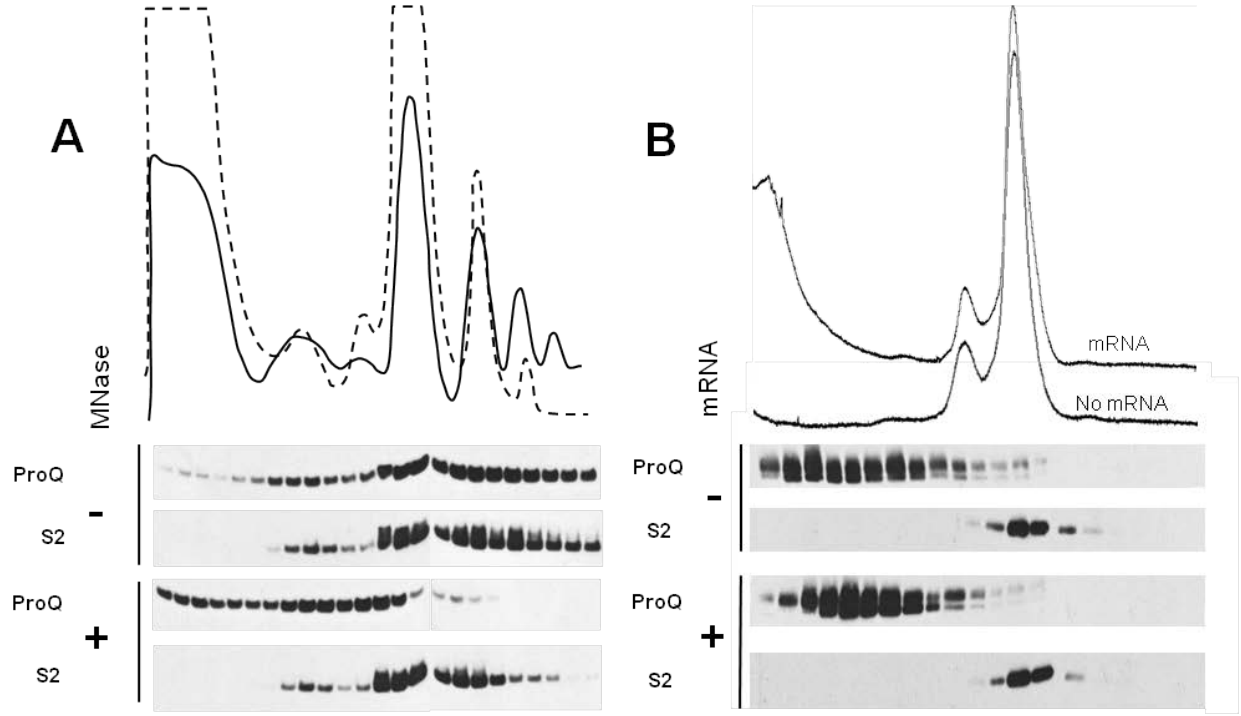

Figure 2.4. mRNA binding kinetics monitored by native tryptophan fluorescence. (A) 20 nM ProQ was titrated with increasing amounts of *in vitro* transcribed mRNAs ("▲" *proP* P1, "●" *proP* P2, "■" *rpoS*). Tryptophan was excited at 295 nm and the fluorescence was monitored at 355 nm. The y-axis is provided in terms of normalized fluorescence (FL_F/FL_I), determined by dividing the fluorescence at each mRNA concentration (FL_F) by the fluorescence for 20nM protein only (FL_I). DNA yielded no measurable fluorescence shift and is included as a negative control ("□" DNA) (B) Summary of binding affinities of ProQ for *in vitro* transcribed mRNAs.

A

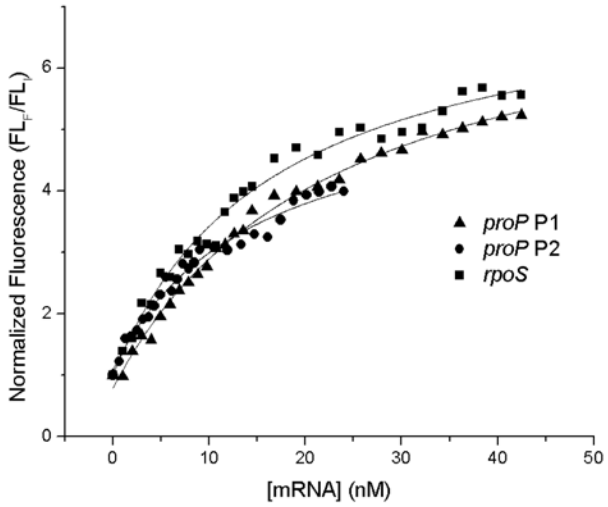

B

mRNA	KD ± SEM (n = 3)
proP P1	17.0 ± 6.1
proP P2	11.6 ± 2.7
rpoS	19.5 ± 7.8

Figure 2.5. Ribosome association of ProQ in various strain backgrounds. Cell lysates from various mutant backgrounds, as indicated, were separated by sucrose density ultracentrifugation and the localization of the ribosomal species (30S, 50S, 70s, polysomes) indicated. The localization of ProQ in the TCA-precipitated fractions is shown by immunoblot. Whole cell extracts from wild type, Δ*proQ* (JM6733), and the soluble lysate (Load) are included as indicated.

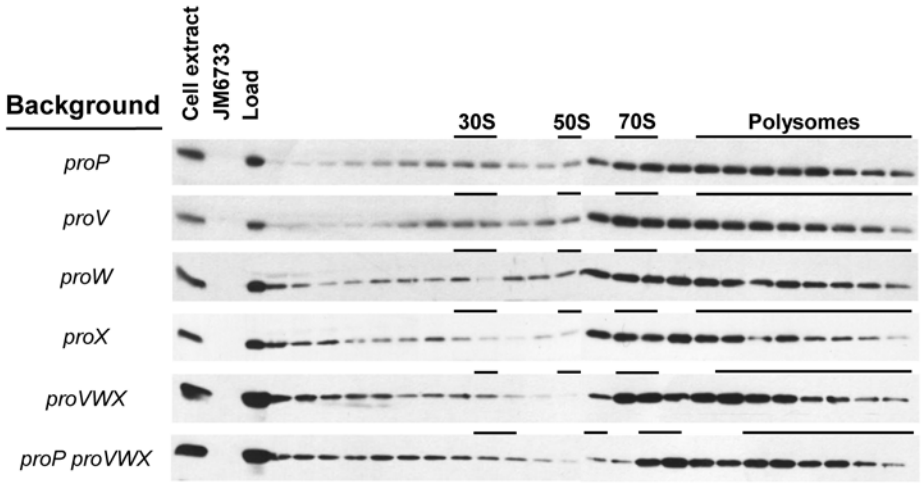

Figure 2.6. Biofilm formation defect in a Δ*proQ* strain. Wild type (BW25113), Δ*proQ* (JM6733), and Δ*proP* (JM6753) strains were examined for formation of biofilms after 6 days. Strains were transformed with either empty vector (pMR20; shaded) or vector containing the *proQ* open reading frame, plus 500 bp of genomic sequence upstream of the translation start site (pMR20-ProQ; unshaded). Error bars represent 95% confidence intervals. A statistical difference is indicated (*) between wild type and Δ*proQ* (JM6733) with a p-value < 0.001.

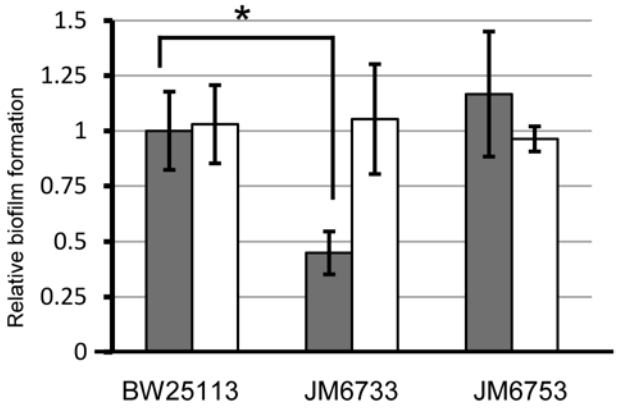

Figure 2.7. Changes in *proP* mRNA and protein levels in response to RNase III deletion. (A) Semi-quantitative RT-PCR of *proP* mRNA in either wild type or RNase III null backgrounds (*rnc*). (B) ProP protein levels in wild type and *rnc* backgrounds. [41].

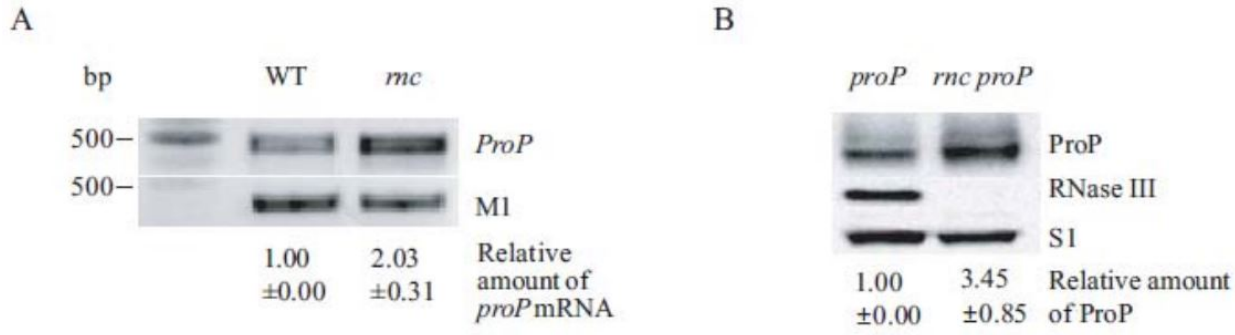

Figure 2.8. Location of the RNase III cleavage site with respect to P1 and P2. The RNase III cleavage site is in a hairpin which resides upstream of the P2 promoter. [41].

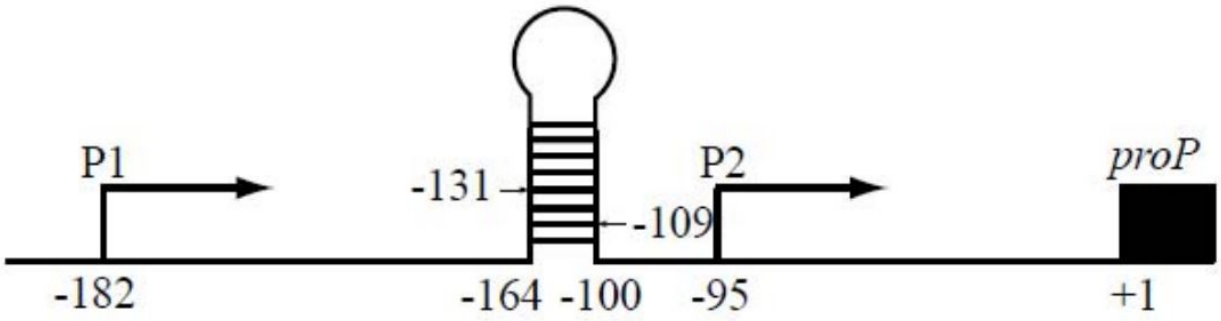

Figure 2.9. Δ*proQ* cells lack appreciable FliC protein. Western blot analysis of whole cell extracts from wild type or Δ*proQ* strains at 37°C and the indicated culture densities.

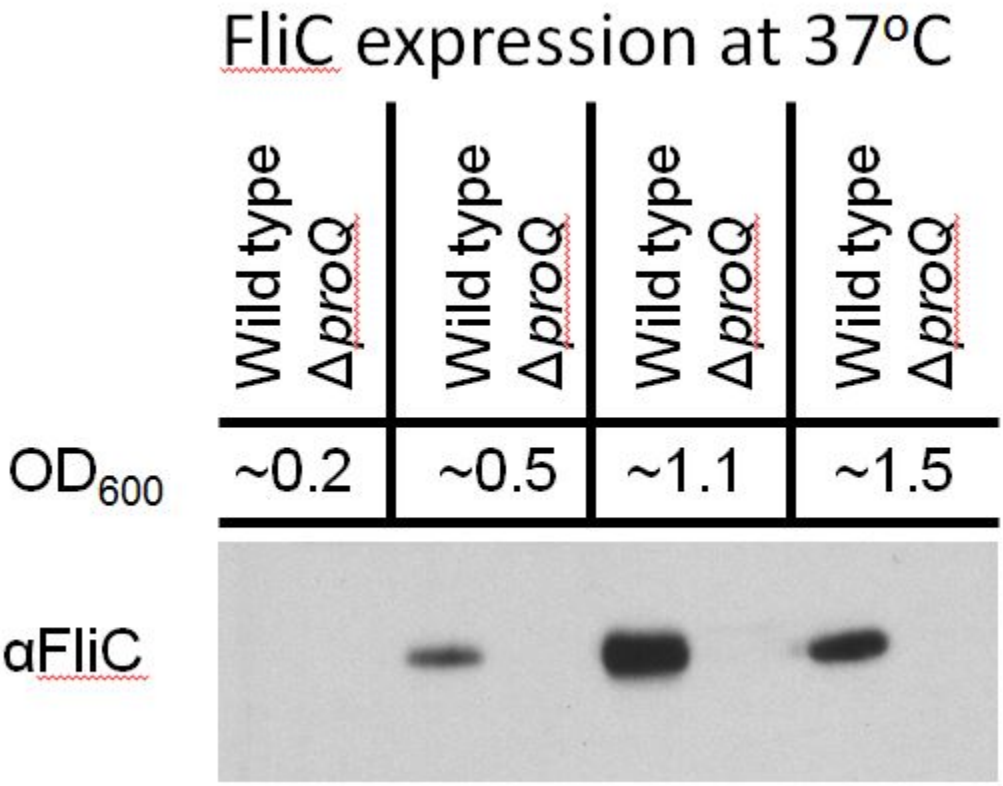

Figure 2.10. Attempted complementation of the Δ*proQ* dependent loss of FliC. Western blot analysis of FliC levels in wild type, Δ*proQ*, and pProQ complemented strains.

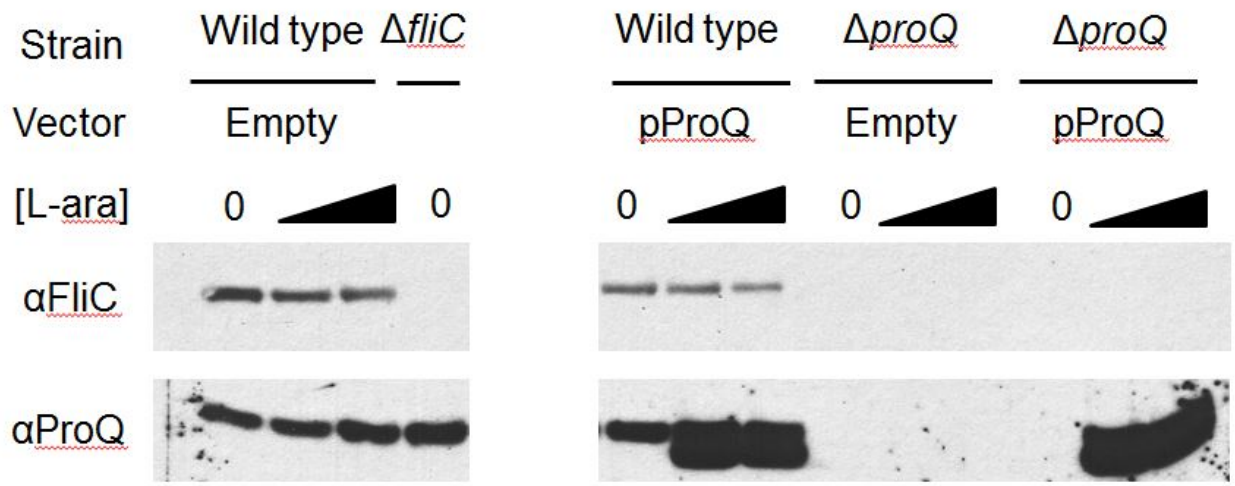

Table 2.1: Strains and Plasmids

Strain	Genotype	Origin
BW25113	Δ*(araD-araB)567*, Δ*lacZ4787*(::rrnB-3), lambda$^-$, *rph-1*, Δ*(rhaD-rhaB)568*, *hsdR514*	[19]
JM6733	BW25113, Δ*proQ*::KAN	[18], This study
JM6753	BW25113, Δ*proP*::KAN	[18], This study
JM6754	BW25113, Δ*proV*::KAN	[18], This study
JM6755	BW25113, Δ*proW*::KAN	[18], This study
JM6877	BW25113, Δ*pro*X:KAN	[18], This study
JM6881	BW25113, Δ*proVWX*::KAN	This study
JM6906	BW25113, Δ*proP*::FRT	This study
JM6926	BW25113, Δ*proP*::FRT, Δ*proVWX*::KAN	This study

Plasmid	Description	Origin
	pCA24N-ProQ	[22]
pDS1	pCA24N-*ProQΔ115N*	This study
pDS2	pCA24N-*ProQΔ181C*	This study
pDS3	pCA24N-*ProQΔ124-180*	This study
pDS4	pCA24N-*ProQ116-180*	This study
pDS5	pCA24N-*ProQ2-123*	This study
pDS6	pMCSG7-ProQ	[23], This study
pMR20	pMR20 empty vector	[26]
pMR20-ProQ	pMR20 containing *proQ* ORF plus 500 bp upstream	This study
pCP20	Flip Recombinase containing vector	[20]

Table 2.2: Oligonucleotide sequences

Name	Sequence (5' - 3')	Function
DS001	GAT CGA GCT CTC TGA CAT TTC AGC TCT GAC T	Construction of *proQΔ124-180*
DS002	GAT CGA GCT CTT CGC GTT TTT TCG CTT GCT G	Construction of *proQΔ124-180* and *proQ1-123*
DS003	GAT CGA GCT CCC CCT ATG CGG CCG CTA A	Construction of *proQΔ181C* and *proQ1-123*
DS004	GAT CGA GCT CAA CCG GGG TGT GCT GTT C	Construction of *proQΔ181C*
DS005	GAT CGA GCT CGA ACA GCA AGC GAA AAA ACG C	Construction of *proQΔ115N* and *proQ181-232*
DS006	GAT CGA GCT CCC TCA GGG CCG GAT CCG T	Construction of *proQΔ115N* and *proQ181-232*
DS007	GAT CGG TAC CCC CCT ATG CGG CCG CTA A	Construction of *proQ116-180*
DS008	GAT CGG TAC CAA CCG GGG TGT GCT GTT C	Construction of *proQ116-180*
DS037	GAT CGA GCT CGT CAT TAA CTG CCC AAT TCA GGC GTC	pBluescript-*proPp1*
DS038	GAT CGA GCT CAG AGA TTG CAT CCT GCA ATT CCC G	pBluescript-*proPp2*
DS039	GAT CGG TAC CTT ATT CAT CAA TTC GCG GAT GTT GCT GC	pBluescript-*proP* reverse
rpoS-T7-forw-SacII	CCG CGG CCG ACA ATT ACG TAT TCT GA	pBluescript-*rpoS*
rpoS-T7-rev-PstI	CTG CAG TTG AGA CTG GCC TTT CTG AC	pBluescript-*rpoS*
DS046	TAC TTC CAA TCC AAT GCC ATG GAA AAT CAA CCT AAG TTG	Construction of 6His-TEV-ProQ
DS047	TTA TCC ACT TCC AAT GTT ATC AGA ACA CCA GGT GTT CTGC	Construction of 6His-TEV-ProQ
DS048	CGC AGG ATA ATC AAC GGA TAA CG	*proQ* genotyping

DS049	ATT TGA TCA GCA CGC GTG ATA TC	*proQ* genotyping
DS054	CAG AGA TTG CAT CCT GCA ATT CCC	*proP* genotyping
DS055	CCT GAT AAG ACA GCG TCA CAT CAG	*proP* genotyping
DS056	GCT CGC ATC AAT ATT CAT GCC ACA	*proV* genotyping
DS057	GTA CTG GTC AGC CAG TCA GCA	*proV* genotyping
DS058	TAG CGA GTT GCT CTC TCA TGT CG	*proW* genotyping
DS059	AGT TTG TGT AGA GAT AAG CGT GGC	*proW* genotyping
DS060	GGC CCT GTT GGT CTG CTG AC	*proX* genotyping
DS061	GTC GCA TCA GGC ATT GTG CAC	*proX* genotyping
DS062	GGT TTC TGG CTG CCG ATG TAT	*proVWX (proU)* genotyping
DS063	CAG CCT ACA CCC TGC TGC GGG TAG TGA TAT	*proVWX (proU)* genotyping
DS076	GAT CTC ACT AGC CAT CCT GCA AAC CTT CAC G	*proP in vitro* transcription template
DS077	ATT GGG TAA TAT ATC GAC ATA GAC AAA TAA AGG AAT CTT TCT ATT GCA TGG TGT AGG CTG GAG CTG CTT CG	*proVWX* (*proU*) deletion
DS078	CAA AAA CGC CTT ATC CGC CCG AAT AAA AAT TAC TTC TGC GCT GCC AGC GCC ATA TGA ATA TCC TCC TTA G	*proVWX* (*proU*) deletion
DS083	GAT CGA GCT CGT GCG TTG TTA TAT GAG CGT C	Construction of pMR20-ProQ
DS084	GAT CGG TAC CTC AGA ACA CCA GGT GTT CTG C	Construction of pMR20-ProQ
pBSIVTforward	CGT TGT AAA ACG ACG GCC AGT G	*proP* and *rpoS in vitro* transcription template
rpoSIVTreverse	GAT CTC ATT AGG TTG CGT ATG TTG AG	*rpoS in vitro* transcription template

References

1. Wood, J.M., *Osmosensing by bacteria.* Sci STKE, 2006. **2006**(357): p. pe43.

2. MacMillan, S.V., et al., *The ion coupling and organic substrate specificities of osmoregulatory transporter ProP in Escherichia coli.* Biochim Biophys Acta, 1999. **1420**(1-2): p. 30-44.

3. Milner, J.L., S. Grothe, and J.M. Wood, *Proline porter II is activated by a hyperosmotic shift in both whole cells and membrane vesicles of Escherichia coli K12.* J Biol Chem, 1988. **263**(29): p. 14900-5.

4. Wood, J.M., *Osmosensing by bacteria: signals and membrane-based sensors.* Microbiol Mol Biol Rev, 1999. **63**(1): p. 230-62.

5. Mellies, J., A. Wise, and M. Villarejo, *Two different Escherichia coli proP promoters respond to osmotic and growth phase signals.* J Bacteriol, 1995. **177**(1): p. 144-51.

6. McLeod, S.M., et al., *The C-terminal domains of the RNA polymerase alpha subunits: contact site with Fis and localization during co-activation with CRP at the Escherichia coli proP P2 promoter.* J Mol Biol, 2002. **316**(3): p. 517-29.

7. Xu, J. and R.C. Johnson, *Activation of RpoS-dependent proP P2 transcription by the Fis protein in vitro.* J Mol Biol, 1997. **270**(3): p. 346-59.

8. Xu, J. and R.C. Johnson, *Cyclic AMP receptor protein functions as a repressor of the osmotically inducible promoter proP P1 in Escherichia coli.* J Bacteriol, 1997. **179**(7): p. 2410-7.

9. Landis, L., J. Xu, and R.C. Johnson, *The cAMP receptor protein CRP can function as an osmoregulator of transcription in Escherichia coli.* Genes & Development, 1999(13): p. 3081-3091.

10. Milner, J.L. and J.M. Wood, *Insertion proQ220::Tn5 alters regulation of proline porter II, a transporter of proline and glycine betaine in Escherichia coli.* J Bacteriol, 1989. **171**(2): p. 947-51.

11. Smith, M.N., et al., *Overexpression, purification, and characterization of ProQ, a posttranslational regulator for osmoregulatory transporter ProP of Escherichia coli.* Biochemistry, 2004. **43**(41): p. 12979-89.

12. Smith, M.N., et al., *Structural and functional analysis of ProQ: an osmoregulatory protein of Escherichia coli.* Biochemistry, 2007. **46**(11): p. 3084-95.

13. Ghetu, A.F., et al., *Crystal structure of the bacterial conjugation repressor finO.* Nat Struct Biol, 2000. **7**(7): p. 565-9.

14. Chaulk, S.G., et al., *ProQ is an RNA chaperone that controls ProP levels in Escherichia coli.* Biochemistry, 2011. **50**(15): p. 3095-106.

15. Kunte, H.J., et al., *Protein ProQ influences osmotic activation of compatible solute transporter ProP in Escherichia coli K-12.* J Bacteriol, 1999. **181**(5): p. 1537-43.

16. Jiang, M., et al., *Identification of novel Escherichia coli ribosome-associated proteins using isobaric tags and multidimensional protein identification techniques.* J Bacteriol, 2007. **189**(9): p. 3434-44.

17. Schrenk, W.J. and J.H. Miller, *Specialized transducing phages carrying fusions of the trp and lac regions of the E. coli chromosome.* Mol Gen Genet, 1974. **131**(1): p. 9-19.

18. Baba, T., et al., *Construction of Escherichia coli K-12 in-frame, single-gene knockout mutants: the Keio collection.* Mol Syst Biol, 2006. **2**: p. 2006 0008.

19. Datsenko, K.A. and B.L. Wanner, *One-step inactivation of chromosomal genes in Escherichia coli K-12 using PCR products.* Proc Natl Acad Sci U S A, 2000. **97**(12): p. 6640-5.

20. Cherepanov, P.P. and W. Wackernagel, *Gene disruption in Escherichia coli: TcR and KmR cassettes with the option of Flp-catalyzed excision of the antibiotic-resistance determinant.* Gene, 1995. **158**(1): p. 9-14.

21. Jiang, M., et al., *The Escherichia coli GTPase CgtAE is involved in late steps of large ribosome assembly.* J Bacteriol, 2006. **188**(19): p. 6757-70.

22. Kitagawa, M., et al., *Complete set of ORF clones of Escherichia coli ASKA library (a complete set of E. coli K-12 ORF archive): unique resources for biological research.* DNA Res, 2005. **12**(5): p. 291-9.

23. Eschenfeldt, W.H., et al., *A family of LIC vectors for high-throughput cloning and purification of proteins.* Methods Mol Biol, 2009. **498**: p. 105-15.

24. Brandi, A., et al., *Post-transcriptional regulation of CspA expression in Escherichia coli.* Mol Microbiol, 1996. **19**(2): p. 231-40.

25. Lakowicz, J.R., *Principles of Fluorescence Spectroscopy: CD-ROM*. 2006: Springer.

26. Roberts, R.C., et al., *Identification of a Caulobacter crescentus operon encoding hrcA, involved in negatively regulating heat-inducible transcription, and the chaperone gene grpE.* J Bacteriol, 1996. **178**(7): p. 1829-41.

27. Niba, E.T., et al., *A genome-wide approach to identify the genes involved in biofilm formation in E. coli.* DNA Res, 2007. **14**(6): p. 237-46.

28. O'Toole, G.A., et al., *Genetic approaches to study of biofilms.* Methods Enzymol, 1999. **310**: p. 91-109.

29. Lederberg, S. and V. Lederberg, *Hybridization between bacterial ribosomes.* Exp Cell Res, 1961: p. 198-200.

30. Wang, L. and S.J. Brown, *BindN: a web-based tool for efficient prediction of DNA and RNA binding sites in amino acid sequences.* Nucleic Acids Res, 2006. **34**(Web Server issue): p. W243-8.

31. McGuffin, L.J., K. Bryson, and D.T. Jones, *The PSIPRED protein structure prediction server.* Bioinformatics, 2000. **16**(4): p. 404-5.

32. Ward, J.J., et al., *The DISOPRED server for the prediction of protein disorder.* Bioinformatics, 2004. **20**(13): p. 2138-9.

33. Young, K., *The Selective Value of Bacterial Shape.* Microbiol Mol Biol Rev, 2006. **70**(3): p. 660-703.

34. Ishihama, Y., et al., *Protein abundance profiling of the Escherichia coli cytosol.* BMC Genomics, 2008. **9**: p. 102.

35. Smith-Frieday, M.N., *Characterization of ProQ: An RNA Binding Protein Modulating Expression of the Osmosensor and Osmoregulator ProP of Escherichia Coli*. 2009, The University of Guelph: Guelph. p. 273.

36. Fuentes, J.L., et al., *In vivo functional characterization of the Saccharomyces cerevisiae 60S biogenesis GTPase Nog1.* Mol Genet Genomics, 2007. **278**(1): p. 105-23.

37. Shajani, Z., M.T. Sykes, and J.R. Williamson, *Assembly of bacterial ribosomes.* Annu Rev Biochem. **80**: p. 501-26.

38. Koraimann, G., et al., *The FinOP repressor system of plasmid R1: analysis of the antisense RNA control of traJ expression and conjugative DNA transfer.* Mol Microbiol, 1996. **21**(4): p. 811-21.

39. van Biesen, T. and L.S. Frost, *The FinO protein of IncF plasmids binds FinP antisense RNA and its target, traJ mRNA, and promotes duplex formation.* Mol Microbiol, 1994. **14**(3): p. 427-36.

40. Xu, J. and R.C. Johnson, *Fis activates the RpoS-dependent stationary-phase expression of proP in Escherichia coli.* J Bacteriol, 1995. **177**(18): p. 5222-31.

41. Lim, B. and K. Lee, *Stability of the Osmoregulated Promoter-Derived proP mRNA Is Posttranscriptionally Regulated by RNase III in Escherichia coli.* J Bacteriol, 2015. **197**(7): p. 1297-305.

42. McCullen, C.A., et al., *Mechanism of positive regulation by DsrA and RprA small noncoding RNAs: pairing increases translation and protects rpoS mRNA from degradation.* J Bacteriol, 2010. **192**(21): p. 5559-71.

Chapter III
Coordinating the sensing of and response to nutrient availability in *Saccharomyces cerevisiae*

3.1. Consequences of nitrogen and glucose stresses

Essential to the survival of any organism is its ability to respond to changes in the nutrient availability presented to it by its environment. During times of nutrient excess, yeast cells rapidly grow and divide, doubling in population approximately every 90 minutes [1]. As the population grows, it eventually consumes the available nutrients, and the growth rate slows down or stops. As with everything, the process is more nuanced, and yeast can shift from fermenting glucose to oxidizing the ethanol produced during that fermentation, a phase of growth known as the diauxic shift [2]. For the sake of discussion, nutrient excess will be defined as growth in liquid culture or on solid media containing sufficient sources of available carbon (most often glucose) and nitrogen, and growth under these conditions will be referred to as “vegetative growth”. Limiting nitrogen, glucose, or both, can cause dramatic phenotypic changes. Here, I will discuss two such events and some of the processes governing them.

3.1.1. Pseudohyphal growth

During conditions where nitrogen is scarce, some strains of *Saccharomyces cerevisiae* are able to switch from vegetative growth to a growth morphology termed filamentous or pseudohyphal growth (PHG) (Figure 3.1 [3]) due to its similarities to the

hyphal growth of other fungi. During PHG, cells elongate and bud in a unipolar fashion. In addition, daughter cells remain physically attached after division. The result is a chain of cells [4], and this physical change can be seen by simple light microscopy of colonies, as the changed PHG morphology causes perturbation of the normally smooth colony edges (Figure 3.2). It is thought that this gross change in cell morphology acts as a scavenging mechanism, allowing the non-motile yeast to explore the surrounding area for nutrients [5]. It is useful to note two additional points. First, most common laboratory strains of *S. cerevisiae* do not undergo this change to PGH at least partially because of a non-functional version of the *FLO8* gene, a transcription factor essential to the process [6]. Second, surface-spread filamentation (Figure 3.2) is most readily observed under conditions of nitrogen stress in diploid cells.

3.1.2. Formation of cytoplasmic mRNP granules

A second response to nutrient stress is the formation of cytoplasmic aggregates of mRNA and proteins called messenger ribonucleoprotein (mRNP) granules. The exact dynamics and composition of these granules varies depending upon induction conditions, but this discussion will focus on what is known about mRNP granule formation in response to glucose stress [7]. These structures are generally classified into two different categories: processing bodies (P-bodies) and stress granules (For review see [8]).

In general, stress granules are comprised of mRNAs which have been stalled at the level of translation initiation and proteins important for that process, including translation initiation factors and ribosomal species. These granules are considered to be

a sort of “storage site” for components which will be translated after the glucose stress has been cleared [9]. P-bodies tend to accumulate mRNAs and protein decay machinery. This led to the belief that they are the sites of mRNA turnover, but formation of P-bodies is not necessary for mRNA turnover on a global scale [10, 11], and their exact purpose is less well understood. Whatever their ultimate purpose, both P-bodies and stress granules play an important role in cellular survival and adaptation to stress, as numerous studies implicate the proper regulation of their formation and clearance in disease (For review see [12]).

3.2. Nutrient responsive pathways in PHG and mRNP formation

Chapter IV of this document focuses on the role of one particular protein in the regulation of both PHG and mRNP formation. Ksp1p is a kinase whose signaling activity is necessary for the switch from vegetative to pseudohyphal growth and for proper mRNP granule dynamics, but before looking at Ksp1p specifically, it is important to develop the wider context of signal transduction in yeast and how PHG and mRNP granule formation are regulated by other known signaling pathways. In *Saccharomyces cerevisiae*, many pathways exist to gather information from outside of the cell and turn that information into an appropriate response. These pathways are complex and often converge and diverge along the way. For example, it is an over simplification to say that glucose levels have no effect on whether or not a cell chooses to switch from vegetative to pseudohyphal growth, and *vice versa*. What follows is a brief introduction into the signals coordinated by four different pathways, and ultimately, an overview of how these pathways affect the switch to PHG and the formation of mRNPs.

3.2.1. The cAMP/PKA pathway

In *Saccharomyces cerevisiae*, PKA, in its inactive form, exists as a heterotetrameric protein comprised of two copies of the regulatory subunit Bcy1p and two copies of a catalytic subunit, Tpk [13, 14]. There are three different Tpk subunits, not surprisingly called Tpk1p, Tpk2p, and Tpk3p [14]. These subunits are semi-redundant, but they do appear to differentially regulate pseudohyphal growth, as will be discussed later. When the membrane bound G-protein coupled receptor (GPCR), Gpr1, senses glucose, it releases the G-protein, Gpa2p [15]. Gpa2p works with the adenylate cyclase Cyr1 to stimulate the conversion of ATP into the second messenger cyclic AMP (cAMP) [16]. Once formed, cAMP can bind to Bcy1p. This binding of cAMP to the regulatory subunits of PKA causes the dissociation of the catalytic subunits. Once liberated, the catalytic subunits can influence transcription of genes involved in glucose metabolism and stress responses (Figure 3.3 [17]). In addition to Gpr1/Gpa2, Cyr1p activity is regulated by the GTPases Ras1p and Ras2p, which also interact with Cyr1p to increase cellular levels of cAMP (Figure 3.3 [4]).

How the cAMP/PKA pathway responds to nitrogen is not well understood. A study of the transcription pattern of cells starved for glucose or nitrogen yielded a correlation value just below 0.8, suggesting overlap between glucose and nitrogen responsive pathways. More interestingly, the same study demonstrated that after adding back the depleted nutrient, recovery was cAMP dependent, and both nitrogen and glucose addition inhibited stress responsive genes (Figure 3.3 [18]).

3.2.1.1. The cAMP/PKA pathway in pseudohyphal growth

The regulation of pseudohyphal growth by PKA is dependent upon the accumulation of cAMP. Overexpression of the phosphodiesterase Pde2p, which converts cAMP into AMP causes the loss of PHG [4, 19]. As mentioned, binding of cAMP to Bcy1p causes the release of the Tpk subunits of PKA. Depending upon the Tpk subunit which is activated, PHG is differentially affected. Tpk2p has the most straightforward effect on PHG. To stimulate filament formation, Tpk2p phosphorylates the transcription factor Flo8p which, in turn, enhances transcription of the major flocculence gene, *FLO11* [20]. Deletion of Tpk3 causes cells to be hyperfilamentous, suggesting that Tpk3p is a negative regulator of PHG. Tpk1p acts more indirectly to regulate the kinase Yak1p via phosphorylation. Phosphorylation of Yak1p inactivates it. Yak1p transduces its signal through two transcription factors, Sok2p and Phd1p, which also regulate *FLO11* transcription (Figure 3.3 [20-22]).

3.2.1.2. The cAMP/PKA pathway in mRNP regulation

Several studies have been conducted looking at the localization of the Tpk subunits of PKA during conditions which induce mRNP formation and the role of PKA signaling on mRNP formation. What has been found is that both Tpk2p and Tpk3p can localize to P-bodies (Figure 3.3 [23]), constitutive activation of the PKA pathway in a specific *ras2p* mutant background blocks P-body formation, and overexpression of any of the catalytic subunits of PKA also inhibits P-body formation, likely by phosphorylating the P-body associated protein Pat1 [24]. PKA appears to play less of a role in the

regulation of stress granule formation, but in light of our study presented in Chapter IV, this may be dependent upon induction conditions.

3.2.2. The MAPK pathways

Saccharomyces cerevisiae have five well characterized mitogen-activated protein kinase (MAPK) pathways. In general, a signal is received by a receptor protein at the cell surface, and a signal is transduced via a triplet of kinases, a MAPKKK (or MAP3K), a MAPKK (MAP2K), and finally the MAPK [25]. The MAPK in turn regulates transcription factors via phosphorylation to generate a cellular response appropriate to the signal. The pathways regulated and their respective MAPKs are as follows: sporulation via Smk1p [26], cell wall integrity via Slt2p [27], osmotic balance via Hog1p [28], mating and pheromone response via Fus3p [29], and filamentation via Kss1p [30].

At first glance, MAPK pathways appear fairly linear (Figure 3.4 [31]). Upon closer examination it can be seen that many components are shared among the pathways, especially among the mating, filamentation, and osmo-responsive pathways. Upstream of the MAPKKK, Ste20p is involved in regulation of all three pathways. The MAPKKK Ste11p is also shared among these MAPK cascades (Figure 3.4). It seems likely that a particular stimulus may have unintended consequences, by increasing signaling through overlapping pathways, but inter-pathway inhibition by specific proteins helps to prevent this. That said, these interdependencies serve to add complexity to the MAPK pathways ([32] and for review see [33]).

3.2.2.1 The MAPK pathway in pseudohyphal growth

As mentioned above, pseudohyphal growth is stimulated by nutrient limiting conditions, allowing cells to forage for nutrients in the surrounding areas. Low nitrogen conditions have been traditionally used to examine PHG, but glucose limitation can also stimulate PHG [34]. The MAPK pathway is capable of responding to both nitrogen and glucose levels. At the membrane, nutrient limitation is sensed by three proteins: Msb2p, Sho1p, and Opy2p. Once sensed, the GEF Cdc24p and GTPase Cdc42p activate Ste20p. Phosphorylation of the MAPKKK Ste11p by Ste20p eventually leads to activation of the transcription factors Ste12p and Tec1p by the MAPK Kss1p. Once activated Ste12p and Tec1p bind upstream of the *FLO11* promoter and stimulate transcription [35] (Figure 3.4).

3.2.2.2. The MAPK pathway in mRNP regulation

The role of the MAPK pathways in mRNP formation is not well characterized, but there are a few proteins involved in MAPK signaling which do play a regulatory role in granule formation or dynamics. Ste20p is one such protein. It has been shown that Ste20p phosphorylates the P-body protein Dcp2p, and this phosphorylation event is important for Dcp2p localization to P-bodies. Also, failure of Dcp2p to localize to P-bodies results in aberrant stress granule formation [36]. Also, in a screen for mRNA binding proteins whose localization becomes punctate in low glucose stress, Ste20p was occasionally, though not consistently found to form puncta (Figure 3.4 [37]). This is consistent with our results, presented in Chapter IV.

3.2.3. The SNF1 pathway

SNF1 is a heterotrimeric complex comprised of the catalytic alpha subunit Snf1p, the gamma subunit Snf4, which serves a regulatory function, and one of three beta subunits: Sip1p, Sip2p, or Gal83p [38]. The name SNF1 stands for *Sucrose NonFermenting* as *SNF* genes were originally identified in mutants unable to grow on sucrose as a carbon source [39]. When glucose is limiting, SNF1 is phosphorylated on the Snf1p subunit by one of three upstream kinases: Sak1p, Elm1p, or Tos3p [40-42]. Upon activation, the cellular localization of the Snf1p complex shifts from cytoplasmic to nuclear, and the complex can act to activate glucose-repressed genes (Figure 3.7 [43]).

Inactivation of SNF1 occurs when glucose is present. To achieve inactivation, the phosphatase, PP1, dephosphorylates threonine 210 which is phosphorylated by the upstream activating kinases. PP1 is comprised of two proteins Reg1p and Glc7p. It is the Glc7p subunit of PP1 which is responsible for the dephosphorylation and inactivation of SNF1 [44, 45].

3.2.3.1. The SNF1 pathway in pseudohyphal growth

The regulation of PHG by *SNF1* is complicated by the fact that the conditions needed to induce *SNF1*-dependent PHG seem to differ between haploids and diploids. Haploid strains are not able to undergo surface spread filamentation, but they are able to invade agar. When glucose is depleted in haploid cells, Snf1p represses two *FLO11* transcriptional repressors Nrg1p and Nrg2p. Haploid cells expressing Flo11p are able to invade the solid agar surface (Figure 3.6) [46, 47]. *SNF1* diploid mutants grown on low nitrogen media were also deficient for PHG, and deletion of *nrg1* and *nrg2* suppress the defect, again placing them in the same pathway, but this time responding to nitrogen

stress (Figure 3.5 [47]). Upstream of *SNF1*, the kinase Elm1p also acts as a regulator of PHG. Deletion of Elm1p causes strains to become hyperfilamentous, so Elm1p acts as a negative regulator of PHG through a *SNF1*-independent pathway [48].

3.2.3.2. The SNF1 pathway in mRNP regulation

Formation of mRNPs is a response to glucose limitation, so it seems obvious that the glucose sensing SNF1 pathway would be involved. However, it has been shown that defects in the Snf1p kinase do not alter P-body formation [24]. There is evidence to suggest that Snf1p might be involved in localizing some proteins to stress granules, however. Snf1p has been shown to directly phosphorylate the kinase Psk1p both *in vitro* and *in vivo*. This activates Psk1p to phosphorylate the known stress granule associated protein Pbp1p. Pbp1p has been shown to recruit the growth regulating TOR complex (discussed in more detail below) to stress granules [49]. Circumstantial evidence suggests that phosphorylation of Pbp1p by Psk1p may activate Pbp1p to accomplish this sequestration when nutrients are limited (Figure 3.5 [50]).

3.2.4. The TOR pathway

The Target of Rapamycin (TOR) pathway is named for its central kinase, the TOR kinase. TOR kinase is part of a multisubunit complex. In yeast there are two different TOR kinases, TOR1 and TOR2, which means that two distinct complexes exist, namely TORC1 and TORC2, but TORC1 may contain either TOR1 or TOR2. The differentiation comes from the other proteins in the complex (For review see [51]). Unless otherwise noted, this discussion will focus on TORC1. At its heart, the TOR

complex senses the nutrient availability and stimulates growth when nutrients are not limiting. When stresses are present, the complex is inactivated, arresting growth until the stress has passed [51].

Processes regulated by TORC1 are generally involved in proliferation and utilization of nutrients. TORC1 stimulates general translation [52], as well as expression of ribosomal biogenesis genes [53] and ribosomal proteins [54]. It also promotes the transcription of genes involved in nitrogen utilization, such as permeases to facilitate import of nitrogen sources [55] (Figure 3.6 [56]). It is this response to nutrient levels, specifically to nitrogen availability that well positions TORC1 to regulate PHG.

3.2.4.1. The TOR pathway in pseudohyphal growth

A large source of nitrogen available for cells comes from amino acids, specifically glutamine. When this preferred source of nitrogen is present, TOR inhibits the genes involved in utilization of suboptimal sources of nitrogen [57]. This inhibition is achieved by phosphorylation of the transcription factor Gln3p. Phosphorylated Gln3p is bound by the cytoplasmic protein Ure2p and sequestered from the nucleus. Nitrogen limitation results in the dephosphorylation of Gln3p by the TOR-dependent phosphatase Sit4p [57]. This allows Gln3p to localize to the nucleus and regulate transcription of nitrogen repressed genes. One such gene is Mep2p, an ammonium permease which is necessary for proper PHG [58]. TOR also stimulates the translation of Gcn4p under nitrogen stress [59]. In turn, Gcn4p binds in the promoter for *FLO11* and activates transcription [60] (Figure 3.6). Yet more evidence of TOR signaling in pseudohyphal

growth is that chemical inhibition of the TOR complex inhibits PHG during nitrogen stress, but overexpression of the downstream target Tap42p restored PHG [61].

3.2.4.2. The TOR pathway in mRNP regulation

As mentioned in section 3.2.3.2. TORC1 has been found to be associated with stress granules, and this sequestration to granules is mediated by Pbp1p (Figure 3.5) [50]. Heat stress can also cause TORC1 to localize to stress granules [49]. Also, stress granule formation is induced upon inhibition of translation, and TORC1 is known to positively regulate translation by phosphorylating and inhibiting proteins which bind to initiation factor eIF4E [62]. Therefore, inactivation of TORC1 leads to inhibition of translation initiation, which leads to the formation of stress granules.

3.3. Summary

This chapter has introduced some of the many ways in which cells sense nutrient levels, transduce signals, and elicit an appropriate response. There are processes which have been omitted for the sake of concision but which certainly merit discussion. Decades of study have been undertaken to flesh out these pathways, and there is still work to be done. Noticeably missing from this discussion is the crosstalk among all of these pathways. All four pathways discussed above converge on the *FLO11* promoter (Figure 3.8) [63]. Cells integrate signals regarding carbon and nitrogen availability, as well as physical stresses such as osmotic shock and heat stress, and each pathway weighs in on how to react. The net result is a response fine-tuned by eons of evolution. The complexity of these pathways makes controlling for unexpected consequences very

difficult, and any firm claims require copious verification via other experiments. Chapter IV highlights the signaling network of the Ksp1p kinase, and attempts to place it within the context of the signaling pathway milieu by using both a high-throughput proteomic approach and more targeted experimentation on putative targets of regulation.

Figure 3.1. Haploid and diploid *Saccharomyces cerevisiae* growth forms. Yeast can exists as a stable haploid or diploid. During haploid growth, mother cells grow, bud, and divide, yielding two separate and identical cells. If complementary mating types "fuse", a diploid is formed. Under normal growing conditions, diploid yeast grow, bud, and divide in a manner analogous to haploid yeast. However, if nitrogen stress is encountered, yeast can switch to filamentous growth. During filamentous growth, cells elongate, bud in a unipolar fashion, and remain physically attached at the cell wall. Adapted from [3].

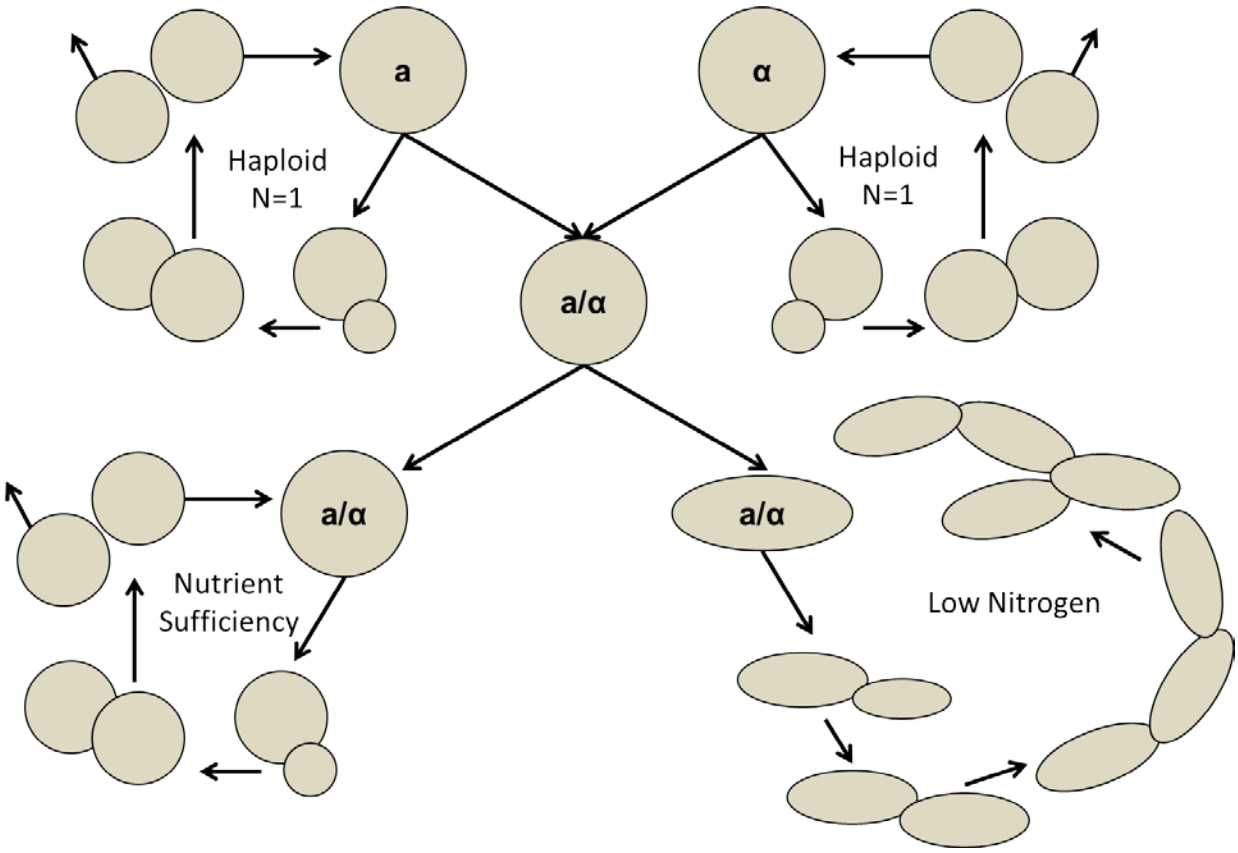

Figure 3.2. Pseudohyphal growth causes changes in colony morphology. Wild type s1278b strain grown under normal conditions (left) or in nitrogen limiting conditions (right).

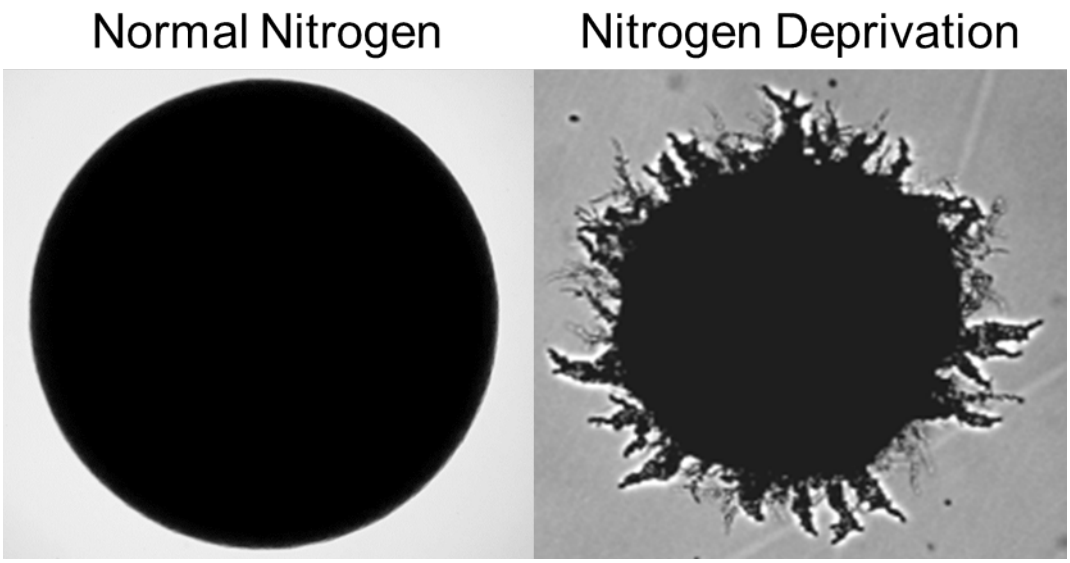

Figure 3.3. The cAMP/PKA/Ras pathway in filamentous growth and mRNP regulation. The membrane bound GPCR Gpr1 responds to glucose in the extracellular environment. The presence of glucose causes the release of the G-protein Gpa2 and activation of Ras. Both Gpa2 and Ras enhance the activity of the adenylate cyclase, Cyr1, which turns ATP in to cAMP. cAMP binds to the regulatory subunit of PKA, Bcy1, and the catalytic subunits, Tpk1/2/3 are activated. Tpk subunits differentially affect transcription of the major flocculence gene, *FLO11*. Tpk1 and Tpk2 are positive regulators of *FLO11*, while deletion of Tpk3 leads to hyperfilamentation. Tpk2 directs Flo8 to the *FLO11* promoter between ˉ1.4 Kb-ˉ1.0 Kb. The Phd1 binding site is not reported. Additionally, Tpk2 and Tpk3 localize to P-bodies during stationary phase. Tpk3 also localizes to P-bodies during glucose and osmotic stress. Deletion of Tpk3 causes an increase in the percentage of cells containing P-bodies during glucose stress. Compiled from [4, 17, 18, 20-23].

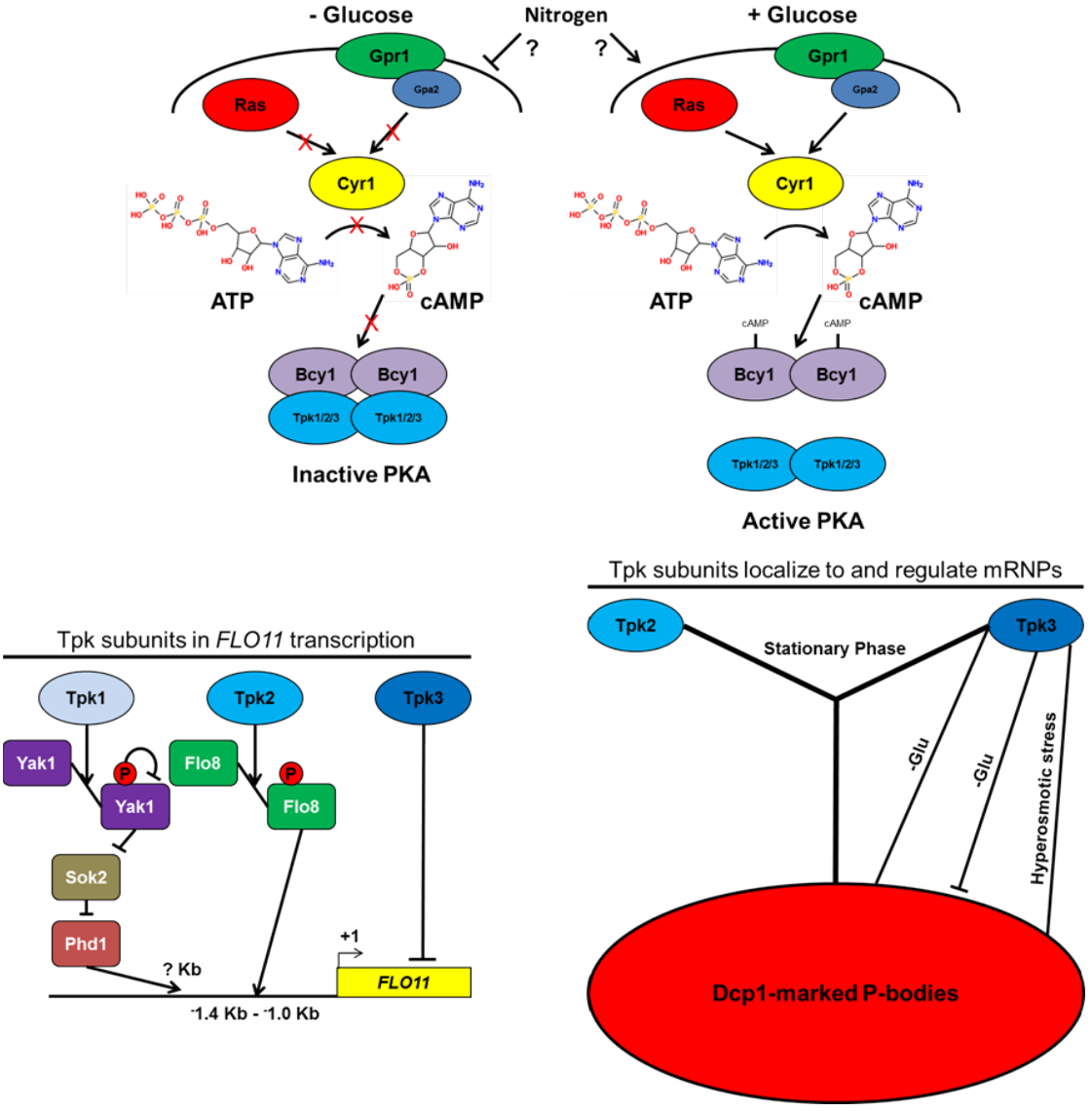

Figure 3.4. Five MAPK pathways and MAPK signaling in filamentous growth and mRNP regulation. MAPK signaling is involved in filamentous growth, mating, osmotic balance, cell wall integrity, and sporulation. These seemingly linear pathways also share many components, especially the filamentous growth, mating, and osmotic balance pathways (red dashed box). The MAPK Kss1 signals through the transcription factors Ste12 and Tec1 to affect transcription of *FLO11*. Also, the protein kinase Ste20, which functions upstream of many MAPK pathways, regulates the formation of stress granules by phosphorylating the P-body protein Dcp2. It also localizes, though inconsistently (dashed line), to stress granules during glucose stress. Compiled and adapted from [26-31, 34-37].

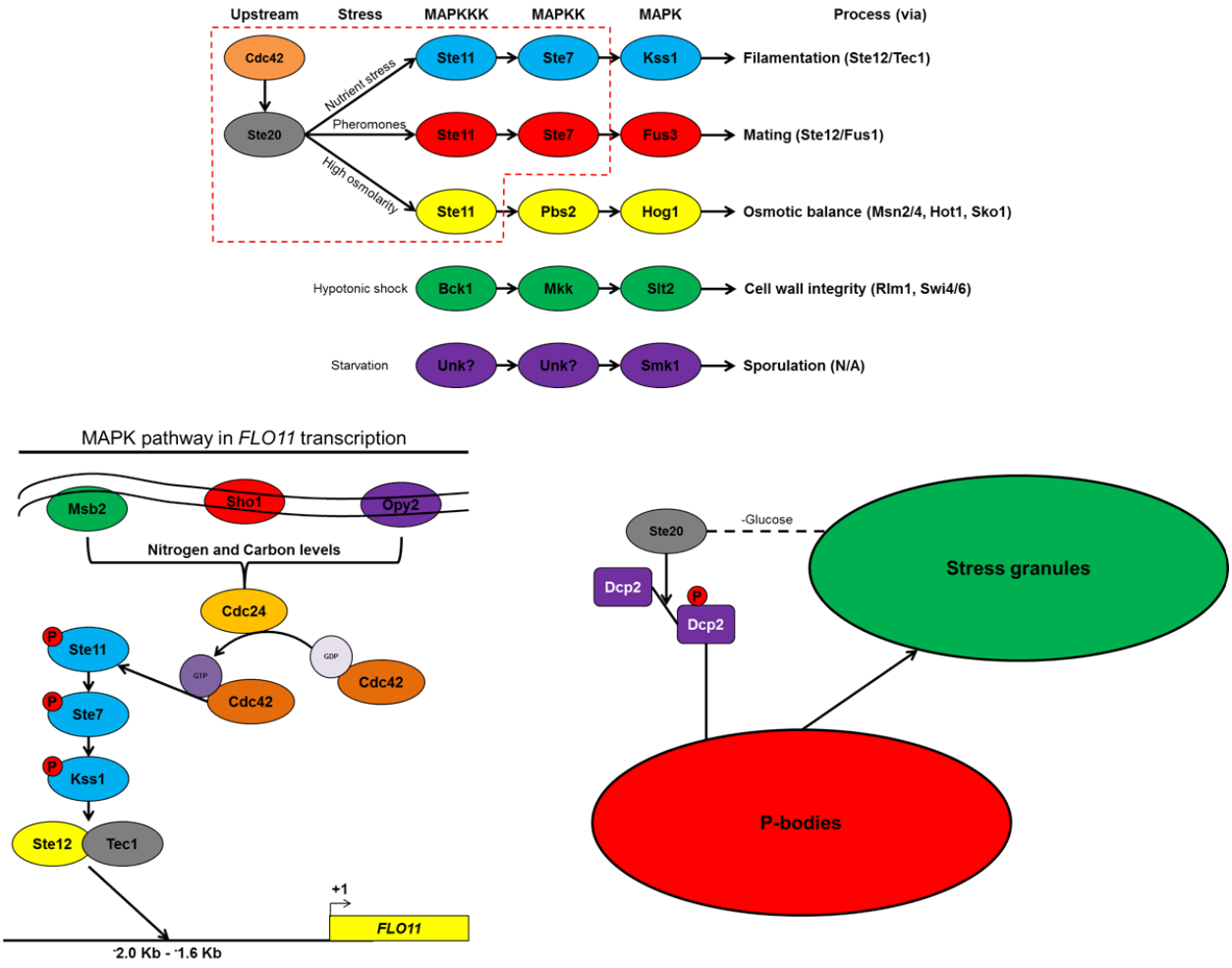

Figure 3.5. The SNF1 pathway in filamentous growth and mRNP regulation. The *SNF1* complex functions to suppress glucose related genes when cells are grown on alternate carbon sources. Phosphorylation of the complex is performed by one of three upstream complexes, and dephosphorylation is performed by PP1. *SNF1* also regulates *FLO11* transcription by repressing the *FLO11* transcriptional repressor Nrg1/2. Nrg1/2 competes with Flo8 for binding to the *FLO11* promoter. *SNF1* dependent phosphorylation events may also help to sequester TORC1 to stress granules when nutrients are limited. Compiled and adapted from [24, 40-50, 64, 65].

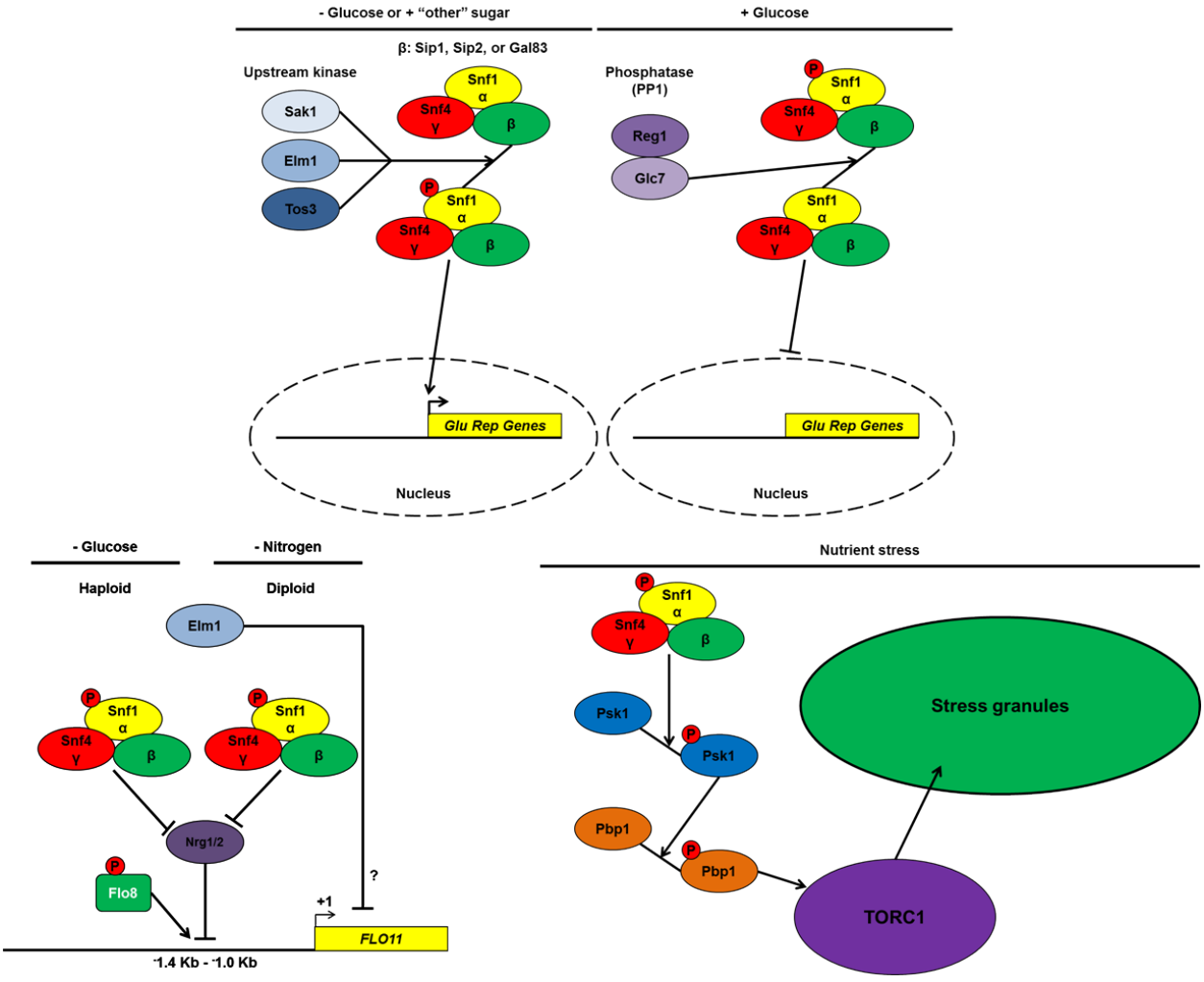

Figure 3.6. Invasion of a solid surface by haploid filamentous strains. Haploid filamentous strains were struck to rich media and allowed to grow for 3-5 days (Left; pre-wash). After incubation, plates were washed with deionized water and gently rubbed with a finger to remove surface cells. The degree of agar invasion is qualitatively measured by examining the density of the remaining cells below the surface (Right; post-wash).

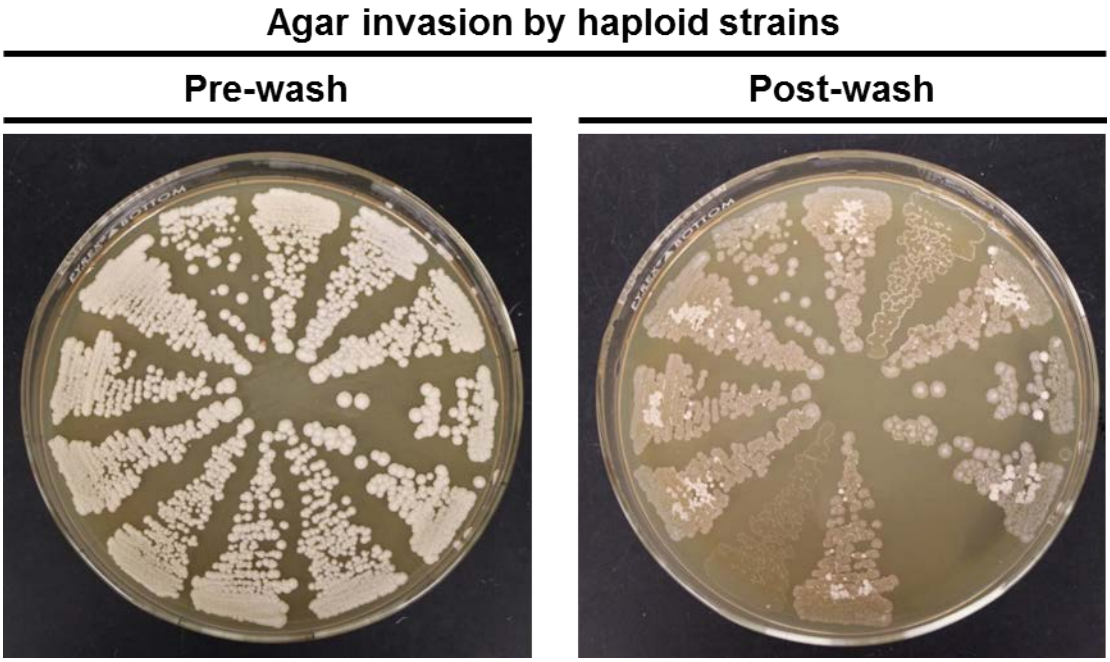

Figure 3.7. The TOR pathway in filamentous growth and mRNP regulation. The TOR pathway responds to the extracellular nutrient availability, especially the availability of nitrogen. When conditions are favorable, TOR directs pathways which are involved in growth of the cells and inhibits stress responses. The TOR pathway also affects transcription of several genes involved in PHG, including *FLO11*. Compiled and adapted from [51-60, 66].

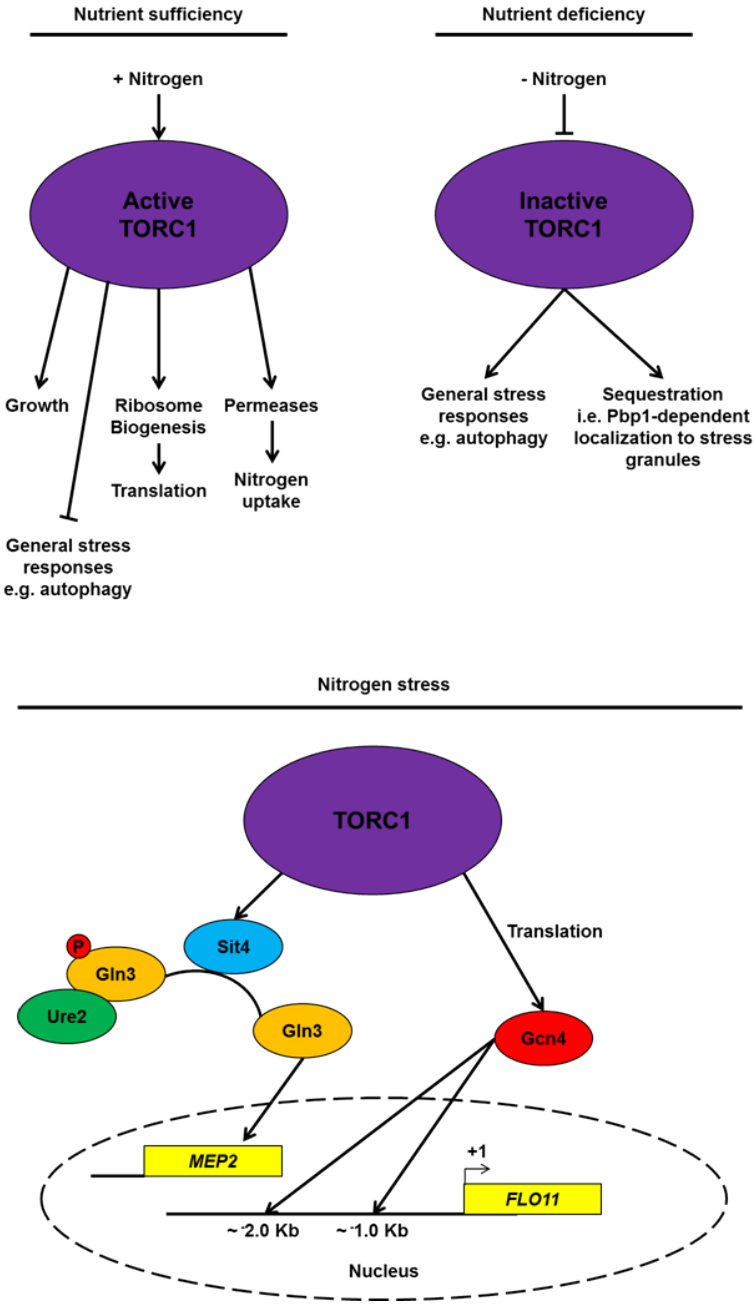

Figure 3.8. Summary of *FLO11* transcriptional regulation by four different signaling pathways. The transcription of *FLO11* is influenced by all four pathways discussed (L to R: MAPK, PKA, SNF1, and TOR). Additionally, much of the regulation by these pathways is concentrated within the -2000 to -1000 range with respect to the transcriptional start site. The Phd1 binding site is not reported.

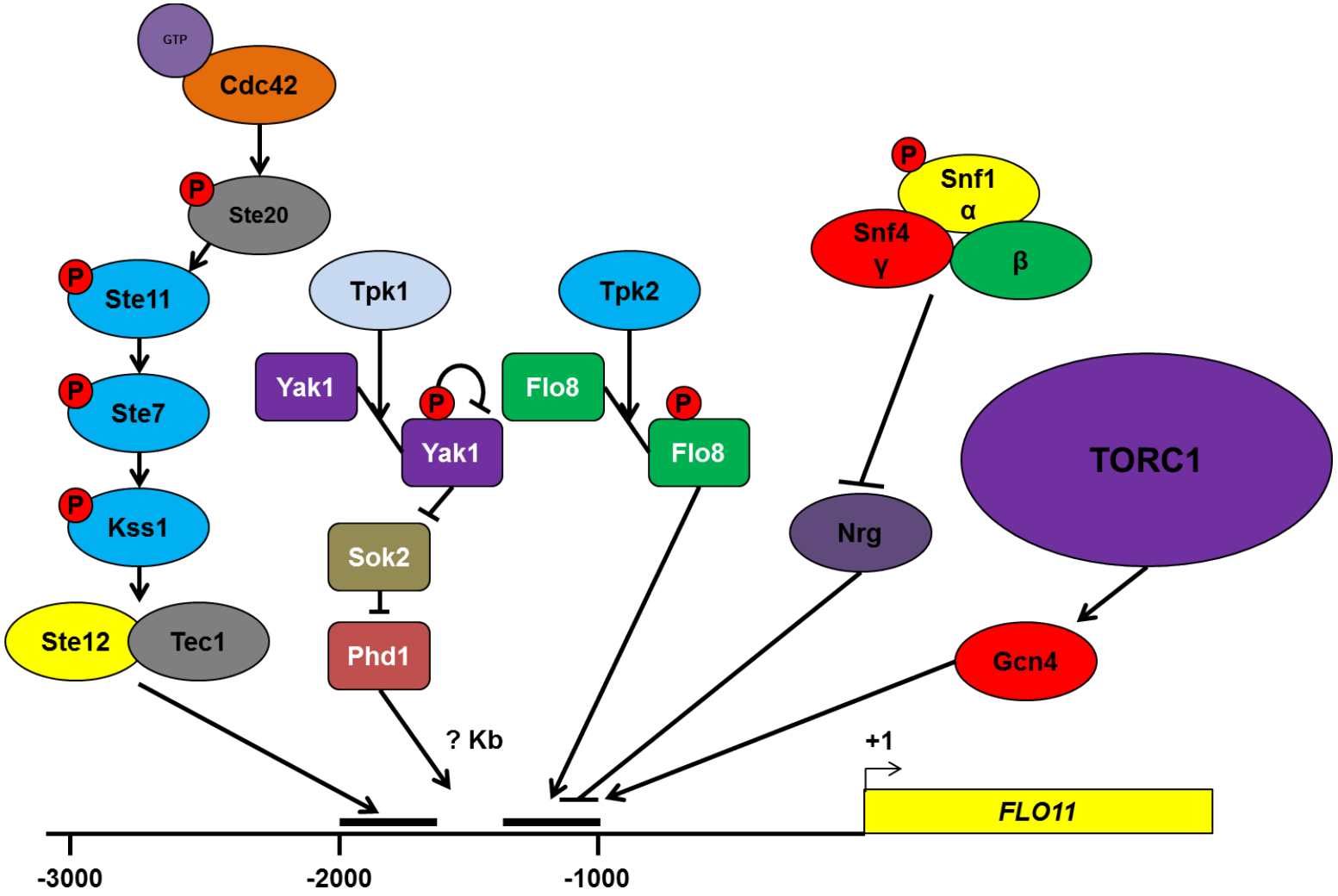

References

1. Herskowitz, I., *Life cycle of the budding yeast Saccharomyces cerevisiae.* Microbiol Rev, 1988. **52**(4): p. 536-53.

2. Dickinson, J.R., Schweizer, M., ed. *The Metabolism and Molecular Physiology of Saccharomyces cerevisiae*. 2nd ed. 2004, CRC Press: Philadelphia.

3. Lengeler, K.B., et al., *Signal transduction cascades regulating fungal development and virulence.* Microbiol Mol Biol Rev, 2000. **64**(4): p. 746-85.

4. Gimeno, C.J., et al., *Unipolar cell divisions in the yeast S. cerevisiae lead to filamentous growth: regulation by starvation and RAS.* Cell, 1992. **68**(6): p. 1077-90.

5. Lee, B.N. and E.A. Elion, *The MAPKKK Ste11 regulates vegetative growth through a kinase cascade of shared signaling components.* Proc Natl Acad Sci U S A, 1999. **96**(22): p. 12679-84.

6. Pan, X. and J. Heitman, *Cyclic AMP-dependent protein kinase regulates pseudohyphal differentiation in Saccharomyces cerevisiae.* Mol Cell Biol, 1999. **19**(7): p. 4874-87.

7. Buchan, J.R., J.H. Yoon, and R. Parker, *Stress-specific composition, assembly and kinetics of stress granules in Saccharomyces cerevisiae.* J Cell Sci, 2011. **124**(Pt 2): p. 228-39.

8. Erickson, S.L. and J. Lykke-Andersen, *Cytoplasmic mRNP granules at a glance.* J Cell Sci, 2011. **124**(Pt 3): p. 293-7.

9. Buchan, J.R. and R. Parker, *Eukaryotic stress granules: the ins and outs of translation.* Mol Cell, 2009. **36**(6): p. 932-41.

10. Eulalio, A., et al., *P-body formation is a consequence, not the cause, of RNA-mediated gene silencing.* Mol Cell Biol, 2007. **27**(11): p. 3970-81.

11. Stalder, L. and O. Muhlemann, *Processing bodies are not required for mammalian nonsense-mediated mRNA decay.* Rna, 2009. **15**(7): p. 1265-73.

12. Anderson, P. and N. Kedersha, *Stress granules: the Tao of RNA triage.* Trends Biochem Sci, 2008. **33**(3): p. 141-50.

13. Toda, T., et al., *Cloning and characterization of BCY1, a locus encoding a regulatory subunit of the cyclic AMP-dependent protein kinase in Saccharomyces cerevisiae.* Mol Cell Biol, 1987. **7**(4): p. 1371-7.

14. Toda, T., et al., *Three different genes in S. cerevisiae encode the catalytic subunits of the cAMP-dependent protein kinase.* Cell, 1987. **50**(2): p. 277-87.

15. Xue, Y., M. Batlle, and J.P. Hirsch, *GPR1 encodes a putative G protein-coupled receptor that associates with the Gpa2p Galpha subunit and functions in a Ras-independent pathway.* Embo J, 1998. **17**(7): p. 1996-2007.

16. Nakafuku, M., et al., *Isolation of a second yeast Saccharomyces cerevisiae gene (GPA2) coding for guanine nucleotide-binding regulatory protein: studies on its structure and possible functions.* Proc Natl Acad Sci U S A, 1988. **85**(5): p. 1374-8.

17. Zaman, S., et al., *How Saccharomyces responds to nutrients.* Annu Rev Genet, 2008. **42**: p. 27-81.

18. Conway, M.K., D. Grunwald, and W. Heideman, *Glucose, nitrogen, and phosphate repletion in Saccharomyces cerevisiae: common transcriptional responses to different nutrient signals.* G3 (Bethesda), 2012. **2**(9): p. 1003-17.

19. Ward, M.P., et al., *SOK2 may regulate cyclic AMP-dependent protein kinase-stimulated growth and pseudohyphal development by repressing transcription.* Mol Cell Biol, 1995. **15**(12): p. 6854-63.

20. Cullen, P.J. and G.F. Sprague, Jr., *The regulation of filamentous growth in yeast.* Genetics, 2012. **190**(1): p. 23-49.

21. Zhang, Z., M.M. Smith, and J.S. Mymryk, *Interaction of the E1A oncoprotein with Yak1p, a novel regulator of yeast pseudohyphal differentiation, and related mammalian kinases.* Mol Biol Cell, 2001. **12**(3): p. 699-710.

22. Malcher, M., S. Schladebeck, and H.U. Mosch, *The Yak1 protein kinase lies at the center of a regulatory cascade affecting adhesive growth and stress resistance in Saccharomyces cerevisiae.* Genetics, 2011. **187**(3): p. 717-30.

23. Tudisca, V., et al., *Differential localization to cytoplasm, nucleus or P-bodies of yeast PKA subunits under different growth conditions.* Eur J Cell Biol, 2010. **89**(4): p. 339-48.

24. Shah, K.H., et al., *Processing body and stress granule assembly occur by independent and differentially regulated pathways in Saccharomyces cerevisiae.* Genetics, 2013. **193**(1): p. 109-23.

25. Widmann, C., et al., *Mitogen-activated protein kinase: conservation of a three-kinase module from yeast to human.* Physiol Rev, 1999. **79**(1): p. 143-80.

26. Pierce, M., et al., *Transcriptional regulation of the SMK1 mitogen-activated protein kinase gene during meiotic development in Saccharomyces cerevisiae.* Mol Cell Biol, 1998. **18**(10): p. 5970-80.

27. Verna, J., et al., *A family of genes required for maintenance of cell wall integrity and for the stress response in Saccharomyces cerevisiae.* Proc Natl Acad Sci U S A, 1997. **94**(25): p. 13804-9.

28. Tatebayashi, K., M. Takekawa, and H. Saito, *A docking site determining specificity of Pbs2 MAPKK for Ssk2/Ssk22 MAPKKKs in the yeast HOG pathway.* Embo J, 2003. **22**(14): p. 3624-34.

29. van Drogen, F., et al., *MAP kinase dynamics in response to pheromones in budding yeast.* Nat Cell Biol, 2001. **3**(12): p. 1051-9.

30. Palecek, S.P., A.S. Parikh, and S.J. Kron, *Sensing, signalling and integrating physical processes during Saccharomyces cerevisiae invasive and filamentous growth.* Microbiology, 2002. **148**(Pt 4): p. 893-907.

31. Qiagen. *MAPK Pathways in Budding Yeast*. [cited 2015 April 4]; MAPK Pathways in Budding Yeast]. Available from: https://www.qiagen.com/us/products/genes%20and%20pathways/pathway%20details.aspx?pwid=281.

32. Saito, H., *Regulation of cross-talk in yeast MAPK signaling pathways.* Curr Opin Microbiol, 2010. **13**(6): p. 677-83.

33. Schwartz, M.A. and H.D. Madhani, *Principles of MAP kinase signaling specificity in Saccharomyces cerevisiae.* Annu Rev Genet, 2004. **38**: p. 725-48.

34. Karunanithi, S. and P.J. Cullen, *The filamentous growth MAPK Pathway Responds to Glucose Starvation Through the Mig1/2 transcriptional repressors in Saccharomyces cerevisiae.* Genetics, 2012. **192**(3): p. 869-87.

35. Rupp, S., et al., *MAP kinase and cAMP filamentation signaling pathways converge on the unusually large promoter of the yeast FLO11 gene.* Embo J, 1999. **18**(5): p. 1257-69.

36. Yoon, J.H., E.J. Choi, and R. Parker, *Dcp2 phosphorylation by Ste20 modulates stress granule assembly and mRNA decay in Saccharomyces cerevisiae.* J Cell Biol, 2010. **189**(5): p. 813-27.

37. Mitchell, S.F., et al., *Global analysis of yeast mRNPs.* Nat Struct Mol Biol, 2013. **20**(1): p. 127-33.

38. Zhang, J., L. Olsson, and J. Nielsen, *The beta-subunits of the Snf1 kinase in Saccharomyces cerevisiae, Gal83 and Sip2, but not Sip1, are redundant in glucose derepression and regulation of sterol biosynthesis.* Mol Microbiol, 2010. **77**(2): p. 371-83.

39. Carlson, M., B.C. Osmond, and D. Botstein, *Mutants of yeast defective in sucrose utilization.* Genetics, 1981. **98**(1): p. 25-40.

40. Hong, S.P., et al., *Activation of yeast Snf1 and mammalian AMP-activated protein kinase by upstream kinases.* Proc Natl Acad Sci U S A, 2003. **100**(15): p. 8839-43.

41. Nath, N., R.R. McCartney, and M.C. Schmidt, *Yeast Pak1 kinase associates with and activates Snf1.* Mol Cell Biol, 2003. **23**(11): p. 3909-17.

42. Sutherland, C.M., et al., *Elm1p is one of three upstream kinases for the Saccharomyces cerevisiae SNF1 complex.* Curr Biol, 2003. **13**(15): p. 1299-305.

43. Hedbacker, K. and M. Carlson, *SNF1/AMPK pathways in yeast.* Front Biosci, 2008. **13**: p. 2408-20.

44. Tu, J. and M. Carlson, *REG1 binds to protein phosphatase type 1 and regulates glucose repression in Saccharomyces cerevisiae.* Embo J, 1995. **14**(23): p. 5939-46.

45. Sanz, P., et al., *Regulatory interactions between the Reg1-Glc7 protein phosphatase and the Snf1 protein kinase.* Mol Cell Biol, 2000. **20**(4): p. 1321-8.

46. Cullen, P.J. and G.F. Sprague, Jr., *Glucose depletion causes haploid invasive growth in yeast.* Proc Natl Acad Sci U S A, 2000. **97**(25): p. 13619-24.

47. Kuchin, S., V.K. Vyas, and M. Carlson, *Snf1 protein kinase and the repressors Nrg1 and Nrg2 regulate FLO11, haploid invasive growth, and diploid pseudohyphal differentiation.* Mol Cell Biol, 2002. **22**(12): p. 3994-4000.

48. Edgington, N.P., et al., *Control of Saccharomyces cerevisiae filamentous growth by cyclin-dependent kinase Cdc28.* Mol Cell Biol, 1999. **19**(2): p. 1369-80.

49. Takahara, T. and T. Maeda, *Transient sequestration of TORC1 into stress granules during heat stress.* Mol Cell, 2012. **47**(2): p. 242-52.

50. DeMille, D., Badal, B.D., Evans, J.B., Mathis, A.D., Anderson, J.F., Grose, J.H., *PAS kinase is activated by direct Snf1-dependent phophorylation and mediates inhibition of TORC1 through phophorylation and activation of Pbp1.* Mol. Biol. Cell, 2015.

51. Loewith, R. and M.N. Hall, *Target of rapamycin (TOR) in nutrient signaling and growth control.* Genetics, 2011. **189**(4): p. 1177-201.

52. Barbet, N.C., et al., *TOR controls translation initiation and early G1 progression in yeast.* Mol Biol Cell, 1996. **7**(1): p. 25-42.

53. Zaragoza, D., et al., *Rapamycin induces the G0 program of transcriptional repression in yeast by interfering with the TOR signaling pathway.* Mol Cell Biol, 1998. **18**(8): p. 4463-70.

54. Lempiainen, H. and D. Shore, *Growth control and ribosome biogenesis.* Curr Opin Cell Biol, 2009. **21**(6): p. 855-63.

55. Cardenas, M.E., et al., *The TOR signaling cascade regulates gene expression in response to nutrients.* Genes Dev, 1999. **13**(24): p. 3271-9.

56. Qiagen. *TOR Complexes in yeast*. 2015 [cited 2015 April 7]; TOR complexes in yeast]. Available from: https://www.qiagen.com/us/products/genes%20and%20pathways/pathway%20details.aspx?pwid=447.

57. Hardwick, J.S., et al., *Rapamycin-modulated transcription defines the subset of nutrient-sensitive signaling pathways directly controlled by the Tor proteins.* Proc Natl Acad Sci U S A, 1999. **96**(26): p. 14866-70.

58. Lorenz, M.C. and J. Heitman, *The MEP2 ammonium permease regulates pseudohyphal differentiation in Saccharomyces cerevisiae.* Embo J, 1998. **17**(5): p. 1236-47.

59. Valenzuela, L., C. Aranda, and A. Gonzalez, *TOR modulates GCN4-dependent expression of genes turned on by nitrogen limitation.* J Bacteriol, 2001. **183**(7): p. 2331-4.

60. Braus, G.H., et al., *Amino acid starvation and Gcn4p regulate adhesive growth and FLO11 gene expression in Saccharomyces cerevisiae.* Mol Biol Cell, 2003. **14**(10): p. 4272-84.

61. Cutler, N.S., et al., *The TOR signal transduction cascade controls cellular differentiation in response to nutrients.* Mol Biol Cell, 2001. **12**(12): p. 4103-13.

62. Wullschleger, S., R. Loewith, and M.N. Hall, *TOR signaling in growth and metabolism.* Cell, 2006. **124**(3): p. 471-84.

63. Busti, S., et al., *Glucose signaling-mediated coordination of cell growth and cell cycle in Saccharomyces cerevisiae.* Sensors (Basel), 2010. **10**(6): p. 6195-240.

64. Gagiano, M., et al., *Divergent regulation of the evolutionarily closely related promoters of the Saccharomyces cerevisiae STA2 and MUC1 genes.* J Bacteriol, 1999. **181**(20): p. 6497-508.

65. Kim, T.S., S.B. Lee, and H.S. Kang, *Glucose repression of STA1 expression is mediated by the Nrg1 and Sfl1 repressors and the Srb8-11 complex.* Mol Cell Biol, 2004. **24**(17): p. 7695-706.

66. Herzog, B., et al., *Mutual cross talk between the regulators Hac1 of the unfolded protein response and Gcn4 of the general amino acid control of Saccharomyces cerevisiae.* Eukaryot Cell, 2013. **12**(8): p. 1142-54.

Chapter IV
Proteomic analysis of the signaling network of the *Saccharomyces cerevisiae* kinase Ksp1p and discovery of a novel role in mRNP regulation.

4.1. Introduction

The yeast kinase Ksp1p was first identified in a screen for high-copy suppressors of a mutation in the nucleotide exchange factor Srm1p [1]. However, almost two decades later Ksp1p remains mostly uncharacterized, especially with respect to its signaling network. Work in our lab has shown that Ksp1p, and specifically its kinase activity, is necessary for cells to transition from vegetative to pseudohyphal growth during nitrogen stress [2]. Briefly, under conditions of nutrient sufficiency, cells grow, bud, and divide rapidly and exhibit a mostly round morphology. When these same cells are starved for nitrogen, they become elongated and bud in a uni-polar fashion. Daughter cells do not completely separate from the mother cell and long chains of cells are formed [3]. This switch is often described as a foraging mechanism for the otherwise nonmotile yeast [4]. We also demonstrated that Ksp1p kinase activity is necessary for the wild type localization of three other pseudohyphal growth regulating kinases: Fus3p, Sks1p, and Bcy1p, the regulatory subunit of PKA [2].

Several kinase signaling pathways are intimately involved in regulating pseudohyphal growth. The filamentous growth MAPK pathway and the MAP kinase Kss1p acts on the transcription factors Ste12p and Tec1p to stimulate transcription of the major flocculence gene *FLO11* [5-7] (For review see [8]). The cAMP/PKA pathway

also acts on *FLO11* via the transcription factor Flo8p [9], a pseudogene in most common laboratory strains [10]. An additional layer of regulation is provided by the TOR pathway [11].

The TOR pathway, and specifically the TOR1 complex (TORC1), acts to stimulate cell growth during nutrient sufficiency and activate stress response pathways during nutrient limitation [12]. The TOR pathway is especially necessary for sensing of nitrogen stress and amino acid availability [13]. Ksp1p has been linked to TORC1 in several ways. Most notably, Ksp1p has been shown to physically interact with TORC1 via coimmunoprecipitation with complexes precipitated with the Kog1p subunit, and the same study showed that inhibition of TORC1 with rapamycin changes the phosphorylation state of Ksp1p [14]. Ksp1p has also been shown to be phosphorylated by PKA on Ser827 in a TOR dependent manner [15].

Ksp1p has been shown to have an inhibitory effect on general autophagy, the trafficking of vesicles encompassing cytosolic proteins to the central yeast vacuole for processing and recycling under conditions of nitrogen stress. This inhibitory effect also appears to be mediated via TOR and PKA, as mutation of Ser827 of Ksp1p to alanine results in increased autophagy in low nitrogen conditions. A phosphomimetic Ser827Asp mutation conversely results in a decrease in autophagy [16].

Despite the mounting circumstantial evidence, the location of Ksp1p within the network of these pathways and processes remains a mystery, and as yet, no direct targets of Ksp1p phosphorylation have been definitively identified. Because of our interest in understanding the kinase signaling cascades involved in the regulation of pseudohyphal growth, we endeavored to examine global changes in the

phosphoproteome of a *ksp1* kinase dead mutant as compared to a wild type strain under conditions which invoke a filamentous stress response. To do this, we employed a technique known as stable isotope labeling by amino acids in cell culture (SILAC) [17]. In this technique, wild type and mutant strains are differentially labeled with either “light” or “heavy” isotopes of lysine and arginine allowing for quantitative comparisons of their proteomes under a given growth condition . Here we present our findings, including differential phosphorylation states observed in 146 genes and 47 novel phosphorylation sites.

To complement our proteomic study, we mined our data for Gene Ontology (GO) term enrichment [18] and found statistically significant enrichment for proteins involved in mRNA binding and stress granule assembly. Stress granules are ribonucleoprotein aggregates which form in the cytoplasm during many kinds of cellular stress [19, 20], though they are best characterized for their formation during glucose stress [21]. The general composition of these mRNPs includes mRNAs which have been stalled in translation, translation factors, and other mRNA binding proteins, but as they are studied further, the list becomes more diverse to include the likes of many kinases [22] and even TORC1 [23]. Though Ksp1p has been reported to localize to stress granules upon depletion of glucose, the GO term enrichment for stress granule assembly came as a surprise to us, as Ksp1p has never previously been reported to affect the dynamics of stress granule formation. Here, we show that Ksp1p does affect granule dynamics in response to high culture density, a known inducer of mRNP formation [24, 25]. Recent work in our lab has begun to draw connections between the improper formation of mRNP granules and defects in pseudohyphal growth (Shively, et al. manuscript in

progress). To that end, we followed up on three specific genes known to localize to, or regulate the formation of, stress granules which were differentially phosphorylated in a *ksp1* kinase dead background as revealed by SILAC. We found that mutation of specific residues in Pbp1p, Tif4631p, and Ste20p had differential effects on pseudohyphal growth phenotypes and localization of these proteins to cytoplasmic foci after growth to high optical density.

With this study, we have generated a putative target list for Ksp1p kinase activity. We have also demonstrated a role for Ksp1p in regulating the formation of stress granules under some conditions. More importantly, we have succeeded in implicating specific residues of three proteins from our SILAC data as being important for pseudohyphal growth, localization to mRNP granules, or both. These results, as well as targeted follow-up studies, will eventually place Ksp1p in the complex network of the yeast signaling pathways.

4.2. Materials and methods

4.2.1. Strains, media, and growth conditions

The strains used in this study are listed in Table 4.1. Diploid filamentous strains were constructed in the Σ1278b background by mating the Y825 and HLY337 haploid strains [26]. Fluorescence microscopy was performed using the S288C derivatives BY4742 and BY4741 [27].

Standard yeast techniques and growth media were used to culture cells [28]. Under normal conditions, cells were grown in complete media, either YPD (2% peptone, 1% yeast extract, and 2% glucose, with or without 2% agar) or Synthetic Complete (SC)

(0.67% yeast nitrogen base, 2% glucose, and 0.2% of the appropriate amino acid dropout mix, with or without 2% agar). Low nitrogen conditions were achieved by growth in or on Synthetic Low Ammonia Dextrose (SLAD) (0.17% yeast nitrogen base without amino acids and without ammonium sulfate, 2% glucose, 50µM ammonium sulfate, and the appropriate amino acids to complement auxotrophies).

Plasmids used in this study are listed in Table 4.2. The plasmid pDS7 (U1A-mCherry) was made by amplification of the mCherry protein from plasmid pBS35 [29] using DSK116 and DSK117, and amplification of the pRP1194 backbone [30] using DSK114 and DSK115. PCR products obtained were used for Gibson Assembly using Gibson Assembly Master Mix (NEB).

4.2.2. Construction of chromosomal mutants and fusions

Chromosomal deletions of genes were made using a one-step PCR-based protocol for gene disruption by amplifying the kanMX6 gene from plasmid pFA6a-kanMX6 [31]. Transformants were selected by plating on YPD + G418 plates and verified by PCR. Deletion of *KSP1* was done using oCK0327 and oCK0328. Deletion of *TIF4631* was done using oCK0265 and oCK0266. Deletion of *PBP1* was done using oCK0259 and oCK0260. Deletion of *STE20* was done using oCK0263 and oCK0264. Similarly, C-terminal GFP fusions were made by transformation of strains with PCR product obtained after amplification of the GFP::HisMX6 cassette from pFA6a-GFP::HisMX6 [31]. *PBP1* was tagged using DSK009 and DSK010. *STE20* was tagged using DSK118 and DSK119.

Chromosomally integrated point mutants were made using a *URA3* knock-in-knock-out method as previously described [32]. Briefly, the *URA3* gene was amplified from vector pRS406 with primers containing homology to 45 base pairs of sequence on either side of the mutational target site. Strains were transformed with PCR product and selected for on media lacking uracil. Strains with successful *URA3* insertions were transformed with annealed 120-mer oligonucleotides containing the desired mutant sequence and homology to flanking regions. Successful loss of *URA3* was monitored by screening on 5-FOA plates. Mutations in *KSP1* were made using DSK096, DSK097, DSK100, and DSK101. Mutations in *TIF4631* were made using oCK0448, oCK0449, oCK0450, oCK0451, oCK0452, oCK0453, DSK024, and DSK025. Mutations in *PBP1* were made using DSK028, DSK029, DSK034, DSK035, DSK0121, and DSK122. Mutations in *STE20* were made using oCK0656, oCK0657, oCK0658, and oCK0659.

4.2.3. Peptide sample preparation and phosphopeptide enrichment

S. cerevisiae Y825 control and *ksp1*^{K47D} mutant cells were isotopically labeled with heavy (Lys-8/Arg-10) amino acids during cell culture (SILAC). Cell cultures were lysed by bead beating in lysis buffer; the lysis buffer was composed of 50 mM tris buffer (pH 8.2), 8 M urea, and protease inhibitors (Roche) and phosphatase inhibitors (50 mM NaF, 50 mM beta-glycerophosphate, 1 mM sodium vanadate, 10 mM sodium pyrophosphate, 1 mM phenylmethylsulfonyl fluoride). Frozen cells were suspended in 400 µl lysis buffer and were lysed by applying three cycles of bead beating (for one minute each) with a 2-minute rest on ice between cycles. Supernatants containing protein extract were recovered by centrifugation at 14,000 g for 10 minutes, and protein

concentrations were measured by Bradford assay. Equal amounts of protein from three SILAC-labeled cells were combined, treated for disulfide reduction and alkylation, and digested with TMPK-treated trypsin (Worthington Biochemical Corp., Lakewood, NJ) at a trypsin:protein ratio of 1:10 at 37 °C overnight.

Peptide mixtures were desalted with C18 (Waters) and separated into 12 strong cation exchange (SCX) fractions on a PolySulfoethyl A column (PolyLC, 150 x 4 mm) over a 48 minute salt gradient with two mobile phases: 100% solvent A (5 mM KH_2PO_4, 30% acetonitrile, pH 2.7) for 5 minutes, a linear gradient of 0-40% solvent B (250 mM KH_2PO_4, 30% acetonitrile, pH 2.7) in the following 35 min, a stiff increase of 40-100% B in 3 min, and flushing with 100% B for 5 min. Collected SCX fractions were desalted with C18 (Waters) and subjected to selective phosphopeptide enrichment using ZrO_2 (Glygen, 50 µm i.d. resin) under acidic conditions in the presence of 2,5-dihydroxy benzoic acid (52, 53). Phosphopeptides selectively bound on ZrO_2 were eluted with 4% NH_4OH. The ZrO_2 eluate of enriched phosphopeptides and the flow-through of each SCX fraction were analyzed by nanoLC-tandem mass spectrometry (MSMS).

4.2.4. Mass spectrometric analysis and SILAC quantification

NanoLC-MSMS experiments were performed on a hybrid type mass spectrometer (Thermo, LTQ-Orbitrap XL) coupled to a nanoLC system (Eksigent, 2D nanoLC). Samples were separated on a custom capillary column (150 mm x 75 µm, 3 µm Sepax HP-C18) using a 120 min linear aqueous gradient (9-90% acetonitrile, 0.01% formic acid) delivered at 250 nL/min. The eluent was introduced on-line to the LTQ-Orbitrap via an electrospray device (Advion, TriVersa NanoMate) in positive ion mode.

The LTQ-Orbitrap was operated in a data-dependent mode alternating a full MS scan (300-1700 m/z at 60,000 resolution power at 400 m/z) in the Orbitrap analyzer and collision-induced dissociation scans (CID-MSMS) for the 7 most abundant ions with signal intensity above 500 from the previous MS scan in LTQ. Recurring precursor ions were dynamically excluded for 30 sec by applying charge-state monitoring, ions with 1 or unassigned charge states were rejected to increase the fraction of ions producing useful fragmentation. Lock mass ($[(Si(CH_3)_2O)_6]_1+$, m/z = 445.120029) was used for internal calibration. Each sample was analyzed by two LC-MS experiments. Raw LC-MS data file sets were processed, database searched, and quantified using MaxQuant (ver 1.0.13.8) (54) and the Mascot search engine together. Mascot database searches were performed against a composite database of forward and reverse sequences of verified yeast open reading frames from the Saccharomyces Genome Database. Variable modifications were allowed for oxidation (M) and phosphorylations (STY), as well as a fixed modification of carbamidomethylation (C). Peptide, protein, and phosphorylation site identifications were filtered at a false discover rate of 5%. The MaxQuant normalized H/L (heavy/light) ratios with significance scores less than 0.05 were considered statistically significant.

4.2.5. Surface spread filamentation and invasion assays

Cultures of diploid wild type or mutant strains were grown overnight in YPD, back diluted 1:20 in fresh YPD, and grown for 4-6 h. Cells were washed 3 times with sterile deionized water and normalized to a final OD_{600} of 1.0 before being diluted and plated to SLAD plus uracil at a density of approximately 50 cells/plate. Plates were incubated

at 30^{o}C for until filamentation was observed in wild type strains (about 7-8 days) before being visualized. After images were taken of representative colonies, invasion into the agar was assayed by running plates under deionized water and gently removing surface cells with a finger. Plates were dried and reimaged.

4.2.6. β-galactosidase assays of *FLO11* transcription activity

Diploid strains harboring plasmid pGL669-Z FLO11 6/7 [33] were grown overnight in SC minus uracil. Cells were washed 3 times with 2% glucose, diluted 1:5 in SLAD media, and grown at 30^{o}C for 4-6 h. B-galactosidase assays were performed in triplicate using Thermo Scientific Yeast β-Galactosidase Assay Kit according to the manufacturer's protocols.

4.2.7. Induction and visualization of mRNP granules

Strains harboring pPS2037 and pDS7 were grown overnight in SC minus uracil and leucine. Cultures were back diluted to OD600 of 0.1, and incubated at 30^{o}C. Formation of granules and colocalization was monitored at 24 h and 48 h using a Nikon Eclipse 80i microscope, X-Cite 120 lamp, and MetaMorph imaging software (Version 7.1.2.0).

4.3. Results

4.3.1. Analysis of the Ksp1p signaling network

SILAC experiments, performed and quantified in the lab of Phil Andrews, comparing phosphorylation states between a wild type strain and a kinase dead version

of *ksp1* (Figure 4.1) yielded 180 peptides with altered phosphorylation (Figure 4.2A and Table 4.7) across 146 unique genes. Of those, 43 were observed to be hyperphosphorylated (Table 4.3) and 147 hypophosphorylated (Table 4.4). In addition, 6 genes were observed to contain both hyper and hypophosphorylated peptides (Figure 4.2B). Though a decrease in phosphorylation must be an indirect effect, these changes can still give insight into the regulatory network of Ksp1p and are useful in looking at possible connections among various signaling pathways and Ksp1p. Within the 180 peptides identified, we also report discovery of 47 novel phosphorylation sites (Table 4.6).

To begin analyzing the proteomic data a little deeper, we used available computational tools to look at Gene Ontology (GO) Terms which are enriched in our data set compared to background. These programs compare the proportion of genes within a specified dataset which are annotated for a particular cellular process or function to the overall proportion of genes which are ascribed that same process or function in the entire genome. The results of this analysis are highlighted in Figure 4.3. It was not surprising to us that our data set was enriched for protein kinases and kinase activity, but it is worth noting that these kinases represent diverse signaling pathways. For example, we observe differential phosphorylation of the MAPK-pathway kinase Ste20p, the PKA-regulated kinase Yak1p, and Hxk1, a kinase downstream of the glucose sensing Snf1 pathway. Also statistically enriched in our data set were genes involved in trehalose metabolism (Figure 4.3B). Trehalose is a disaccharide and is hydrolyzed into two glucose molecules by Nth1p or Nth2p. Together, these results seem

to position Ksp1p to facilitate crosstalk among several pathways, perhaps coordinating a less linear, and more nuanced, response to extracellular nutrient levels.

In addition to kinase activity and metabolic pathways, we were struck by the large number of genes in the data set which are known to bind to mRNA and regulate the formation of stress granules (Figure 4.3B). Ksp1p had been previously shown to localize to cytoplasmic foci upon glucose stress, but it was reported that Ksp1p did not affect the formation of stress granules. In light of this enrichment, and previous results from our lab demonstrating the link between mRNP formation and pseudohyphal growth, we to examined the phenotypic consequences of mutations of several of these genes. In particular, because of the reported localization of Ksp1p, we were interested in the genes which have been most closely linked to stress granules. Pbp1p and Tif4631 have both been shown to localize to stress granules, and Ste20p has been implicated in regulating the formation of stress granules via phosphorylation of Dcp2p and has been reported to occasionally localize to granules.

4.3.2. Mutation of SILAC-identified residues affects pseudohyphal growth and invasion

Diploid integrated point mutants in *PBP1*, *TIF4631*, *STE20,* and *KSP1*, in the filamentous Σ1278b background, were assayed for their ability to undergo pseudohyphal growth and invade the agar surface on low nitrogen media (Figure 4.4 and Figure 4.5). As we have previously reported, Ksp1p is necessary for robust pseudohyphal growth, and mutation of the kinase activity is sufficient to cause this defect. In this way, *ksp1* mutants serve as a negative control.

Complete deletions of *KSP1, TIF4631, PBP1,* and *STE20* cause severe pseudohyphal growth defects, with little to no filamentation observed in *PBP1* and *STE20* (Figure 4.4). Deletion of *PBP1* or *STE20* also ablates invasion (Figure 4.5). The kinase dead mutant *ksp1*^{K47D} is also defective for pseudohyphal growth.

More interestingly, non-phosphorylatable alleles of *tif4631* suggest that Ser176 is necessary for robust pseudohyphal growth. Though filaments can be observed in this strain, they are abnormal in appearance. Ser180 did not have an effect on filamentation, and the double mutant exhibited an intermediate phenotype. Mutations of *TIF4631* did not greatly alter the invasive phenotype of these cells (data not shown).

Ser456 of Pbp1p was hyperphosphorylated in our SILAC experiment. Here, we changed Ser456 to alanine, essentially making it constitutively hypophosphorylated. In the pseudohyphal growth assay, we observed very large colonies with little to no surface-spread filamentation, but this mutation confers a hyperinvasive phenotype. For its part, the *ste20*^{T203A} mutant did not have a consistently appreciable effect on surface spread filamentation or invasive growth.

4.3.3. Mutants are defective for PKA control of *FLO11* transcription

As a complement to the more qualitative pseudohyphal and invasive growth assays, we used a LacZ reporter construct to measure transcription of the *FLO11* gene, a gene essential for formation of filaments. The *FLO11* promoter is unusually large and is controlled by both the filamentous growth MAPK pathway and the PKA pathway. Reporter constructs have been made which separate the MAPK-responsive and PKA-responsive locations of the *FLO11* promoter and active transcription can be measured

by standard β-galactosidase assays. No differences were observed using the MAPK-responsive construct (data not shown), but statistically significant differences were seen among the mutants with the PKA-responsive reporter (Figure 4.6).

Again, all null mutants were decreased for transcription of *FLO11*, even *ste20*Δ, which is known to function upstream of the MAPK pathway. It should be noted, however, that Thr203 of Ste20p resides in a consensus PKA kinase motif, so Ste20p may also facilitate crosstalk between pathways, but there was no statistically significant change in the *FLO11* transcription in a *ste20*^{T203A} background.

The *FLO11* transcriptional activity in the *pbp1*Δ and *pbp1*^{S436A} mutants complemented the observed phenotypes in plate assays. The null mutant exhibited a 70% decrease in PKA-dependent *FLO11* transcription, while the non-phosphorylatable mutant showed a 30% increase.

In the various *TIF4631* backgrounds, transcription of this reporter is varied, as are the pseudohyphal growth phenotypes. Here again the *tif4631*^{S180A} mutant did not cause a significant change in transcription. Oddly, even though the *tif4631*^{S176A} and *tif4631*Δ mutants both led to decreased activity, the point mutant exhibited a greater decrease (about 30% of wild type activity in the point mutant versus 80% of wild type activity in the null mutant). This result is slightly perplexing, and it will require a greater understanding of the role of Ser176 *in vivo*. The *tif4631*^{S176,180A} mutant was again intermediately defective compared to the single mutants. Though it still exhibits about 90% of the activity of wild type, the difference was consistent and statistically significant.

4.3.4. Ksp1p affects mRNP granules formed during high-OD stress

Ksp1p has not previously been implicated in regulating the formation of mRNP granules. It is important to note that the composition of mRNP granules and dynamics of their assembly can vary greatly depending on induction conditions. Most commonly, mRNP formation is induced by acutely starving cells in the logarithmic-growth phase for glucose. Other induction conditions commonly used include: heat stress, inhibition of translation, or high culture density. In our assay, the most consistent results were obtained using this latter method, and mRNP formation was observed after growth to high OD. To monitor the formation of mRNPs, we replaced the GFP moiety of the plasmid pRP1194 with mCherry via Gibson Assembly (see methods). This also allowed us to examine colocalization with GFP-tagged strains from the available GFP collection.

Wild type and *ksp1* mutant strains were transformed with the reporter plasmids, allowing us to track the formation of mCherry-marked PGK-mRNA containing foci through U1A binding. High optical density stress was induced by back dilution of overnight cultures into Synthetic Complete media to a starting OD_{600} of 0.1 and growth at $30^{o}C$ for 24-48 hours. After 48 hours, both the null and kinase dead mutants of *ksp1* consistently exhibited nearly a 3-fold increase in the percentage of cells containing at least 1 focus with the modified *PGK1* transcript. This result suggests that Ksp1p may play a role in inhibiting, or at least slowing, the formation of stress granules in aging cultures

4.3.5. Pbp1p and Ste20p point mutants have aberrant mRNP phenotypes

As mentioned, Pbp1p and Tif4631p have been classified as stress granule components. Ste20p has been shown to regulate stress granule formation by

phosphorylating the P-body associating protein Dcp2p, a necessary step in the formation of stress granules. We wished to examine the localization pattern of wild type Tif4631p-GFP, Pbp1p-GFP, Ste20p-GFP, as well as the localization of the point mutants used in the pseudohyphal growth assays. Here we utilized the PGK/mCherry system in combination with GFP-tagged wild type and mutant versions of Tif4631p, Pbp1p, and Ste20p to allow for quantification of both GFP focus formation and potential changes in the colocalization patterns. No consistent phenotypes were observed in the various *TIF4631* backgrounds (data not shown).

For Pbp1p, we compared the relative granule formation between wild type and the *pbp1*^{S436A} mutant as well as between wild type and a phosphomimetic *pbp1*^{S436D} mutant (Figure 4.8). The most striking phenotypic differences were observed at 24 h, when both mutants consistently had a higher percentage of cells containing foci relative to wild type (Figure 4.8 and quantified in Figure 4.9). No marked differences from wild type were observed after 48 h (see discussion). Interestingly, the colocalization phenotypes are different between the two strains at 24 h (Figure 4.8). Though both mutants had more foci, the Ser456Ala mutant was slightly, though statistically significantly, decreased for colocalization with the mCherry-marked *PGK1*-U1A-binding site foci. The Ser456Asp showed almost 2-fold more colocalization than wild type Pbp1p-GFP. Based on these results Ser456 is important for wild type formation and localization of Pbp1p granules.

The *ste20*^{T203A} mutant also had differential localization patterns compared to wild type (Figure 4.10 and quantified in Figure 4.11). At 48 h the *ste20*^{T203A} mutant had a 2.5-fold increase in foci formation compared to wild type. The increase in foci formation

at 48 h was concomitant with an increase in colocalization with PGK containing foci. It is possible that Thr203 is necessary for movement of Ste20p out of these granules.

4.4. Discussion

Here we present a proteomic survey of the kinase signaling network of Ksp1p and potential downstream targets of Ksp1p regulation. Of particular note is the breadth of the potential Ksp1p targets which include members of three major filamentous growth signaling pathways: the PKA pathway, the MAPK pathway, and the Snf1 pathway (Figure 4.2). There were no observed changes in the phosphorylation of any TORC1 proteins, but Tsc11p (Avo3p), a member of the TORC2 complex was hypophosphorylated in the mutant *ksp1* background (Table 4.5).

Utilizing the phosphoproteomic data presented here, and previous data showing Ksp1p to immunoprecipitate with TORC1 [14], regulate autophagy in a TOR-dependent manner [16], as well as data showing Ksp1p phosphorylation by PKA to be dependent upon TOR [15], it is possible to speculate as to the location of Ksp1p within these many signaling networks, with respect to pseudohyphal growth (Figure 4.12). Likely, Ksp1p resides downstream of both TORC1 and PKA, and though Ksp1p is necessary for the proper response to nitrogen limitation, it may help cells to respond to glucose stress. Evidence of this comes from the fact that putative targets of Ksp1p include genes involved in trehalose metabolism (Figure 4.3), as well as the aberrant formation of stress granules in *ksp1* mutant strains (Figure 4.7, Figure 4.13), as stress granule formation is a response to glucose depletion.

Further bolstering the position of Ksp1p at least partially within the PKA pathway are the results of the *FLO11* transcriptional reporter assay (Figure 4.6). Both the null and kinase dead alleles of *ksp1* exhibited decreased PKA-dependent transcription of *FLO11*. Moreover, point mutations of residues implicated by the SILAC data also exhibited a decrease in transcription of *FLO11*.

Proteomic data has begun to help us place Ksp1p within its signaling network, but it has also yielded a potentially novel role for Ksp1p in the regulation of stress granule formation (Figure 4.12, Figure 4.13). Because of the enrichment of stress granule associating and regulatory proteins present in our data set, we looked at the effects, not only on general granule formation in the *ksp1*Δ and *ksp1*^{K47D} backgrounds, but also at the effects of SILAC-implicated residues on the localization of Tif4631p, Ste20p, and Pbp1p after growth to high OD (Figures 4.7-4.11).

Mutation of *ksp1* resulted in a higher percentage of cells containing PGK foci after 48 hours (Figure 4.7, Figure 4.13). Again, this suggests that Ksp1p plays a role in inhibiting granule formation, and this inhibition is dependent upon Ksp1p kinase activity. If Ksp1p is acting to stimulate the hydrolysis of trehalose into glucose by Nth1p and Nth2p, this may explain why granules form more quickly in these strains. A decrease in trehalose hydrolysis would exacerbate any glucose stress present. While Nth2p is hypophosphorylated in our data set, Nth1p exhibits a “mixed” state with one peptide being identified as being hypophosphorylated and one peptide being hyperphosphorylated.

Mutations of two of the three individual stress granule proteins yielded changes in their localizations (Figure 4.8-4.11, 4.13). The *tif4631* alleles tested showed no

consistent phenotypes and were not examined further in this study. Mutation of Thr203 of Ste20p led to an increase in the number of *ste20*^{T203A}p-GFP foci present at 48 h. These foci were also 1.5 times more likely to colocalize with foci containing the modified *PGK1* transcript. It is possible that the phosphorylation state of Thr203 acts to mediate whether or not Ste20p enters granules, or this residue may facilitate the exit of Ste20p from the U1A-marked granules.

The results seen in the *PBP1* alleles are intriguing. First, it must be addressed that the most significant difference in granule formation compared to wild type was seen at 24 h (Figure 4.8 and Figure 4.9). At the 48 h time point, neither allele exhibited a localization pattern different from that of wild type (data not shown). One possible explanation for this could be that at 24 h, cells are either still in late logarithmic phase, at the cusp of undergoing diauxic shift., or have just undergone the shift. Diauxic shift occurs when nearly all of the available glucose is consumed by fermentation, and the yeast must shift to respiration and growth on the alcohols produced by fermentation [34]. Both PKA and TOR are negative regulators of this diauxic shift (For review see [35]), and Pbp1p has been demonstrated to help recruit TORC1 to stress granules [23]), possibly as a means of sequestering it. It will be interesting to determine if the increased foci formation affects timing of the diauxic shift in the *pbp1* mutant relative to wild type. Nevertheless, both the nonphosphorylatable *pbp1*^{S456D}p-GFP and the phosphomimetic *pbp1*^{S456D}p-GFP constructs formed more foci than wild type at 24 h. This suggests that this residue is important for regulating wild type levels of Pbp1p-GFP granule formation, but the phosphorylation state of this residue is not sufficient to govern its localization to granules.

When colocalization of these mutant alleles with U1A-marked granules is examined, we find that the *pbp1*^{S456A} mutant is slightly decreased for the proportion of GFP foci which colocalize with mCherry-marked foci. Conversely, the *pbp1*^{S436D} mutant shows nearly a 2-fold increase in colocalization. This seems to implicate this residue in trafficking Pbp1p to the "correct" cytoplasmic granule. The immutable nature of these mutants may decrease the ability of Pbp1p to move between different types of mRNP granules. Lastly, it is possible that these point mutants could be having an effect on formation of foci with the modified *PGK1* transcript, but we observed no significant differences between U1A-marked foci formation in wild type and our point mutants (data not shown).

Synthesis of the results yields a speculative model for Ksp1p function during stress (Figure 4.12 and Figure 4.13). Ksp1p kinase activity is a positive regulator of pseudohyphal growth, but a negative regulator of mRNP formation. As these two processes are both activated in response to nutrient limitation, it seems Ksp1p is playing somewhat divergent roles. Traditionally, filamentous growth is a response to low nitrogen, while mRNP formation is a response to glucose stress. As the signaling pathways discussed respond to diverse stimuli, Ksp1p may play differing roles during nitrogen and glucose stresses. During nitrogen stress, Ksp1p signals, at least indirectly, through several known mRNP associated proteins to affect PKA-dependent transcription of *FLO11.* The catalytic subunits of PKA, either Tpk1 or Tpk2, then cause an increase in the transcription of *FLO11*, and consequently, filamentous growth (Figure 4.6 and Figure 4.12). Formation of mRNPs is not traditionally studied during nitrogen

stress, so it remains unknown if Pbp1p, Ste20p, or Tif4631p form foci under these conditions, but it is unlikely.

I do not observe an effect for Ksp1p on mRNA granule formation during acute glucose stress. Ksp1p foci form consistently when cells are grown to high OD by culturing for 24-48 hours. This long growth naturally leads to the consumption of glucose via fermentation, stressing the cells, though more gradually. Under these conditions, mRNA granules form in the presence of Ksp1p, but only in approximately 5% of cells. Loss of Ksp1p, or its kinase activity, results in mRNA foci occurring in approximately 15% of cells (Figure 4.7). Mutation of phosphorylation sites on Ste20p and Pbp1p whose phosphorylation states have been shown by SILAC to be regulated by Ksp1p also leads to an increase in foci formation by these proteins, further demonstrating that Ksp1p acts to retard formation of granules.

Ksp1p kinase activity may inhibit RNP granule formation through several means. Ksp1p may directly phosphorylate a protein component of RNP granules, thereby decreasing affinity for other granule proteins. Ksp1p may phosphorylate a component of the TORC1 complex, affecting nutrient-responsive signaling, and indirectly, RNP granule formation. Ksp1p may also regulate mRNP granule number through the PKA pathway, which is known to negatively regulate P-body formation in response to glucose stress. Our data, as well as data indicating TORC1-dependent PKA phosphorylation of Ksp1p, most directly relates to the latter two possibilities, although the mechanism of this regulatory control remains to be determined. Collectively, the retardation of granule formation by Ksp1p may be a mechanism by which the cells prevent the unnecessary formation of granules in the absence of *dire* stress conditions. However, once a

particular threshold has been reached, Ksp1p may signal through Pbp1p to sequester TORC1 and PKA, and potentially itself via a physical interaction with TORC1, to granules, completely releasing the brake on granule formation (Figures 4.7-4.11 and Figure 4.13). At present, further experimentation is needed to test this model.

Figure 4.1. Experimental design for discovery of differentially phosphorylated peptides. Filamentous strains harboring a *ksp1*Δ allele were transformed with either wild type or a kinase dead mutant of *KSP1* under control of its native promoter. Strains were grown in minimal media with "light" or "heavy" amino acids, plus 1% butanol to induce filamentation in liquid culture. Protein preparations were mixed, digested, and enriched for phosphopeptides before being subjected to LC-MS/MS. Adapted from [26].

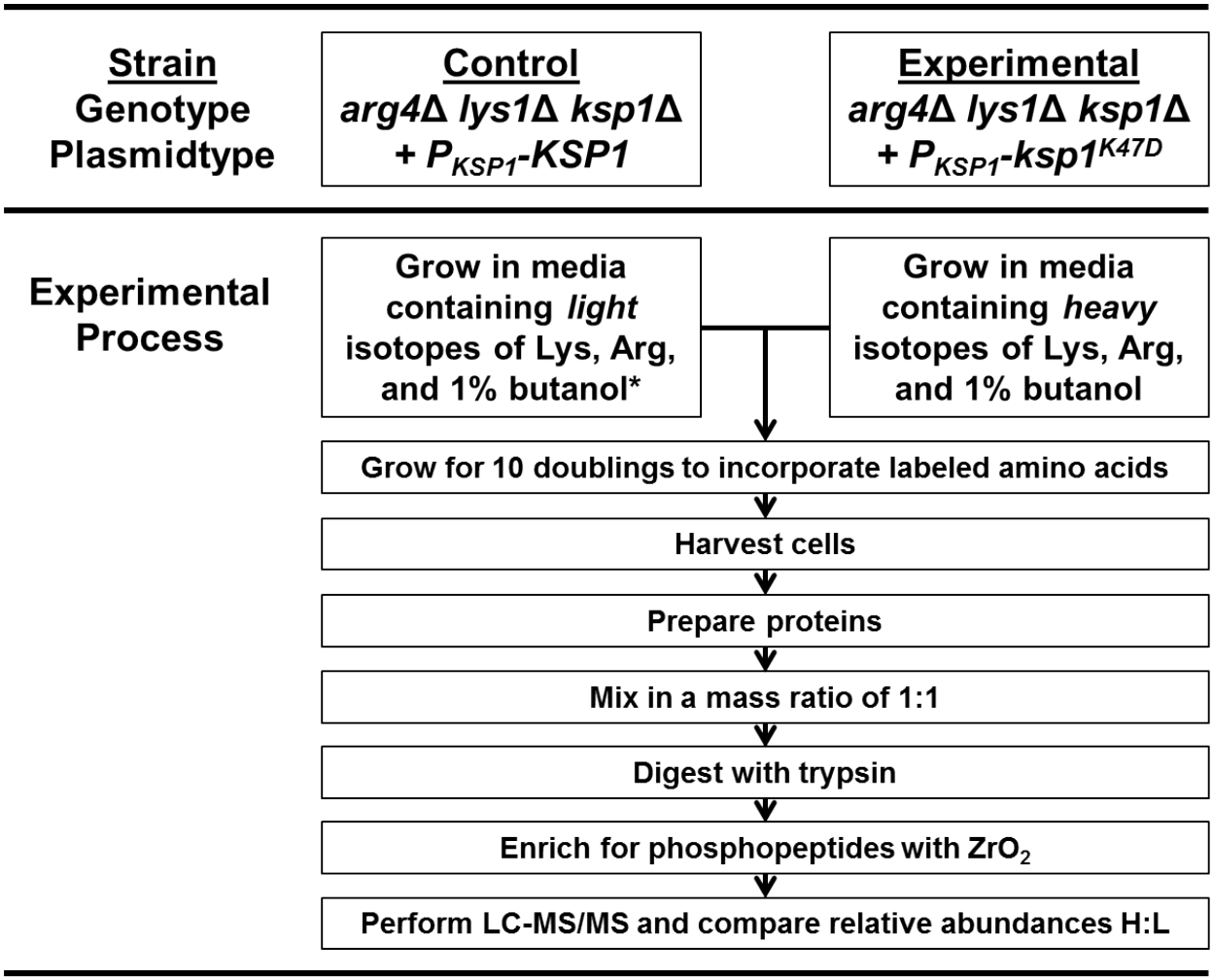

Figure 4.2. Overview of genes with altered phosphorylation in a *ksp1*^{K47D} strain. (A) List of all non-redundant genes to which a peptide was mapped and observed to be hyperphosphorylated (green) or hypophosphorylated (red). Relevant numbers are given in green and red boxes to the right. (B) Genes to which independent peptides showed both types of aberrant phosphorylation.

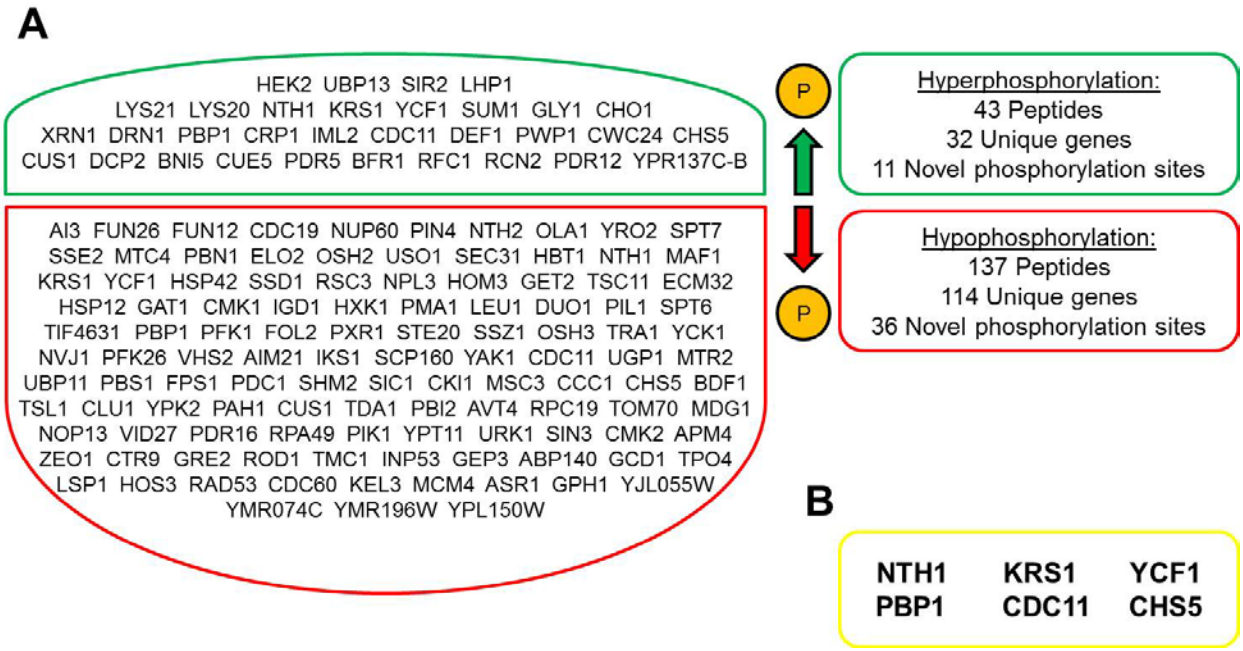

Figure 4.3. Analysis of Gene Ontology (GO) Terms. (A) Highlights of some GO Terms for Cellular Function, their p-values for enrichment, and their member genes. (B) Highlights of some GO Terms for Cellular Process, their p-values for enrichment, and their member genes.

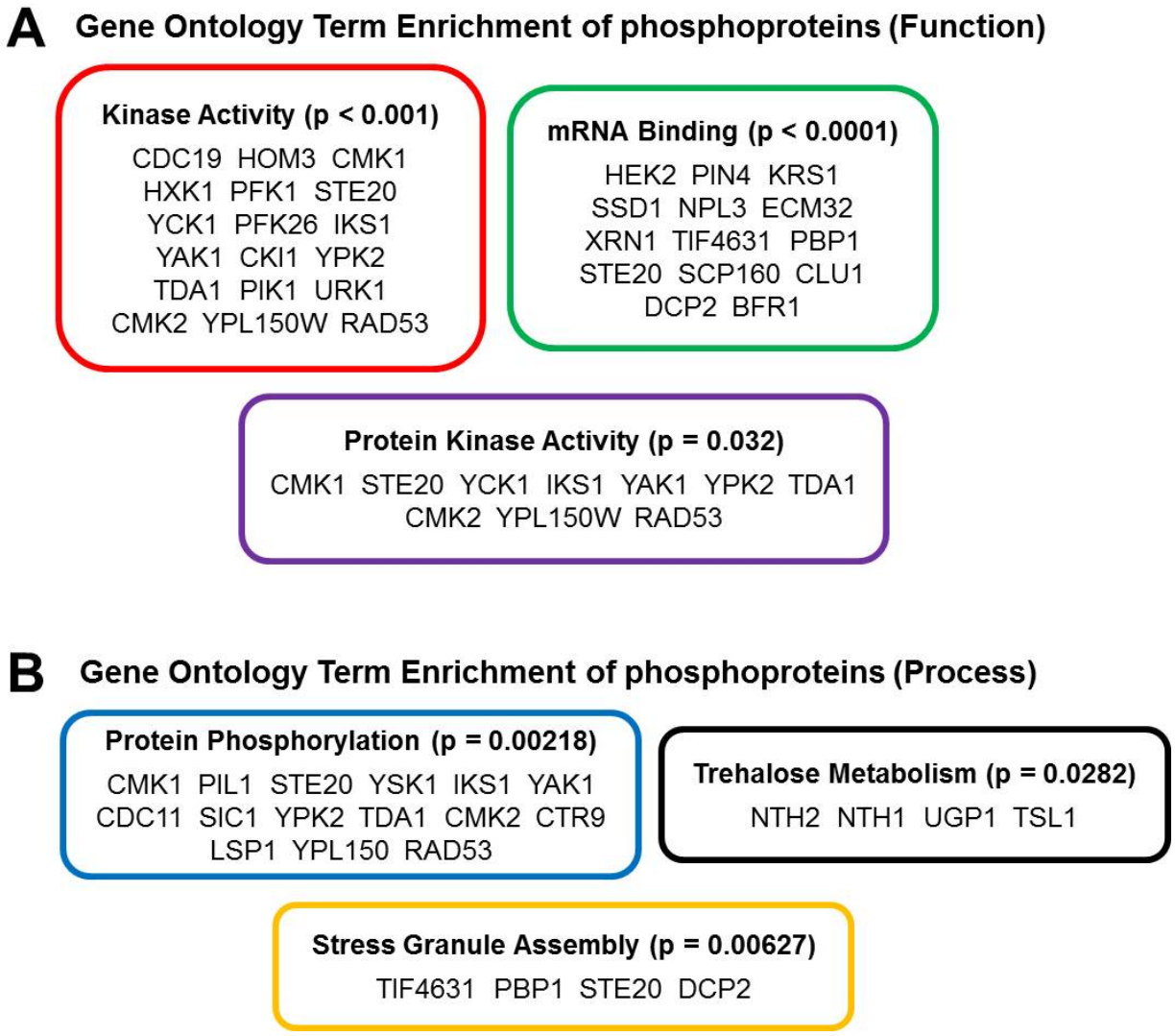

Figure 4.4. Diploid pseudohyphal growth phenotypes. Cells in the logarithmic growth phase were washed with sterile water and approximately 50 cells/plate were spread to SLAD (low nitrogen) plates. Representative images of multiple replicates of surface spread filamentation assays with diploid cells are shown. Relative phenotypes are represented by "+" (wild type) and "-" (decreased) pseudohyphal growth.

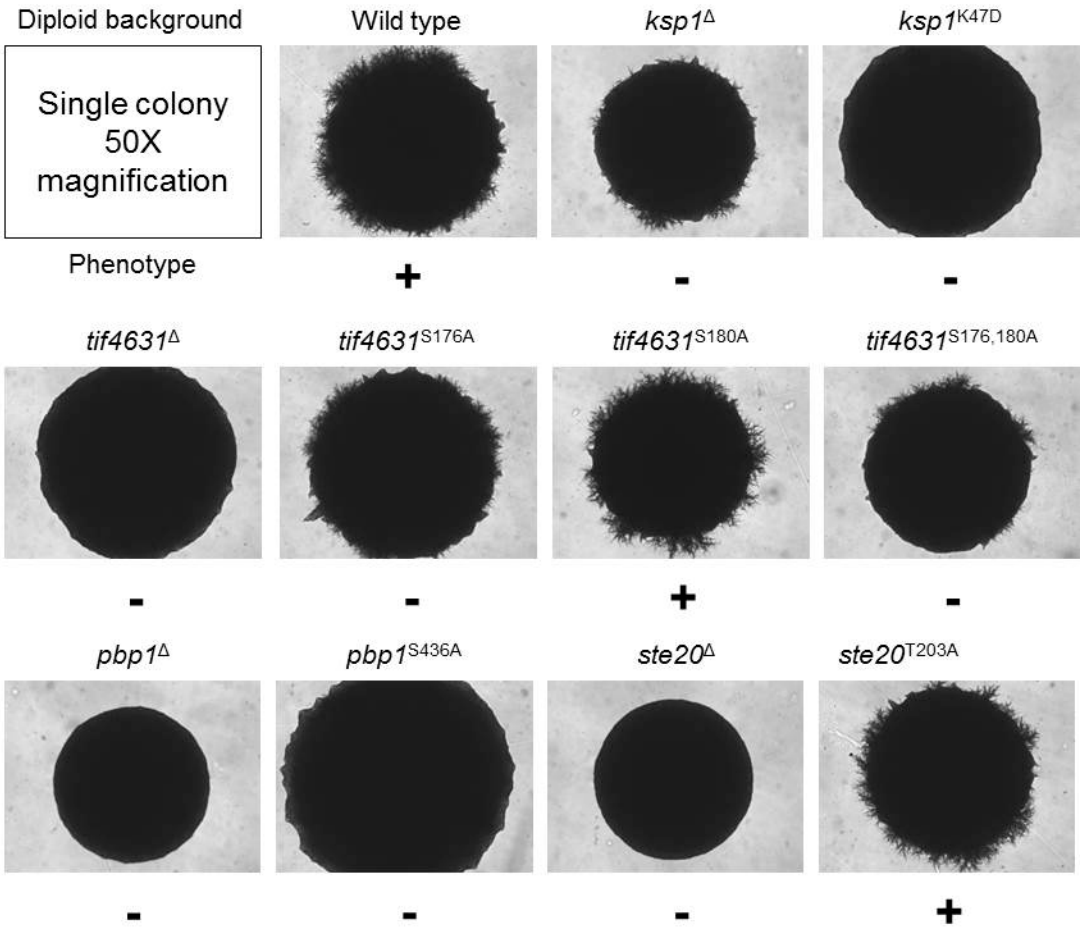

Figure 4.5. Diploid agar invasion phenotypes. Cells in the logarithmic growth phase were washed with sterile water and approximately 50 cells/plate were spread to SLAD (low nitrogen) plates and allowed to invade the agar. Representative images of multiple replicates of agar invasion assays with diploid cells are shown. Relative phenotypes are represented by “+” (wild type), “-“ (decreased), “- -“ (severely decreased) and “++” (increased) invasive growth.

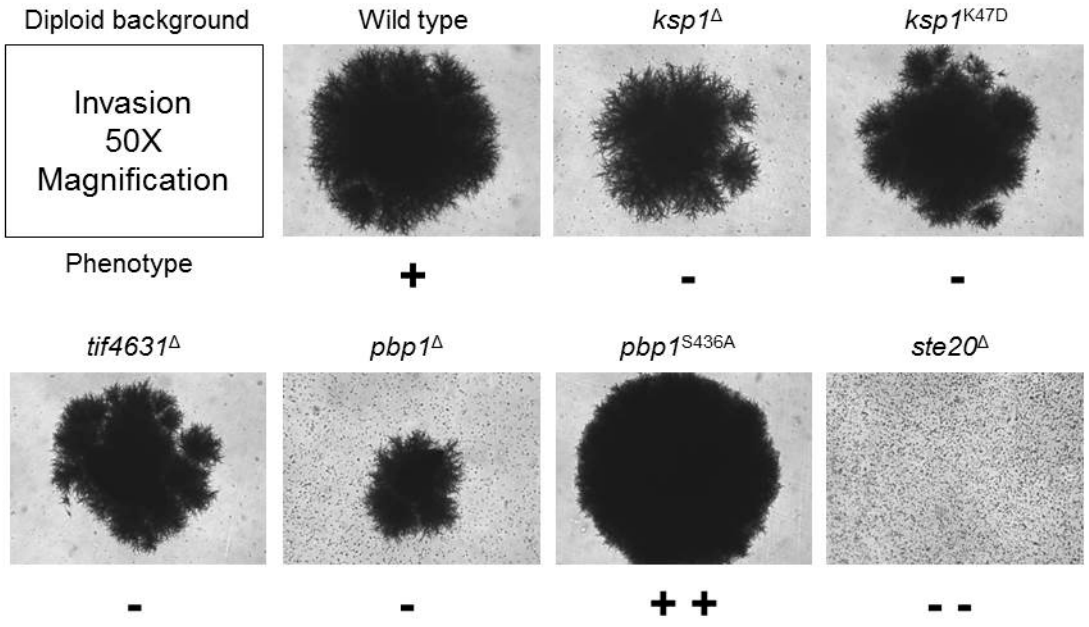

Figure 4.6. Quantification of PKA-dependent *FLO11* transcription. Diploid cells, of the specified genotype, were transformed with pLG669-Z FLO11 6/7 and monitored for PKA-dependent *FLO11* transcription via β-galactosidase assays in triplicate. Miller units of mutants were normalized to wild type and fold-change is reported on the Y-axis. Statistical significance is indicated by asterisks ($p < 0.01$ "***", $p < 0.05$ "**", $p < 0.10$ "*").

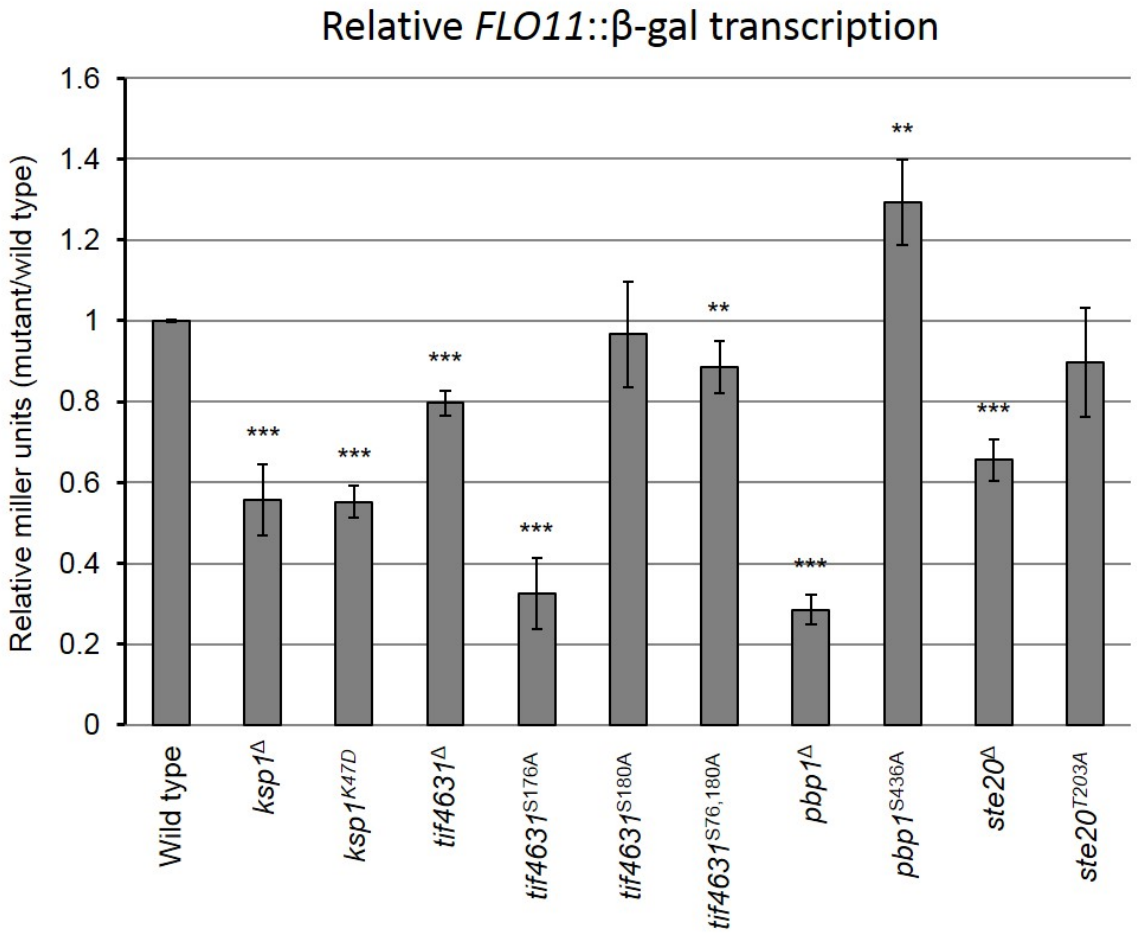

Figure 4.7. Dynamics of PGK mRNA-containing mRNP granules in various *KSP1* backgrounds. (A) The indicated strain was transformed with pPS2037 (PGK-U1A mRNA), and pDS7 (U1A-mCherry) and monitored for focus formation after 48 hour of growth in SC minus uracil, minus leucine. (B) Quantification and statistical analysis of three paired replicates. The percentage of mutant cells exhibiting foci was normalized to wild type and fold-change is reported on the Y-axis. Statistical significance is indicated by asterisks ($p < 0.01$ "***", $p < 0.05$ "**", $p < 0.10$ "*"). (Data is from 3 replicates; $N_{cells} \geq 250$; $\bar{x}_{wildtype} = 4.7\%$).

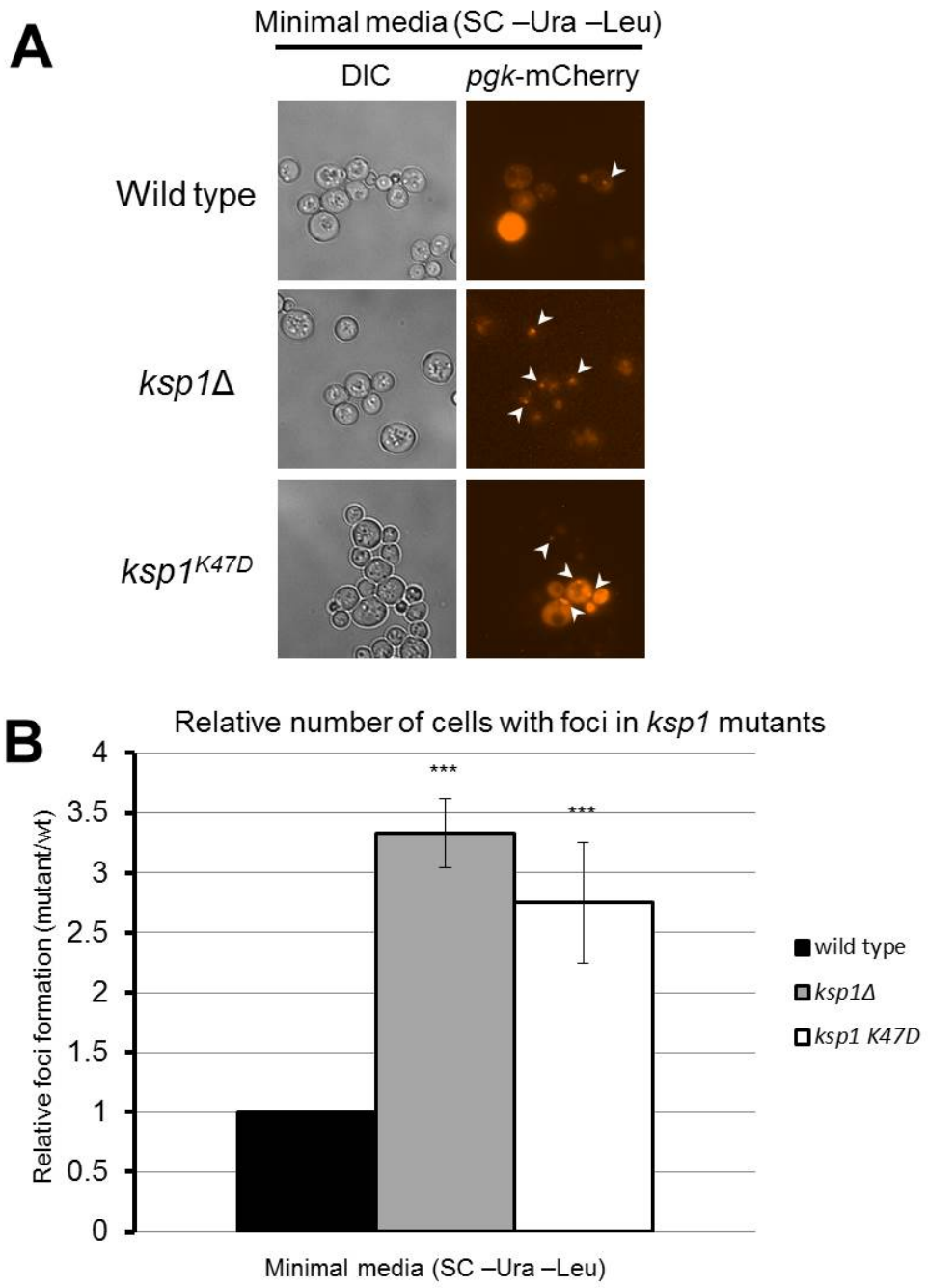

Figure 4.8. Dynamics of Pbp1p-GFP and MS implicated mutant *pbp1*p-GFP foci. Wild type, non-phosphorylatable, and phosphomimetic mutants of Pbp1p were fused to GFP and transformed with pPS2037 and pDS7. Formation of GFP-foci and colocalization with mCherry-marked PGK-foci was monitored after 24 hours of growth in SC minus uracil, minus leucine.

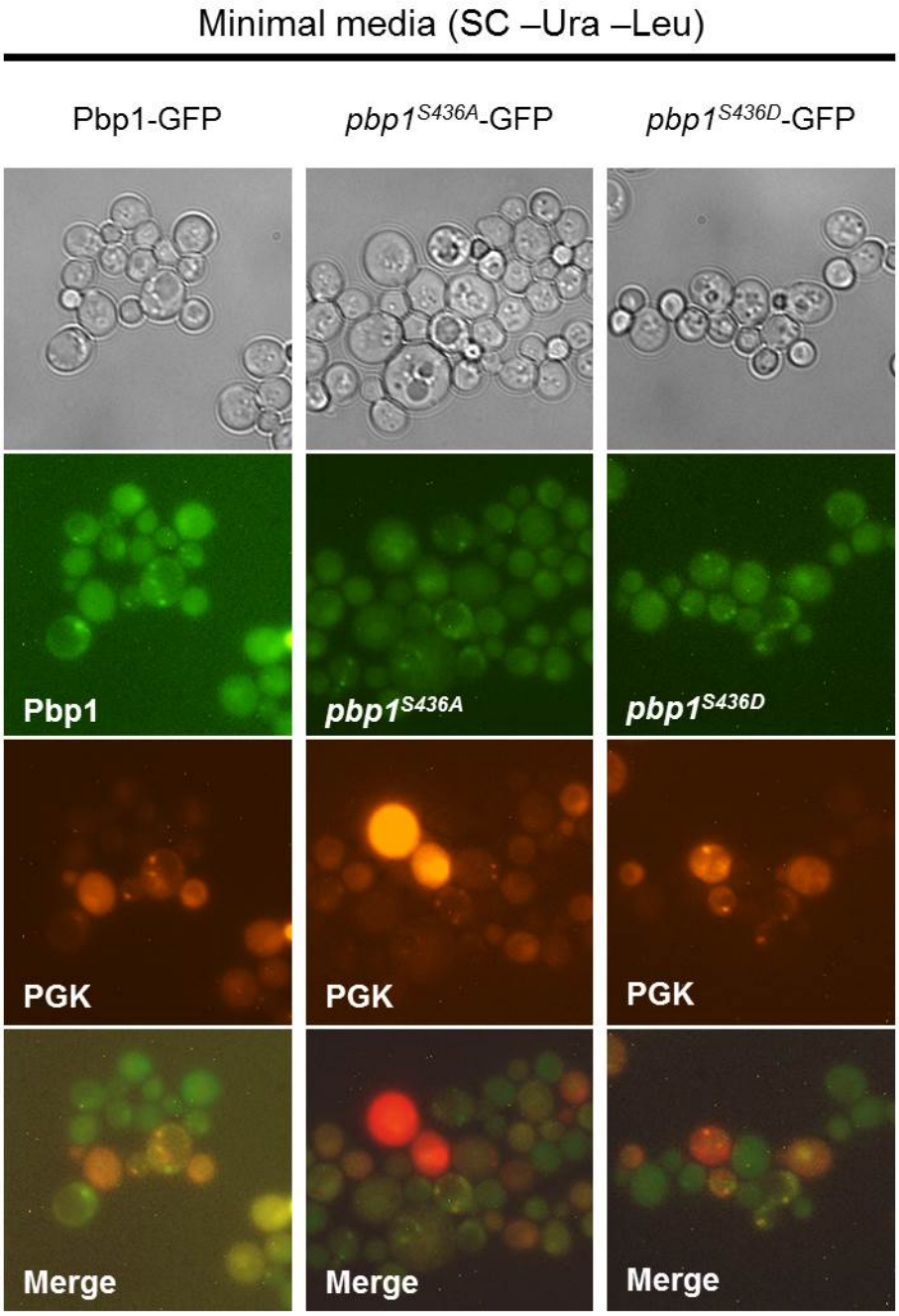

Figure 4.9. Quantification of Pbp1p-GFP and MS implicated mutant *pbp1*p-GFP foci dynamics. Wild type and mutant fusion proteins were imaged after 24 hours of growth in SC minus uracil, minus leucine and the percentage of cells containing GFP foci, as well as the percentage of those foci which colocalized with PGK mRNA-containing foci was determined. The percentage of mutant cells exhibiting foci or colocalizing with PGK granules was normalize to wild type and fold-change is reported on the Y-axis. Statistical significance is indicated by asterisks ($p < 0.01$ "***", $p < 0.05$ "**", $p < 0.10$ "*").(Data is from 4 replicates; $N_{cells} \geq 150$; Foci $\bar{x}_{wildtype} = 9.4\%$; Colocalization $\bar{x}_{wildtype} = 42.6\%$).

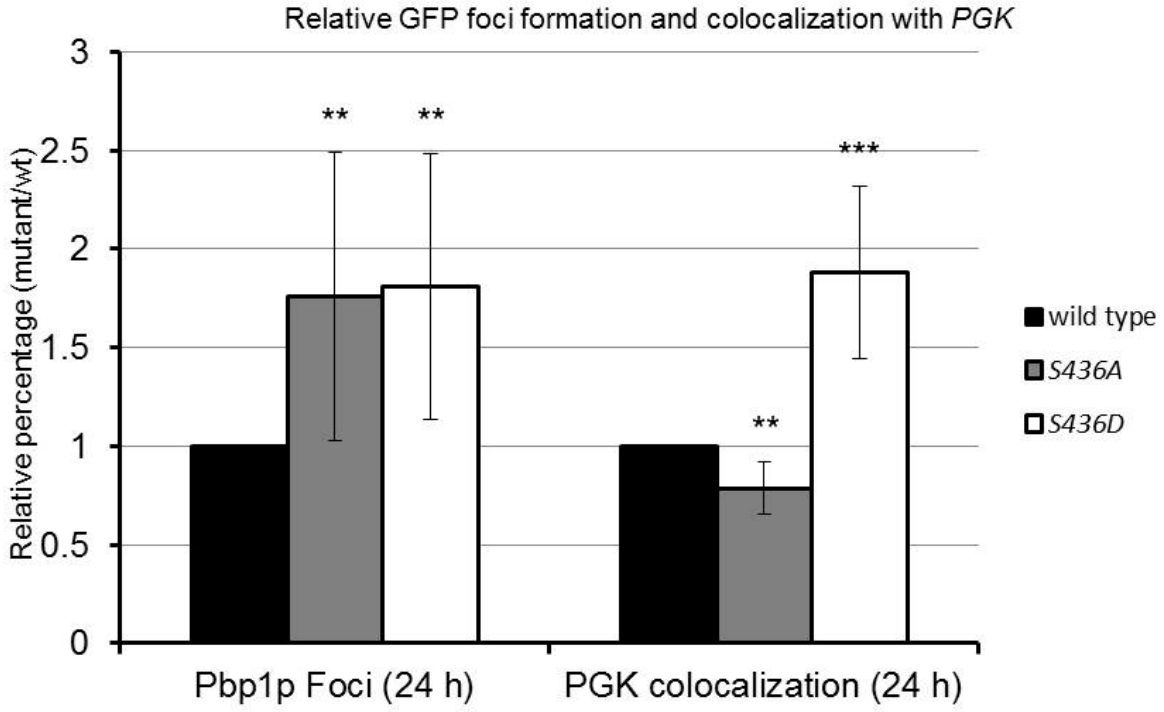

Figure 4.10. Dynamics of Ste20p-GFP and MS implicated mutant *ste20*p-GFP foci. Wild type and a non-phosphorylatable mutant of Ste20p was fused to GFP and transformed with pPS2037 and pDS7. Formation of GFP-foci and colocalization with mCherry-marked PGK-foci was monitored after 48 hours of growth in SC minus uracil, minus leucine.

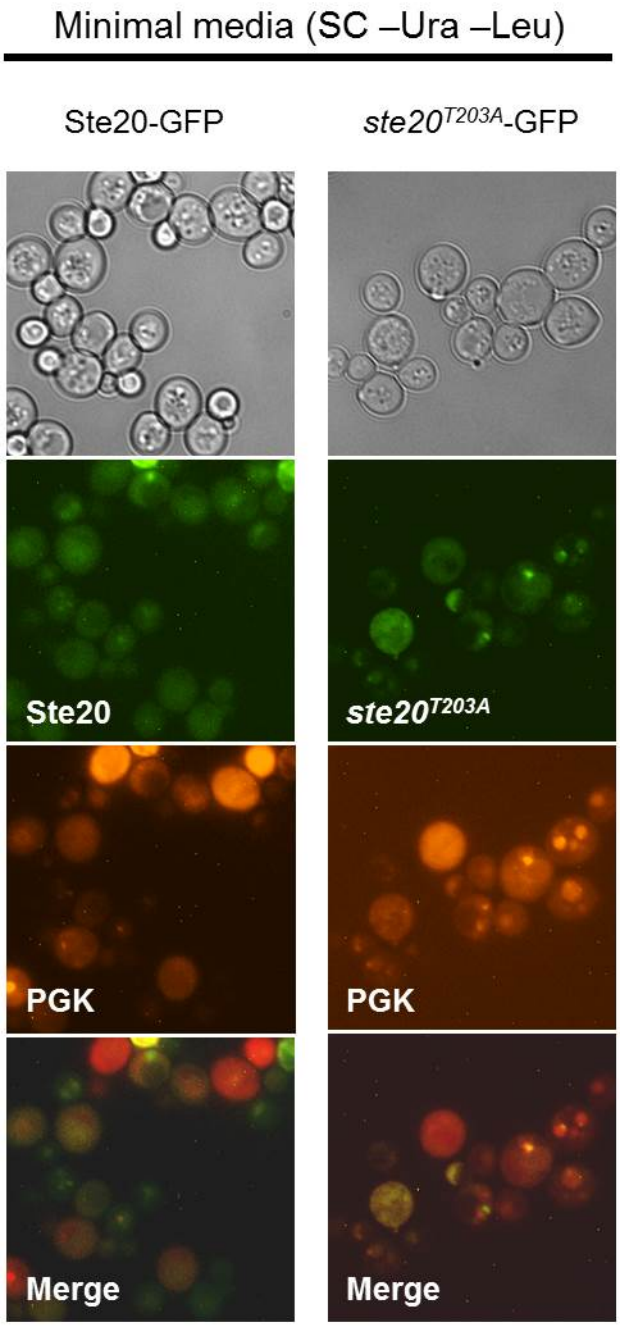

Figure 4.11. Quantification of Ste20p-GFP and MS implicated mutant *ste20*p-GFP foci dynamics. Wild type and mutant fusion proteins were imaged after 48 hours of growth in SC minus uracil, minus leucine, and the percentage of cells containing GFP foci, as well as the percentage of those foci which colocalized with PGK mRNA-containing foci was determined. The percentage of mutant cells exhibiting foci or colocalizing with PGK granules was normalize to wild type and fold-change is reported on the Y-axis. Statistical significance is indicated by asterisks ($p < 0.01$ "***", $p < 0.05$ "**", $p < 0.10$ "*").(Data is from 5 replicates; $N_{cells} \geq 150$; Foci $\bar{x}_{wildtype} = 3.9\%$; Colocalization $\bar{x}_{wildtype} = 38.6\%$).

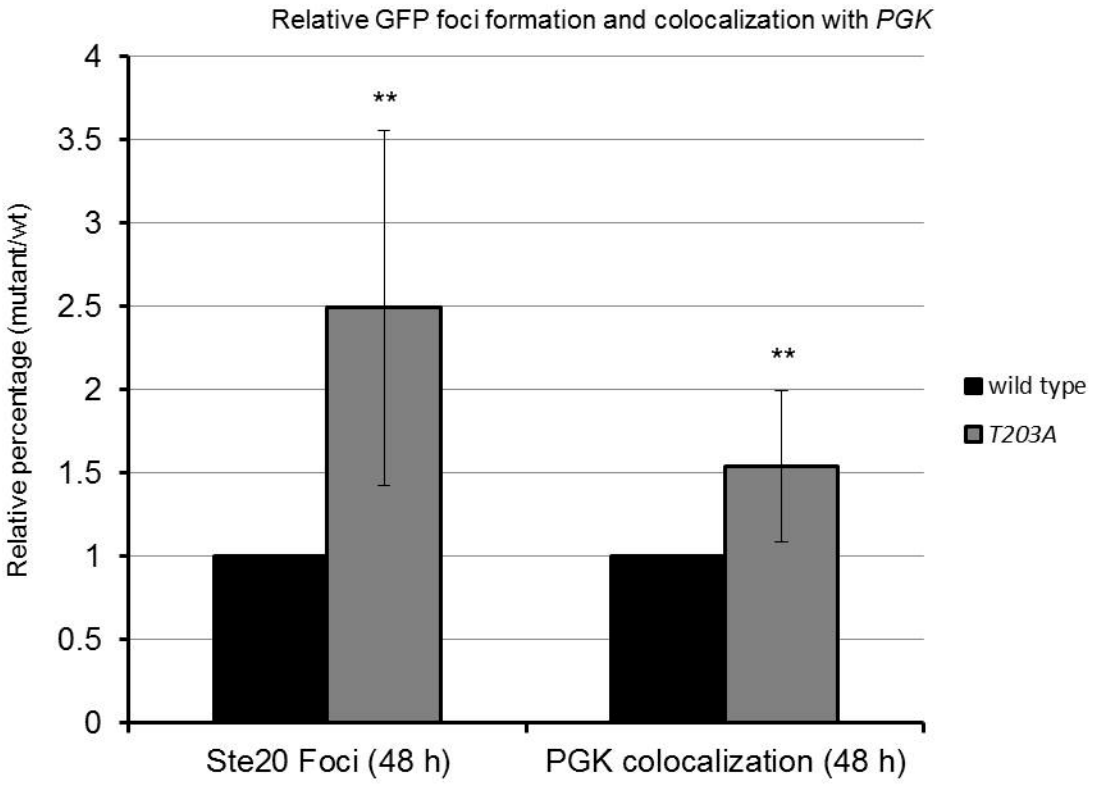

Figure 4.12. A partial Ksp1p signaling network. Deletions of all SILAC implicated genes show an affect on *FLO11* transcription via the PKA pathway, Additionally, some SILAC implicated residues are functionally important for PKA-dependent *FLO11* transcription. PKA also phosphorylates Ksp1p in a TOR-dependent manner, and Ksp1p has an inhibitory effect on mRNP formation during high-OD stress.

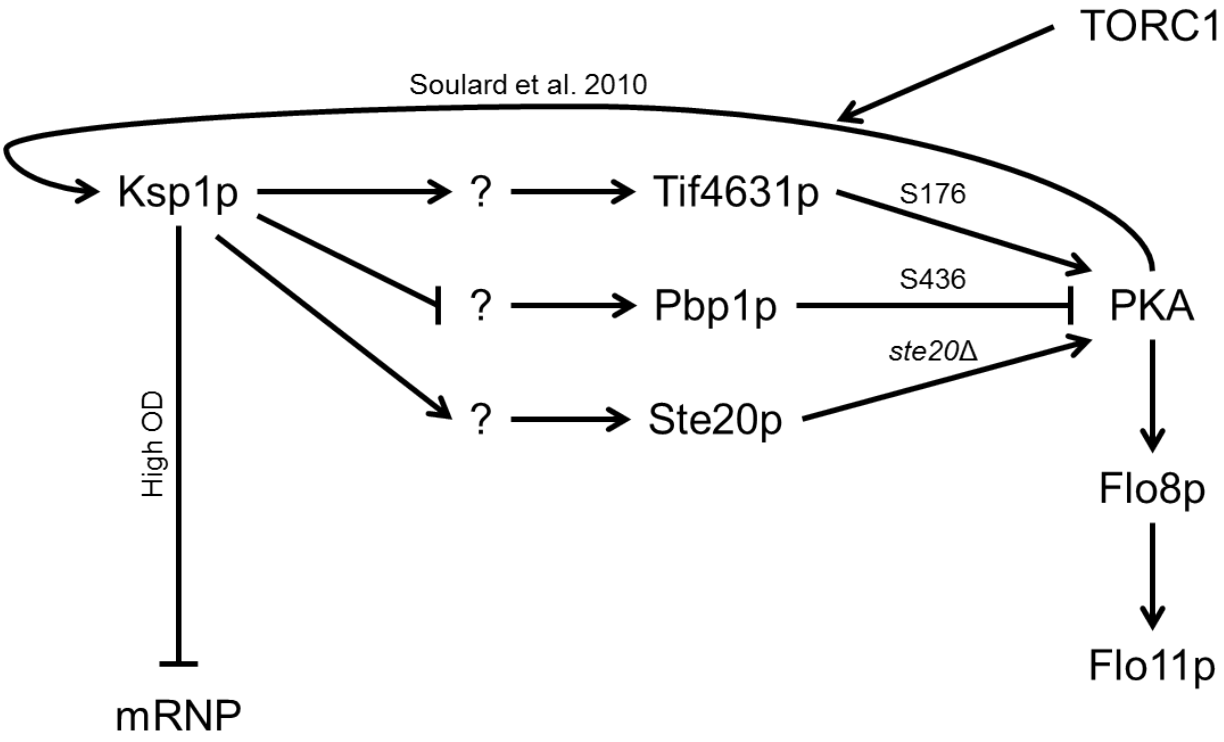

Figure 4.13. Ksp1p in mRNP formation. During high-OD stress, Ksp1p functions as a "brake" on mRNP formation. Mutation of SILAC-implicated residues on Ste20p and Pbp1p results in an increase in those proteins localizing to foci. Additionally, these residues are important for wild type localization of Ste20p and Pbp1p to mRNA foci.

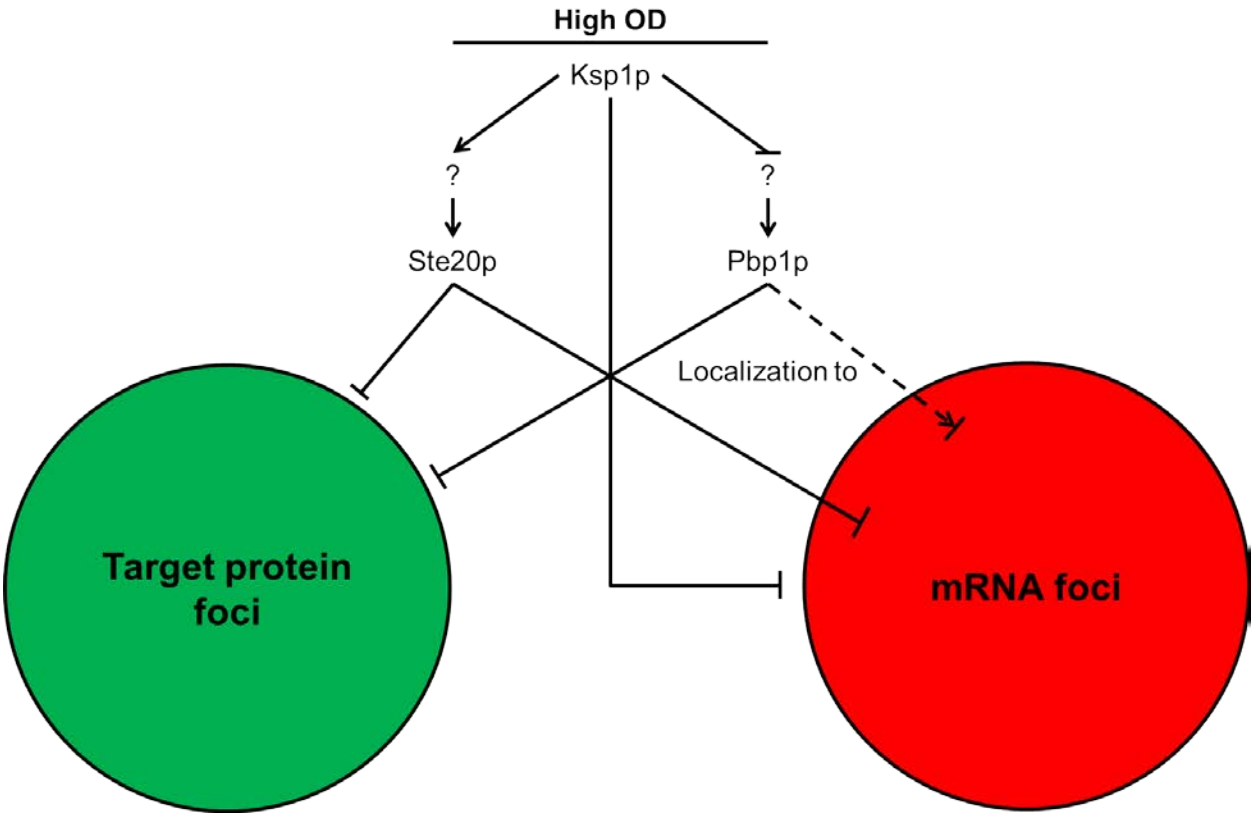

Table 4.1. Yeast strains used in this study

Strain	Genotype	Source
HLY337	*ura3-52 trp1-1 MATα*	
Y825	*ura3-52 leu2Δ0 MATa*	
BY4742	*his3Δ1 leu2Δ0 lys2D0 ura3Δ0 MATα*	[36]
yCK021 (825x337)	*ura3-52/ura3-52 leu2Δ0/LEU2 TRP1/trp1-1 MATa/MATα*	[26]
yCK109	*ura3-52/ura3-52 leu2Δ0/LEU2 TRP1/trp1-1 MATa/MATα ksp1Δ::kanMX/ksp1Δ::kanMX*	This study
yCK186	*ura3-52/ura3-52 leu2Δ0/LEU2 TRP1/trp1-1 MATa/MATα* $ksp1^{K47D}/ksp1^{K47D}$	This study
yCK061	*ura3-52/ura3-52 leu2Δ0/LEU2 TRP1/trp1-1 MATa/MATα tif4631Δ::kanMX/tif4631Δ::kanMX*	This study
yCK190	*ura3-52/ura3-52 leu2Δ0/LEU2 TRP1/trp1-1 MATa/MATα* $tif4631^{S176A}/tif4631^{S176A}$	This study
yCK235	*ura3-52/ura3-52 leu2Δ0/LEU2 TRP1/trp1-1 MATa/MATα* $tif4631^{S180A}/tif4631^{S180A}$	This study
DSY035	*ura3-52/ura3-52 leu2Δ0/LEU2 TRP1/trp1-1 MATa/MATα* $tif4631^{S176,180A}/tif4631^{S176,180A}$	This study
yCK059	*ura3-52/ura3-52 leu2Δ0/LEU2 TRP1/trp1-1 MATa/MATα pbp1Δ::kanMX/pbp1Δ::kanMX*	This study
DSY178	*ura3-52/ura3-52 leu2Δ0/LEU2 TRP1/trp1-1 MATa/MATα* $pbp1^{S436A}/pbp1^{S436A}$	This study
DSY245	*ura3-52/ura3-52 leu2Δ0/LEU2 TRP1/trp1-1 MATa/MATα* $pbp1^{S436D}/pbp1^{S436D}$	This study
yCK083	*ura3-52/ura3-52 leu2Δ0/LEU2 TRP1/trp1-1 MATa/MATα ste20Δ::kanMX*/ste20Δ*::kanMX*	This study
yCK336	*ura3-52/ura3-52 leu2Δ0/LEU2 TRP1/trp1-1 MATa/MATα* $ste20^{T203A}/ste20^{T203A}$	This study
DSY052	*his3Δ1 leu2Δ0 met15Δ0 ura3Δ0* PBP1-GFP-HIS3MX6 *MATa*	[27]
DSY179	*his3Δ1 leu2Δ0 met15Δ0 ura3Δ0* $pbp1^{S436A}$-GFP::HisMX *MATa*	This study
DSY241	*his3Δ1 leu2Δ0 met15Δ0 ura3Δ0* $pbp1^{S436D}$-GFP::HisMX *MATa*	This study

DSY226	*his3Δ1 leu2Δ0 lys2D0 ura3Δ0* Ste20-GFP::His3MX6 *MATα*	[27]
DSY240	*his3Δ1 leu2Δ0 lys2D0 ura3Δ0 ste20^{T203A}*-GFP::His3MX6 *MATα*	This study
DSY160	*his3Δ1 leu2Δ0 lys2D0 ura3Δ0 ksp1Δ::KanMX MATα*	This study
DSY161	*his3Δ1 leu2Δ0 lys2D0 ura3Δ0 ksp1^{K47D} MATα*	This study

Table 4.2. Plasmids used in this study

Short name	Description	Source
	pFA6a-GFP(S65T)-HisMX6	[31]
	pFA6a-kanMX	[31]
pRS406	*URA3*, *Cen,* AMP	[37]
	P_{KSP1}-$ksp1^{K47D}$	This study
	P_{KSP1}-*KSP1*	This study
pLG669-Z FLO11 6/7	*URA3*, 2 µ, AMP, p*FLO11*::LacZ-6/7	[33]
pPS2037	*URA3,* 2µ, AMP, PGK1-U1A-PGK1 3' UTR	[38]
pDS7	*LEU*, 2 µ, AMP, U1A-mCherry	This study

Table 4.3. Oligonucleotides used in this study

Name	Sequence
DSK009	CCACCATGGCCACCATAATAGTAGTACCAGTGGCCATAAACGGATCCCCGGGTTAATTAA
DSK010	TTTATTACTATATATTGCTTTTTCTGACGTGCTTCCTTCAGAATTCGAGCTCGTTTAAAC
DSK024	AGATCTACTGTGTCTCCGCAACCAGAGTCAAAGTTAAAAGAAACTTCTGATGCTACTTCTACTGCTACTCCAACTCCTACCCCTTCCACTAATGACTCTAAGGCCAGTTCTGAAGAAAA
DSK025	TTTTCTTCAGAACTGGCCTTAGAGTCATTAGTGGAAGGGGTAGGAGTTGGAGTAGCAGTAGAAGTAGCATCAGAAGTTTCTTTTAACTTTGACTCTGGTTGCGGAGACACAGTAGATCT
DSK028	ATTAAAATCTAATTCTTCGTTGCCTCCAAAACCGATCAGCAAAACCCCTTCGGCCGAGAGTGCACCATACCACAGC
DSK029	CTTGAGATATGTTGCTGCCACTTCTTCTAGATTCTGATTTCCCTGCAGAAATCTGTTAGTTTTGCTGGCCGCATC
DSK034	CTCCTACTACACAGATTTCTGCAGGGAAATCAGAATCTAGAAGAAGTGGCAGCAACATAGCTCAAGGCCAATCATCTACCGGCCATACCACGAGATCTAGTACTTCATTGAGAAGACGTA
DSK035	TACGTCTTCTCAATGAAGTACTAGATCTCGTGGTATGGCCGGTAGATGATTGGCCTTGAGCTATGTTGCTGCCACTTCTTCTAGATTCTGATTTCCCTGCAGAAATCTGTGTAGTAGGAG
DSK096	TATGTATCATTGGCTAAAGATGTTAGAGAGAAAAGATTGGTTGCAGAGAGAGTGCACCATACCACAGC
DSK097	GTCCTGAGGCCCATCGTACTGGCCGTCATCTTCTAATTTGAAAATTTAGTTTTGCTGGCCGCATC
DSK100	GGTTCATATGGTTATGTATCATTGGCTAAAGATGTTAGAGAGAAAAGATTGGTTGCAGTCGACTACATTTTCAAATTAGAAGATGACGGCCAGTACGATGGGCCTCAGGACGACGAAAAT
DSK101	ATTTTCGTCGTCCTGAGGCCCATCGTACTGGCCGTCATCTTCTAATTTGAAAATGTAGTCGACTGCAACCAATCTTTTCTCTCTAACATCTTTAGCCAATGATACATAACCATATGAACC
DSK114	TCCTCGCCCTTGCTCACCATGAGTTCTTCTCCTTTGCTAGCC
DSK115	TGGACGAGCTGTACAAGTAGCCTCGAGGGGGGGCC
DSK116	CTAGCAAAGGAGAAGAACTCATGGTGAGCAAGGGCGAG
DSK117	TACCGGGCCCCCCCTCGAGGCTACTTGTACAGCTCGTCCATG

DSK118	AAAGAAACCGTAAATTTGGACGTAACTGAAGATGATAAACAAAAGCG GATCCCCGGGTTAATTAA
DSK119	GTGTATATACTTTGTCGATAATAAGGTGTACCCTGCTTGCTACGTGA ATTCGAGCTCGTTTAAAC
DSK121	TCTAATTCTTCGTTGCCTCCAAAACCGATCAGCAAAACCCCTTCGGC CAAGACTGTTGACCCTACTACACAGATTTCTGCAGGGAAATCAGAAT CTAGAAGAAGTGGCAGCAACATATCT
DSK122	AGATATGTTGCTGCCACTTCTTCTAGATTCTGATTTCCCTGCAGAAAT CTGTGTAGTAGGGTCAACAGTCTTGGCCGAAGGGGTTTTGCTGATC GGTTTTGGAGGCAACGAAGAATTAGA
oCK0259	AAACTGACATCCTCAGTCACGGAAGTAATTAAAGGAGTTCATTACAT TGAAACAATTTAGCTTGCCTCGTCCCCG
oCK0260	AAAGTGCATGAATTTATTACTATATATTGCTTTTTCTGACGTGCTTCC TTCACGAGCTCGTTTAAACTGGATGGC
oCK0263	TCACTGCCTCACACCCCATCCTAAATATCCCACAAGATCCTCGACTA ATACAAGAATTAGCTTGCCTCGTCCCCG
oCK0264	CACAACTGTGTATATACTTTGTCGATAATAAGGTGTACCCTGCTTGC TACGTCGAGCTCGTTTAAACTGGATGGC
oCK0265	CTTCTTGCTCATAAATAAGCAAGGTAAGAGGACAACTGTAATTACCT ATTACAATATTAGCTTGCCTCGTCCCCG
oCK0266	AACATCCTTGTATCCAAGTGACATTTTCGATACTTAACATGATCTATT CATGCGAGCTCGTTTAAACTGGATGGC
oCK0327	TTTCAAATACAAAACAAAAAGACACGTAAAGTTAGTGCAATATTTTTT TCTTACAATTTTTTGAAACTCGTTAGCTTGCCTCGTCCCCG
oCK0327	TTTCAAATACAAAACAAAAAGACACGTAAAGTTAGTGCAATATTTTTT TCTTACAATTTTTTGAAACTCGTTAGCTTGCCTCGTCCCCG
oCK0328	GAAAAAAGCTAAAAATGCATTTCAGAAGGGAAGAAAATAATAAGCAA CATAACAGAGGGAATAGGTGCGCCGAGCTCGTTTAAACTGGATGGC
oCK0328	GAAAAAAGCTAAAAATGCATTTCAGAAGGGAAGAAAATAATAAGCAA CATAACAGAGGGAATAGGTGCGCCGAGCTCGTTTAAACTGGATGGC
oCK0428	CAGTGAAGGTTCATATGGTTATGTATCATTGGCTAAAGATGTTAGAG AGAAAAGAGAGAGTGCACCATACCACAGC
oCK0429	TATCACAATCATTTTCGTCGTCCTGAGGCCCATCGTACTGGCCGTCA TCTTCTAATTAGTTTTGCTGGCCGCATC
oCK0430	ATCATTTTCGTCGTCCTGAGGCCCATCGTACTGGCCGTCATCTTCTA ATTTGAAAATGTAATCGACTGCAACCAATCTTTTCTCTCTAACATCTT TAGCCAATGATACATAACCATATGA

oCK0431	TCATATGGTTATGTATCATTGGCTAAAGATGTTAGAGAGAAAAGATTGGTTGCAGTCGATTACATTTTCAAATTAGAAGATGACGGCCAGTACGATGGGCCTCAGGACGACGAAAATGAT
oCK0448	ACAGTCTCAGGAAAGATCTACTGTGTCTCCGCAACCAGAGTCAAAGTTAAAAGAAGAGAGTGCACCATACCACAGC
oCK0449	CAGCTTCAGATATATTTTCTTCAGAACTGGCCTTAGAGTCATTAGTGGAAGGGGTTTAGTTTTGCTGGCCGCATC
oCK0450	CAGGAAAGATCTACTGTGTCTCCGCAACCAGAGTCAAAGTTAAAAGAAACTTCTGATGCTACTTCTACTTCTACTCCAACTCCTACCCCTTCCACTAATGACTCTAAGGCCAGTTCTGAA
oCK0451	TTCAGAACTGGCCTTAGAGTCATTAGTGGAAGGGGTAGGAGTTGGAGTAGAAGTAGAAGTAGCATCAGAAGTTTCTTTTAACTTTGACTCTGGTTGCGGAGACACAGTAGATCTTTCCTG
oCK0452	ACTGTGTCTCCGCAACCAGAGTCAAAGTTAAAAGAAACTTCTGATTCTACTTCTACTGCTACTCCAACTCCTACCCCTTCCACTAATGACTCTAAGGCCAGTTCTGAAGAAAATATATCT
oCK0453	AGATATATTTTCTTCAGAACTGGCCTTAGAGTCATTAGTGGAAGGGGTAGGAGTTGGAGTAGCAGTAGAAGTAGAATCAGAAGTTTCTTTTAACTTTGACTCTGGTTGCGGAGACACAGT
oCK0656	CCAGCAGCCAGTTGCATCTTCCACAGTAAACTCGAATAAGAGCTCCACTGATGAGAGTGCACCATACCACAGC
oCK0657	GAATTGATCTGTCTTGGCGTGGTTGTCATCGATGGTTTAGAGATAACGGGTTAGTTTTGCTGGCCGCATC
oCK0658	CAGCCAGTTGCATCTTCCACAGTAAACTCGAATAAGAGCTCCACTGATATACGAAGGGCTGCACCAGTGTCCACTCCCGTTATCTCTAAACCATCGATGACAACCACGCCAAGACAGATC
oCK0659	GATCTGTCTTGGCGTGGTTGTCATCGATGGTTTAGAGATAACGGGAGTGGACACTGGTGCAGCCCTTCGTATATCAGTGGAGCTCTTATTCGAGTTTACTGTGGAAGATGCAACTGGCTG

Table 4.4. Table of hyperphosphorylated peptides

Systematic name	Common Name	Peptide	H/L Ratio	Significance
YBL032W	HEK2	KLEAAEGDATVVT(ph)ER	3.4028	0.018291
YBL067C	UBP13	KKEELPIADDLDTAIDDSFVS(ph)NTPIK	2.7758	0.041463
YDL042C	SIR2	VQDLGS(ph)AISVTNVEDPLAKK	11.299	1.39E-05
YDL051W	LHP1	RNS(ph)FAVIEFTPEVLDR	6.0467	0.00097901
YDL131W	LYS21	DFHAELS(ph)TPLLKPVNK	2.6429	0.049668
YDL182W	LYS20	NFHAEVS(ph)TPQVLSAK	5.8667	0.0011687
YDL182W	LYS20	NFHAEVST(ph)PQVLSAK	5.5976	0.0015308
YDL182W	LYS20	KNDS(ph)DVPELATIPAAK	4.7171	0.0038843
YDR001C	NTH1	RGS(ph)EDDTYSSSQGNR	3.42	0.017899
YDR037W	KRS1	KKT(ph)DLFADLDPSQYFETR	5.057	0.0026869
YDR135C	YCF1	RASDAT(ph)LGSIDFGDDENIAK	2.8938	0.035396
YDR310C	SUM1	TAGDDGALDQTENTSIS(ph)PK	2.7074	0.045487
YEL046C	GLY1	S(ph)ESTEVDVDGNAIR	4.338	0.0059462
YEL046C	GLY1	SES(ph)TEVDVDGNAIR	3.7774	0.011509
YEL046C	GLY1	SEST(ph)EVDVDGNAIR	3.7555	0.011818
YER026C	CHO1	DENDGY(ph)AS(ph)DEVGGTLS(ph)R	2.7463	0.043148
YGL173C	XRN1	KGEIKPSSGTNSTECQS(ph)PK	3.7551	0.011824
YGR093W	DRN1	RPLETETENS(ph)FDGDK	5.0033	0.0028459
YGR178C	PBP1	TVS(ph)PTTQISAGK	3.5367	0.015466
YHR146W	CRP1	REST(ph)EGVLDGSK	2.8726	0.036411
YJL082W	IML2	TNDS(ph)SLLPGYMDSATLLHPGK	4.2795	0.0063592
YJR076C	CDC11	TEALS(ph)GESVAAESIRPNLTK	70.709	6.80E-14
YJR076C	CDC11	TEALSGES(ph)VAAESIRPNLTK	39.086	9.92E-11
YJR076C	CDC11	T(ph)EALSGESVAAESIRPNLTK	17.243	4.10E-07
YKL054C	DEF1	KTES(ph)PLENVAELKK	4.2887	0.0062922
YKL054C	DEF1	T(ph)ES(ph)PLENVAELKK	3.9251	0.0096348

YLR196W	PWP1	ATLEEAEGES(ph)GVEDDAATGSSNK	2.7351	0.04381
YLR323C	CWC24	RPS(ph)DDNELVLNMSGK	2.7019	0.045824
YLR330W	CHS5	DATESVAVEPS(ph)NEDVKPEEK	3.2382	0.022557
YMR240C	CUS1	HTAEDELEDTPS(ph)DGIEEHLSAR	2.6761	0.047462
YNL118C	DCP2	NPISSTVSSNQQS(ph)PK	3.0876	0.027411
YNL118C	DCP2	NPISSTVSS(ph)NQQSPK	2.8689	0.03659
YNL166C	BNI5	Y(ph)DSPVSSPITSASELGSIAK	2.8891	0.035618
YOR042W	CUE5	VVAETTYIDT(ph)PDT(ph)ETK	4.1676	0.0072385
YOR042W	CUE5	VVAETTYIDT(ph)PDT(ph)ET(ph)K	3.9602	0.0092396
YOR153W	PDR5	MLQESS(ph)EEES(ph)DT(ph)YGEIGLSK	2.6716	0.047758
YOR198C	BFR1	VVADDLVLVT(ph)PK	5.7514	0.001311
YOR217W	RFC1	KMPVSNVIDVS(ph)ET(ph)PEGEK	5.0739	0.0026388
YOR220W	RCN2	NKPLLS(ph)INTDPGVTGVDSSSLNK	3.5556	0.015108
YOR220W	RCN2	NKPLLSINT(ph)DPGVTGVDSSSLNK	3.2771	0.021459
YPL058C	PDR12	HLSNILS(ph)NEEGIER	3.4782	0.016639
YPR137C-B		EVHTNQDPLDVS(ph)ASK	3.3102	0.020571
YPR137C-B		EVHTNQDPLDVSASKT(ph)EECEK	2.8097	0.039612

Table 4.5. Table of hypophosphorylated peptides

Systematic name	Common Name	Peptide	H/L Ratio	Significance
Q0060	AI3	KINRNY(ph)VLWT(ph)IHDLK	0.0013459	1.08E-26
YAL022C	FUN26	KPILAVPEPALADT(ph)HSEEISR	0.23787	0.0094654
YAL035W	FUN12	S(ph)TPAAT(ph)PAAT(ph)PT(ph)PSSASPNKK	0.2656	0.0069482
YAL035W	FUN12	S(ph)T(ph)PAAT(ph)PAATPTPSSASPNKK	0.4093	0.043466
YAL038W	CDC19	T(ph)SIIGTIGPK	0.28288	0.019251
YAL038W	CDC19	RTS(ph)IIGTIGPK	0.35123	0.042438
YAL038W	CDC19	LTS(ph)LNVVAGSDLR	0.36559	0.030004
YAR002W	NUP60	RAS(ph)ATVPSAPYR	0.46713	Not calculated (NC)
YBL051C	PIN4	SLS(ph)GLDLQNQNK	0.33435	0.035781
YBR001C	NTH2	RGS(ph)EDDSFLSSQGNR	0.28923	0.010376
YBR025C	OLA1	S(ph)T(ph)FFQAITR	0.16702	0.00055233
YBR054W	YRO2	KAQEEEEDVATDS(ph)E	0.28881	0.010307
YBR081C	SPT7	VGAENDGDS(ph)S(ph)LFLR	0.23971	0.0041781
YBR169C	SSE2	S(ph)T(ph)PSLVGFGPR	0.36242	0.027288
YBR255W	MTC4	IT(ph)RS(ph)S(ph)IPLIPS(ph)VSNEQQK	0.0024065	0.0024065
YBR255W	MTC4	IT(ph)RS(ph)S(ph)IPLIPS(ph)VSNEQQK	0.015406	0.015406
YCL052C	PBN1	VT(ph)VLY(ph)NAPEDIGNHMR	0.47394	NC
YCR034W	ELO2	NVPT(ph)PS(ph)PS(ph)PKPQHR	0.42681	0.079108
YDL019C	OSH2	S(ph)REDLS(ph)IAEDLNQVSKPLLK	0.39586	NC
YDL058W	USO1	EAT(ph)ETSSAVQTK	0.15064	0.00028981
YDL195W	SEC31	APS(ph)SVSMVSPPPLHK	0.47458	0.10725
YDL195W	SEC31	APSSVS(ph)MVSPPPLHK	0.48265	0.11232
YDL223C	HBT1	S(ph)ISGGTFGFR	0.1964	0.0089925

YDR001C	NTH1	RGS(ph)EDDTYSSSQGNR	0.16791	0.00057059
YDR005C	MAF1	RDS(ph)NSFWEQK	0.29653	0.038968
YDR037W	KRS1	KTDLFADLDPS(ph)QYFETR	0.1385	0.00016771
YDR135C	YCF1	RAS(ph)DAT(ph)LGSIDFGDDENIAK	0.49411	NC
YDR171W	HSP42	KS(ph)S(ph)S(ph)FAHLQAPS(ph)PIPDPLQVSKPETR	0.19955	0.004294
YDR171W	HSP42	DKS(ph)EAPKEEAGETNK	0.30152	0.012529
YDR293C	SSD1	SST(ph)INNDSDSLSSPTK	0.46786	0.1031
YDR303C	RSC3	KLSEDGVT(ph)DGDGKPIPESER	0.47433	0.1071
YDR432W	NPL3	NLPEGCS(ph)WQDLK	0.28623	0.0098887
YDR432W	NPL3	ENS(ph)LETTFSSVNTR	0.38084	0.37625
YER052C	HOM3	KGESTPPHPPENLS(ph)SSFYEK	0.36413	0.027804
YER052C	HOM3	TNT(ph)SNQFEHAIDER	0.39597	0.034153
YER052C	HOM3	KGES(ph)TPPHPPENLSSSFYEK	0.42225	0.048665
YER052C	HOM3	KGESTPPHPPENLSS(ph)SFYEK	0.4318	NC
YER052C	HOM3	KGEST(ph)PPHPPENLSSSFYEK	0.44344	NC
YER052C	HOM3	KGESTPPHPPENLSSS(ph)FYEK	0.46309	NC
YER052C	HOM3	KGESTPPHPPENLSSSFY(ph)EK	0.4715	NC
YER083C	GET2	TTPPAS(ph)VHSAT(ph)PDIK	0.12809	9.90E-05
YER093C	TSC11	NITSSSPS(ph)TITNESSKRNK	0.032525	1.59E-08
YER176W	ECM32	LIYEEGEPLT(ph)R	0.33593	0.057032
YFL014W	HSP12	GKDNAEGQGES(ph)LADQAR	0.17646	0.00076949
YFL021W	GAT1	RNPSPSIVKPGS(ph)R	0.26104	0.0063899
YFR014C	CMK1	VCSS(ph)DSDLPGSDIK	0.28453	0.0095195
YFR017C	IGD1	ERES(ph)S(ph)IGEHAPGAER	0.19861	0.056558
YFR017C	IGD1	RST(ph)NYMDALNSR	0.21785	0.013409
YFR017C	IGD1	ERESS(ph)IGEHAPGAER	0.21964	0.01395
YFR053C	HXK1	KGS(ph)MADVPK	0.214	0.0059332
YGL008C	PMA1	TDTSSSSSSSSASS(ph)VSAHQPTQEKPAK	0.21985	0.0026675
YGL009C	LEU1	DQDQSS(ph)PKVEVTSEDEK	0.31283	0.028169

YGL009C	LEU1	DQDQS(ph)SPKVEVTSEDEK	0.33477	0.03594
YGL009C	LEU1	ELES(ph)AAY(ph)DHAEPVQPEDAPQDIANDELK	0.41354	0.07192
YGL009C	LEU1	VEVTS(ph)EDEK	0.41956	0.075145
YGL009C	LEU1	VEVT(ph)SEDEKELESAAYDHAEPVQPEDAPQDIANDELK	0.4678	0.1031
YGL061C	DUO1	S(ph)T(ph)NS(ph)ILDSWINIHS(ph)QAGYIHK	0.00073996	2.39E-31
YGR086C	PIL1	ALLELLDDSPVTPGETRPAYDGY(ph)EAS(ph)K	0.49393	0.11953
YGR116W	SPT6	VGDEGNAAESESDNVAAS(ph)R	0.48376	0.11302
YGR162W	TIF4631	LKETSDS(ph)TST(ph)S(ph)T(ph)PTPTPSTNDSK	0.30816	0.013804
YGR178C	PBP1	S(ph)GS(ph)NIS(ph)QGQSSTGHTTR	0.30722	0.043544
YGR178C	PBP1	S(ph)GS(ph)NISQGQSSTGHTTR	0.33652	0.057327
YGR240C	PFK1	ASS(ph)DASDLLR	0.43935	NC
YGR267C	FOL2	HET(ph)PLNIRPTS(ph)PYTLNPPVER	0.24449	0.010641
YGR280C	PXR1	SSES(ph)ASNIPDAVNTR	0.30916	0.044402
YHL007C	STE20	RAT(ph)PVS(ph)T(ph)PVISKPSMTTTPR	0.23046	0.016
YHR064C	SSZ1	EENAEEDDES(ph)EWSDDEPEVVR	0.47019	NC
YHR073W	OSH3	RSS(ph)QHSHSSSNGSDNKR	0.09827	8.43E-05
YHR099W	TRA1	KEDINDS(ph)PDVEMTESDK	0.4822	0.11204
YHR135C	YCK1	TPEQHPNDDNSS(ph)LAASHK	0.31692	0.015607
YHR195W	NVJ1	DCSSSS(ph)EVESQSK	0.37556	0.031399
YIL107C	PFK26	RYS(ph)VIPTAPPS(ph)AR	0.20317	0.010271
YIL107C	PFK26	SS(ph)FASDFLSR	0.21215	0.0021954
YIL107C	PFK26	S(ph)S(ph)FASDFLSR	0.28489	0.034271
YIL135C	VHS2	RPS(ph)TIGLDR	0.25572	0.0057768
YIR003W	AIM21	HPESS(ph)LEELQK	0.49275	0.11878
YJL055W		GAT(ph)PISEEYGETTIVPDMHTR	0.40687	0.06842
YJL057C	IKS1	RAS(ph)AGVESESSR	0.38565	0.034781
YJL080C	SCP160	KPT(ph)PLPSLK	0.27114	0.0076709
YJL141C	YAK1	TVYTY(ph)IQSR	0.42105	NC
YJR076C	CDC11	TEALSGESVAAES(ph)IRPNLT(ph)K	0.11266	0.0001977

YKL035W	UGP1	DVTLRGTVIIVCS(ph)DGHK	0.0014192	2.68E-26
YKL186C	MTR2	MGQDATVPIQPNNT(ph)GNR	0.37625	NC
YKR098C	UBP11	FDGSLHEIPNELTKPTNDNS(ph)KEDIVR	0.27347	0.016852
YLL018C	DPS1	AVEES(ph)AEPAQVILGEDGKPLSK	0.34855	0.041343
YLL043W	FPS1	TTGAQTNMESNES(ph)PR	0.33274	0.035176
YLR044C	PDC1	NPVILADACCS(ph)R	0.47529	NC
YLR058C	SHM2	LITSHLVDTDPEVDS(ph)IIKDEIER	0.25724	0.0059479
YLR079W	SIC1	S(ph)QES(ph)EDEEDIIINPVR	0.37671	NC
YLR133W	CKI1	T(ph)IS(ph)IESDVSNITDDDDLR	0.45956	NC
YLR219W	MSC3	RLS(ph)TSS(ph)AAPPTSR	0.10497	0.00051354
YLR220W	CCC1	NSAQDLENS(ph)PM(ox)SVGK	0.37681	0.031807
YLR330W	CHS5	SEPVGT(ph)PNIEENK	0.49899	0.12282
YLR399C	BDF1	WADRPNLDDYDS(ph)DEDSR	0.47849	0.1097
YML100W	TSL1	S(ph)AT(ph)RS(ph)PSAFNR	0.23612	0.0038676
YMR012W	CLU1	DDVKPELANKS(ph)VDELLTFIEGDSSNSK	0.48803	NC
YMR074C		KDFS(ph)EDLNSFDK	0.46394	0.1007
YMR104C	YPK2	INTNET(ph)LPSSLSSPK	0.494	0.11958
YMR165C	PAH1	RAS(ph)SAAATSIDK	0.47664	NC
YMR196W		IGGTHSGLT(ph)PQSSISSDK	0.35338	0.024652
YMR240C	CUS1	HTAEDELEDT(ph)PSDGIEEHLSAR	0.43473	0.083538
YMR291W	TDA1	KNS(ph)T(ph)FVLDPKPPK	0.16011	0.001439
YNL015W	PBI2	HNDVIENVEEDKEVHT(ph)N	0.21859	0.00653
YNL101W	AVT4	RAQSTVLNS(ph)NPFYSRK	0.18975	0.0033778
YNL113W	RPC19	HIQEEEEQDVDMT(ph)GDEEQEEEPDREK	0.17502	0.00073275
YNL121C	TOM70	FGDIDT(ph)ATAT(ph)PT(ph)ELSTQPAK	0.12446	0.00035769
YNL173C	MDG1	DTSTSADAEAS(ph)EDQNKEPLSK	0.25936	0.013607
YNL175C	NOP13	DAQGEES(ph)TINT(ph)PTGDESGEVVK	0.469	0.10379
YNL212W	VID27	SSLTAS(ph)ADDLK	0.31118	0.014411
YNL231C	PDR16	NKS(ph)EDDLKPLEEEEK	0.13005	0.00012349

YNL248C	RPA49	IDSDKLTDS(ph)AIDIVDSVR	0.2025	0.0045994
YNL267W	PIK1	SST(ph)PTSPIDLIDPIK	0.27543	0.030682
YNL304W	YPT11	S(ph)GAFGRS(ph)GSSGS(ph)S(ph)TVIEPSNIK	0.27393	0.016964
YNR012W	URK1	SS(ph)S(ph)FISILDDETR	0.42512	NC
YOL004W	SIN3	VT(ph)T(ph)PMGTTTVNNNISPSGR	0.31864	0.030126
YOL016C	CMK2	NMYSLGDDGDNDIEENS(ph)LNESLLDGVTHSLDDLR	0.38771	0.035478
YOL062C	APM4	SSSFLGQGDS(ph)TSDFYDNNK	0.040522	5.57E-09
YOL109W	ZEO1	NEAT(ph)PEAEQVK	0.48747	0.0065105
YOL145C	CTR9	TLSDS(ph)DEDDDDVVK	0.35743	0.02554
YOL151W	GRE2	ETIDDTAS(ph)QILK	0.31223	0.014753
YOR018W	ROD1	NFVDDS(ph)EEDVIFQR	0.17061	0.0050562
YOR052C	TMC1	S(ph)DS(ph)GTVLGAIPLNSR	0.31177	0.04521
YOR109W	INP53	S(ph)VSAPAPSTSK	0.29675	0.0117
YOR205C	GEP3	Y(ph)AIPPFIGS(ph)IEIVLK	0.0040536	3.83E-19
YOR239W	ABP140	TAEKPLETNLPKPETNEEDEEEGS(ph)MSENK	0.45399	0.094716
YOR260W	GCD1	DSTAATS(ph)GDKLNELVNSALDSTVINEFMQHSTR	0.21058	0.0021082
YOR273C	TPO4	THT(ph)QPVPASFDR	0.30206	0.041304
YPL004C	LSP1	ALLELLDDSPVT(ph)PGEARPAYDGYEASR	0.2247	0.0029868
YPL116W	HOS3	TVEDIT(ph)IDDISR	0.29238	0.037258
YPL150W		RVS(ph)SLLVEDGGNPTA	0.49401	NC
YPL153C	RAD53	DFS(ph)IIDEVAGQGAFATVKK	0.17558	0.00074691
YPL160W	CDC60	NFDNVPAEEEEIKEET(ph)PAEKDHEDVT(ph)K	0.26174	0.014125
YPL160W	CDC60	NFDNVPAEEEEIKEET(ph)PAEK	0.37355	0.052141
YPL263C	KEL3	TKS(ph)FELCEDR	0.3563	0.025487
YPR019W	MCM4	NNS(ph)QNLSQGEGNIR	0.41548	0.045909
YPR093C	ASR1	NSMIFAGELRDKHS(ph)VK	0.0019333	4.59E-24
YPR160W	GPH1	RLT(ph)GFLPQEIK	0.36207	0.047024

Table 4.6. Table of novel phosphorylation sites

Systematic name	Common Name	Peptide	H/L Ratio	Significance
Q0060	AI3	KINRNY(ph)VLWT(ph)IHDLK	0.0013459	1.08E-26
YAL022C	FUN26	KPILAVPEPALADT(ph)HSEEISR	0.23787	0.0094654
YBL032W	HEK2	KLEAAEGDATVVT(ph)ER	3.4028	0.018291
YBL067C	UBP13	KKEELPIADDLDTAIDDSFVS(ph)NTPIK	2.7758	0.041463
YDL019C	OSH2	S(ph)REDLS(ph)IAEDLNQVSKPLLK	0.39586	NC
YDL042C	SIR2	VQDLGS(ph)AISVTNVEDPLAKK	11.299	1.39E-05
YDR171W	HSP42	KS(ph)S(ph)S(ph)FAHLQAPS(ph)PIPDPLQVSKPETR	0.19955	0.004294
YDR303C	RSC3	KLSEDGVT(ph)DGDGKPIPESER	0.47433	0.1071
YER026C	CHO1	DENDGY(ph)AS(ph)DEVGGTLS(ph)R	2.7463	0.043148
YER052C	HOM3	KGESTPPHPPENLS(ph)SSFYEK	0.36413	0.027804
YER052C	HOM3	TNT(ph)SNQFEHAIDER	0.39597	0.034153
YER052C	HOM3	KGES(ph)TPPHPPENLSSSFYEK	0.42225	0.048665
YER052C	HOM3	KGESTPPHPPENLSS(ph)SFYEK	0.4318	NC
YER052C	HOM3	KGESTPPHPPENLSSS(ph)FYEK	0.46309	NC
YER052C	HOM3	KGESTPPHPPENLSSSFY(ph)EK	0.4715	NC
YER093C	TSC11	NITSSSPS(ph)TITNESSKRNK	0.032525	1.59E-08
YGL009C	LEU1	ELES(ph)AAY(ph)DHAEPVQPEDAPQDIANDELK	0.41354	0.07192
YGL061C	DUO1	S(ph)T(ph)NS(ph)ILDSWINIHS(ph)QAGYIHK	0.00073996	2.39E-31
YGR086C	PIL1	ALLELLDDSPVTPGETRPAYDGY(ph)EAS(ph)K	0.49393	0.11953
YGR116W	SPT6	VGDEGNAAESESDNVAAS(ph)R	0.48376	0.11302
YGR162W	TIF4631	LKETSDS(ph)TST(ph)S(ph)T(ph)PTPTPSTNDSK	0.30816	0.013804
YGR267C	FOL2	HET(ph)PLNIRPTS(ph)PYTLNPPVER	0.24449	0.010641
YHR073W	OSH3	RSS(ph)QHSHSSSNGSDNKR	0.09827	8.43E-05
YJL055W		GAT(ph)PISEEYGETTIVPDMHTR	0.40687	0.06842
YJR076C	CDC11	TEALSGESVAAES(ph)IRPNLT(ph)K	0.11266	0.0001977

YJR076C	CDC11	T(ph)EALSGESVAAESIRPNLTK	17.243	4.10E-07
YJR076C	CDC11	TEALSGES(ph)VAAESIRPNLTK	39.086	9.92E-11
YJR076C	CDC11	TEALS(ph)GESVAAESIRPNLTK	70.709	6.80E-14
YKL035W	UGP1	DVTLRGTVIIVCS(ph)DGHK	0.0014192	2.68E-26
YKL054C	DEF1	T(ph)ES(ph)PLENVAELKK	3.9251	0.0096348
YKR098C	UBP11	FDGSLHEIPNELTKPTNDNS(ph)KEDIVR	0.27347	0.016852
YLR133W	CKI1	T(ph)IS(ph)IESDVSNITDDDDLR	0.45956	NC
YLR330W	CHS5	SEPVGT(ph)PNIEENK	0.49899	0.12282
YMR104C	YPK2	INTNET(ph)LPSSLSSPK	0.494	0.11958
YMR240C	CUS1	HTAEDELEDT(ph)PSDGIEEHLSAR	0.43473	0.083538
YMR240C	CUS1	HTAEDELEDTPS(ph)DGIEEHLSAR	2.6761	0.047462
YNL101W	AVT4	RAQSTVLNS(ph)NPFYSRK	0.18975	0.0033778
YNL121C	TOM70	FGDIDT(ph)ATAT(ph)PT(ph)ELSTQPAK	0.12446	0.00035769
YNL173C	MDG1	DTSTSADAEAS(ph)EDQNKEPLSK	0.25936	0.013607
YNL175C	NOP13	DAQGEES(ph)TINT(ph)PTGDESGEVVK	0.469	0.10379
YNL248C	RPA49	IDSDKLTDS(ph)AIDIVDSVR	0.2025	0.0045994
YNL304W	YPT11	S(ph)GAFGRS(ph)GSSGS(ph)S(ph)TVIEPSNIK	0.27393	0.016964
YOR153W	PDR5	MLQESS(ph)EEES(ph)DT(ph)YGEIGLSK	2.6716	0.047758
YOR205C	GEP3	Y(ph)AIPPFIGS(ph)IEIVLK	0.0040536	3.83E-19
YOR220W	RCN2	NKPLLS(ph)INTDPGVTGVDSSSLNK	3.5556	0.015108
YPL160W	CDC60	NFDNVPAEEEEIKEET(ph)PAEKDHEDVT(ph)K	0.26174	0.014125
YPR093C	ASR1	NSMIFAGELRDKHS(ph)VK	0.0019333	4.59E-24

Table 4.7. Table of differentially phosphorylated peptides

Systematic name	Common Name	Peptide	H/L Ratio	Significance
Q0060	AI3	KINRNY(ph)VLWT(ph)IHDLK	0.0013459	1.08E-26
YAL022C	FUN26	KPILAVPEPALADT(ph)HSEEISR	0.23787	0.0094654
YAL035W	FUN12	S(ph)TPAAT(ph)PAAT(ph)PT(ph)PSSASPNKK	0.2656	0.0069482
YAL035W	FUN12	S(ph)T(ph)PAAT(ph)PAATPTPSSASPNKK	0.4093	0.043466
YAL038W	CDC19	T(ph)SIIGTIGPK	0.28288	0.019251
YAL038W	CDC19	RTS(ph)IIGTIGPK	0.35123	0.042438
YAL038W	CDC19	LTS(ph)LNVVAGSDLR	0.36559	0.030004
YAR002W	NUP60	RAS(ph)ATVPSAPYR	0.46713	NC
YBL032W	HEK2	KLEAAEGDATVVT(ph)ER	3.4028	0.018291
YBL051C	PIN4	SLS(ph)GLDLQNQNK	0.33435	0.035781
YBL067C	UBP13	KKEELPIADDLDTAIDDSFVS(ph)NTPIK	2.7758	0.041463
YBR001C	NTH2	RGS(ph)EDDSFLSSQGNR	0.28923	0.010376
YBR025C	OLA1	S(ph)T(ph)FFQAITR	0.16702	0.00055233
YBR054W	YRO2	KAQEEEEDVATDS(ph)E	0.28881	0.010307
YBR081C	SPT7	VGAENDGDS(ph)S(ph)LFLR	0.23971	0.0041781
YBR169C	SSE2	S(ph)T(ph)PSLVGFGPR	0.36242	0.027288
YBR255W	MTC4	IT(ph)RS(ph)S(ph)IPLIPS(ph)VSNEQQK	0.0024065	0.0024065
YBR255W	MTC4	IT(ph)RS(ph)S(ph)IPLIPS(ph)VSNEQQK	0.015406	0.015406
YCL052C	PBN1	VT(ph)VLY(ph)NAPEDIGNHMR	0.47394	NC
YCR034W	ELO2	NVPT(ph)PS(ph)PS(ph)PKPQHR	0.42681	0.079108
YDL019C	OSH2	S(ph)REDLS(ph)IAEDLNQVSKPLLK	0.39586	NC
YDL042C	SIR2	VQDLGS(ph)AISVTNVEDPLAKK	11.299	1.39E-05
YDL051W	LHP1	RNS(ph)FAVIEFTPEVLDR	6.0467	0.00097901
YDL058W	USO1	EAT(ph)ETSSAVQTK	0.15064	0.00028981
YDL131W	LYS21	DFHAELS(ph)TPLLKPVNK	2.6429	0.049668

YDL182W	LYS20	KNDS(ph)DVPELATIPAAK	4.7171	0.0038843
YDL182W	LYS20	NFHAEVST(ph)PQVLSAK	5.5976	0.0015308
YDL182W	LYS20	NFHAEVS(ph)TPQVLSAK	5.8667	0.0011687
YDL195W	SEC31	APS(ph)SVSMVSPPPLHK	0.47458	0.10725
YDL195W	SEC31	APSSVS(ph)MVSPPPLHK	0.48265	0.11232
YDL223C	HBT1	S(ph)ISGGTFGFR	0.1964	0.0089925
YDR001C	NTH1	RGS(ph)EDDTYSSSQGNR	0.16791	0.00057059
YDR001C	NTH1	RGS(ph)EDDTYSSSQGNR	3.42	0.017899
YDR005C	MAF1	RDS(ph)NSFWEQK	0.29653	0.038968
YDR037W	KRS1	KTDLFADLDPS(ph)QYFETR	0.1385	0.00016771
YDR037W	KRS1	KKT(ph)DLFADLDPSQYFETR	5.057	0.0026869
YDR135C	YCF1	RAS(ph)DAT(ph)LGSIDFGDDENIAK	0.49411	NC
YDR135C	YCF1	RASDAT(ph)LGSIDFGDDENIAK	2.8938	0.035396
YDR171W	HSP42	KS(ph)S(ph)S(ph)FAHLQAPS(ph)PIPDPLQVSKPETR	0.19955	0.004294
YDR171W	HSP42	DKS(ph)EAPKEEAGETNK	0.30152	0.012529
YDR293C	SSD1	SST(ph)INNDSDSLSSPTK	0.46786	0.1031
YDR303C	RSC3	KLSEDGVT(ph)DGDGKPIPESER	0.47433	0.1071
YDR310C	SUM1	TAGDDGALDQTENTSIS(ph)PK	2.7074	0.045487
YDR432W	NPL3	NLPEGCS(ph)WQDLK	0.28623	0.0098887
YDR432W	NPL3	ENS(ph)LETTFSSVNTR	0.38084	0.37625
YEL046C	GLY1	SEST(ph)EVDVDGNAIR	3.7555	0.011818
YEL046C	GLY1	SES(ph)TEVDVDGNAIR	3.7774	0.011509
YEL046C	GLY1	S(ph)ESTEVDVDGNAIR	4.338	0.0059462
YER026C	CHO1	DENDGY(ph)AS(ph)DEVGGTLS(ph)R	2.7463	0.043148
YER052C	HOM3	KGESTPPHPPENLS(ph)SSFYEK	0.36413	0.027804
YER052C	HOM3	TNT(ph)SNQFEHAIDER	0.39597	0.034153
YER052C	HOM3	KGES(ph)TPPHPPENLSSSFYEK	0.42225	0.048665
YER052C	HOM3	KGESTPPHPPENLSS(ph)SFYEK	0.4318	NC
YER052C	HOM3	KGEST(ph)PPHPPENLSSSFYEK	0.44344	NC

YER052C	HOM3	KGESTPPHPPENLSSS(ph)FYEK	0.46309	NC
YER052C	HOM3	KGESTPPHPPENLSSSFY(ph)EK	0.4715	NC
YER083C	GET2	TTPPAS(ph)VHSAT(ph)PDIK	0.12809	9.90E-05
YER093C	TSC11	NITSSSPS(ph)TITNESSKRNK	0.032525	1.59E-08
YER176W	ECM32	LIYEEGEPLT(ph)R	0.33593	0.057032
YFL014W	HSP12	GKDNAEGQGES(ph)LADQAR	0.17646	0.00076949
YFL021W	GAT1	RNPSPSIVKPGS(ph)R	0.26104	0.0063899
YFR014C	CMK1	VCSS(ph)DSDLPGSDIK	0.28453	0.0095195
YFR017C	IGD1	ERES(ph)S(ph)IGEHAPGAER	0.19861	0.056558
YFR017C	IGD1	RST(ph)NYMDALNSR	0.21785	0.013409
YFR017C	IGD1	ERESS(ph)IGEHAPGAER	0.21964	0.01395
YFR053C	HXK1	KGS(ph)MADVPK	0.214	0.0059332
YGL008C	PMA1	TDTSSSSSSSSASS(ph)VSAHQPTQEKPAK	0.21985	0.0026675
YGL009C	LEU1	DQDQSS(ph)PKVEVTSEDEK	0.31283	0.028169
YGL009C	LEU1	DQDQS(ph)SPKVEVTSEDEK	0.33477	0.03594
YGL009C	LEU1	ELES(ph)AAY(ph)DHAEPVQPEDAPQDIANDELK	0.41354	0.07192
YGL009C	LEU1	VEVTS(ph)EDEK	0.41956	0.075145
YGL009C	LEU1	VEVT(ph)SEDEKELESAAYDHAEPVQPEDAPQDIANDELK	0.4678	0.1031
YGL061C	DUO1	S(ph)T(ph)NS(ph)ILDSWINIHS(ph)QAGYIHK	0.00073996	2.39E-31
YGL173C	XRN1	KGEIKPSSGTNSTECQS(ph)PK	3.7551	0.011824
YGR086C	PIL1	ALLELLDDSPVTPGETRPAYDGY(ph)EAS(ph)K	0.49393	0.11953
YGR093W	DRN1	RPLETETENS(ph)FDGDK	5.0033	0.0028459
YGR116W	SPT6	VGDEGNAAESESDNVAAS(ph)R	0.48376	0.11302
YGR162W	TIF4631	LKETSDS(ph)TST(ph)S(ph)T(ph)PTPTPSTNDSK	0.30816	0.013804
YGR178C	PBP1	S(ph)GS(ph)NIS(ph)QGQSSTGHTTR	0.30722	0.043544
YGR178C	PBP1	S(ph)GS(ph)NISQGQSSTGHTTR	0.33652	0.057327
YGR178C	PBP1	TVS(ph)PTTQISAGK	3.5367	0.015466
YGR240C	PFK1	ASS(ph)DASDLLR	0.43935	

YGR267C	FOL2	HET(ph)PLNIRPTS(ph)PYTLNPPVER	0.24449	0.010641
YGR280C	PXR1	SSES(ph)ASNIPDAVNTR	0.30916	0.044402
YHL007C	STE20	RAT(ph)PVS(ph)T(ph)PVISKPSMTTTPR	0.23046	0.016
YHR064C	SSZ1	EENAEEDDES(ph)EWSDDEPEVVR	0.47019	NC
YHR073W	OSH3	RSS(ph)QHSHSSSNGSDNKR	0.09827	8.43E-05
YHR099W	TRA1	KEDINDS(ph)PDVEMTESDK	0.4822	0.11204
YHR135C	YCK1	TPEQHPNDDNSS(ph)LAASHK	0.31692	0.015607
YHR146W	CRP1	REST(ph)EGVLDGSK	2.8726	0.036411
YHR195W	NVJ1	DCSSSS(ph)EVESQSK	0.37556	0.031399
YIL107C	PFK26	RYS(ph)VIPTAPPS(ph)AR	0.20317	0.010271
YIL107C	PFK26	SS(ph)FASDFLSR	0.21215	0.0021954
YIL107C	PFK26	S(ph)S(ph)FASDFLSR	0.28489	0.034271
YIL135C	VHS2	RPS(ph)TIGLDR	0.25572	0.0057768
YIR003W	AIM21	HPESS(ph)LEELQK	0.49275	0.11878
YJL055W		GAT(ph)PISEEYGETTIVPDMHTR	0.40687	0.06842
YJL057C	IKS1	RAS(ph)AGVESESSR	0.38565	0.034781
YJL080C	SCP160	KPT(ph)PLPSLK	0.27114	0.0076709
YJL082W	IML2	TNDS(ph)SLLPGYMDSATLLHPGK	4.2795	0.0063592
YJL141C	YAK1	TVYTY(ph)IQSR	0.42105	NC
YJR076C	CDC11	TEALSGESVAAES(ph)IRPNLT(ph)K	0.11266	0.0001977
YJR076C	CDC11	T(ph)EALSGESVAAESIRPNLTK	17.243	4.10E-07
YJR076C	CDC11	TEALSGES(ph)VAAESIRPNLTK	39.086	9.92E-11
YJR076C	CDC11	TEALS(ph)GESVAAESIRPNLTK	70.709	6.80E-14
YKL035W	UGP1	DVTLRGTVIIVCS(ph)DGHK	0.0014192	2.68E-26
YKL054C	DEF1	T(ph)ES(ph)PLENVAELKK	3.9251	0.0096348
YKL054C	DEF1	KTES(ph)PLENVAELKK	4.2887	0.0062922
YKL186C	MTR2	MGQDATVPIQPNNT(ph)GNR	0.37625	NC
YKR098C	UBP11	FDGSLHEIPNELTKPTNDNS(ph)KEDIVR	0.27347	0.016852
YLL018C	DPS1	AVEES(ph)AEPAQVILGEDGKPLSK	0.34855	0.041343

YLL043W	FPS1	TTGAQTNMESNES(ph)PR	0.33274	0.035176
YLR044C	PDC1	NPVILADACCS(ph)R	0.47529	NC
YLR058C	SHM2	LITSHLVDTDPEVDS(ph)IIKDEIER	0.25724	0.0059479
YLR079W	SIC1	S(ph)QES(ph)EDEEDIIINPVR	0.37671	NC
YLR133W	CKI1	T(ph)IS(ph)IESDVSNITDDDDLR	0.45956	NC
YLR196W	PWP1	ATLEEAEGES(ph)GVEDDAATGSSNK	2.7351	0.04381
YLR219W	MSC3	RLS(ph)TSS(ph)AAPPTSR	0.10497	0.00051354
YLR220W	CCC1	NSAQDLENS(ph)PM(ox)SVGK	0.37681	0.031807
YLR323C	CWC24	RPS(ph)DDNELVLNMSGK	2.7019	0.045824
YLR330W	CHS5	SEPVGT(ph)PNIEENK	0.49899	0.12282
YLR330W	CHS5	DATESVAVEPS(ph)NEDVKPEEK	3.2382	0.022557
YLR399C	BDF1	WADRPNLDDYDS(ph)DEDSR	0.47849	0.1097
YML100W	TSL1	S(ph)AT(ph)RS(ph)PSAFNR	0.23612	0.0038676
YMR012W	CLU1	DDVKPELANKS(ph)VDELLTFIEGDSSNSK	0.48803	NC
YMR074C		KDFS(ph)EDLNSFDK	0.46394	0.1007
YMR104C	YPK2	INTNET(ph)LPSSLSSPK	0.494	0.11958
YMR165C	PAH1	RAS(ph)SAAATSIDK	0.47664	NC
YMR196W		IGGTHSGLT(ph)PQSSISSDK	0.35338	0.024652
YMR240C	CUS1	HTAEDELEDT(ph)PSDGIEEHLSAR	0.43473	0.083538
YMR240C	CUS1	HTAEDELEDTPS(ph)DGIEEHLSAR	2.6761	0.047462
YMR291W	TDA1	KNS(ph)T(ph)FVLDPKPPK	0.16011	0.001439
YNL015W	PBI2	HNDVIENVEEDKEVHT(ph)N	0.21859	0.00653
YNL101W	AVT4	RAQSTVLNS(ph)NPFYSRK	0.18975	0.0033778
YNL113W	RPC19	HIQEEEEQDVDMT(ph)GDEEQEEEPDREK	0.17502	0.00073275
YNL118C	DCP2	NPISSTVSS(ph)NQQSPK	2.8689	0.03659
YNL118C	DCP2	NPISSTVSSNQQS(ph)PK	3.0876	0.027411
YNL121C	TOM70	FGDIDT(ph)ATAT(ph)PT(ph)ELSTQPAK	0.12446	0.00035769
YNL166C	BNI5	Y(ph)DSPVSSPITSASELGSIAK	2.8891	0.035618
YNL173C	MDG1	DTSTSADAEAS(ph)EDQNKEPLSK	0.25936	0.013607

YNL175C	NOP13	DAQGEES(ph)TINT(ph)PTGDESGEVVK	0.469	0.10379
YNL212W	VID27	SSLTAS(ph)ADDLK	0.31118	0.014411
YNL231C	PDR16	NKS(ph)EDDLKPLEEEEK	0.13005	0.00012349
YNL248C	RPA49	IDSDKLTDS(ph)AIDIVDSVR	0.2025	0.0045994
YNL267W	PIK1	SST(ph)PTSPIDLIDPIK	0.27543	0.030682
YNL304W	YPT11	S(ph)GAFGRS(ph)GSSGS(ph)S(ph)TVIEPSNIK	0.27393	0.016964
YNR012W	URK1	SS(ph)S(ph)FISILDDETR	0.42512	NC
YOL004W	SIN3	VT(ph)T(ph)PMGTTTVNNNISPSGR	0.31864	0.030126
YOL016C	CMK2	NMYSLGDDGDNDIEENS(ph)LNESLLDGVTHSLDDLR	0.38771	0.035478
YOL062C	APM4	SSSFLGQGDS(ph)TSDFYDNNK	0.040522	5.57E-09
YOL109W	ZEO1	NEAT(ph)PEAEQVK	0.48747	0.0065105
YOL145C	CTR9	TLSDS(ph)DEDDDDVVK	0.35743	0.02554
YOL151W	GRE2	ETIDDTAS(ph)QILK	0.31223	0.014753
YOR018W	ROD1	NFVDDS(ph)EEDVIFQR	0.17061	0.0050562
YOR042W	CUE5	VVAETTYIDT(ph)PDT(ph)ET(ph)K	3.9602	0.0092396
YOR042W	CUE5	VVAETTYIDT(ph)PDT(ph)ETK	4.1676	0.0072385
YOR052C	TMC1	S(ph)DS(ph)GTVLGAIPLNSR	0.31177	0.04521
YOR109W	INP53	S(ph)VSAPAPSTSK	0.29675	0.0117
YOR153W	PDR5	MLQESS(ph)EEES(ph)DT(ph)YGEIGLSK	2.6716	0.047758
YOR198C	BFR1	VVADDLVLVT(ph)PK	5.7514	0.001311
YOR205C	GEP3	Y(ph)AIPPFIGS(ph)IEIVLK	0.0040536	3.83E-19
YOR217W	RFC1	KMPVSNVIDVS(ph)ET(ph)PEGEK	5.0739	0.0026388
YOR220W	RCN2	NKPLLSINT(ph)DPGVTGVDSSSLNK	3.2771	0.021459
YOR220W	RCN2	NKPLLS(ph)INTDPGVTGVDSSSLNK	3.5556	0.015108
YOR239W	ABP140	TAEKPLETNLPKPETNEEDEEEGS(ph)MSENK	0.45399	0.094716
YOR260W	GCD1	DSTAATS(ph)GDKLNELVNSALDSTVINEFMQHSTR	0.21058	0.0021082
YOR273C	TPO4	THT(ph)QPVPASFDR	0.30206	0.041304
YPL004C	LSP1	ALLELLDDSPVT(ph)PGEARPAYDGYEASR	0.2247	0.0029868
YPL058C	PDR12	HLSNILS(ph)NEEGIER	3.4782	0.016639

YPL116W	HOS3	TVEDIT(ph)IDDISR	0.29238	0.037258
YPL150W		RVS(ph)SLLVEDGGNPTA	0.49401	NC
YPL153C	RAD53	DFS(ph)IIDEVAGQGAFATVKK	0.17558	0.00074691
YPL160W	CDC60	NFDNVPAEEEEIKEET(ph)PAEKDHEDVT(ph)K	0.26174	0.014125
YPL160W	CDC60	NFDNVPAEEEEIKEET(ph)PAEK	0.37355	0.052141
YPL263C	KEL3	TKS(ph)FELCEDR	0.3563	0.025487
YPR019W	MCM4	NNS(ph)QNLSQGEGNIR	0.41548	0.045909
YPR093C	ASR1	NSMIFAGELRDKHS(ph)VK	0.0019333	4.59E-24
YPR137C-B		EVHTNQDPLDVSASKT(ph)EECEK	2.8097	0.039612
YPR137C-B		EVHTNQDPLDVS(ph)ASK	3.3102	0.020571
YPR160W	GPH1	RLT(ph)GFLPQEIK	0.36207	0.047024

References

1. Fleischmann, M., I. Stagljar, and M. Aebi, *Allele-specific suppression of a Saccharomyces cerevisiae prp20 mutation by overexpression of a nuclear serine/threonine protein kinase.* Mol Gen Genet, 1996. **250**(5): p. 614-25.

2. Bharucha, N., et al., *Analysis of the yeast kinome reveals a network of regulated protein localization during filamentous growth.* Mol Biol Cell, 2008. **19**(7): p. 2708-17.

3. Gimeno, C.J., et al., *Unipolar cell divisions in the yeast S. cerevisiae lead to filamentous growth: regulation by starvation and RAS.* Cell, 1992. **68**(6): p. 1077-90.

4. Lee, B.N. and E.A. Elion, *The MAPKKK Ste11 regulates vegetative growth through a kinase cascade of shared signaling components.* Proc Natl Acad Sci U S A, 1999. **96**(22): p. 12679-84.

5. Liu, H., C.A. Styles, and G.R. Fink, *Elements of the yeast pheromone response pathway required for filamentous growth of diploids.* Science, 1993. **262**(5140): p. 1741-4.

6. Madhani, H.D., C.A. Styles, and G.R. Fink, *MAP kinases with distinct inhibitory functions impart signaling specificity during yeast differentiation.* Cell, 1997. **91**(5): p. 673-84.

7. Roberts, R.L. and G.R. Fink, *Elements of a single MAP kinase cascade in Saccharomyces cerevisiae mediate two developmental programs in the same cell type: mating and invasive growth.* Genes Dev, 1994. **8**(24): p. 2974-85.

8. Gustin, M.C., et al., *MAP kinase pathways in the yeast Saccharomyces cerevisiae.* Microbiol Mol Biol Rev, 1998. **62**(4): p. 1264-300.

9. Pan, X. and J. Heitman, *Cyclic AMP-dependent protein kinase regulates pseudohyphal differentiation in Saccharomyces cerevisiae.* Mol Cell Biol, 1999. **19**(7): p. 4874-87.

10. Liu, H., C.A. Styles, and G.R. Fink, *Saccharomyces cerevisiae S288C has a mutation in FLO8, a gene required for filamentous growth.* Genetics, 1996. **144**(3): p. 967-78.

11. Cutler, N.S., et al., *The TOR signal transduction cascade controls cellular differentiation in response to nutrients.* Mol Biol Cell, 2001. **12**(12): p. 4103-13.

12. Heitman, J., N.R. Movva, and M.N. Hall, *Targets for cell cycle arrest by the immunosuppressant rapamycin in yeast.* Science, 1991. **253**(5022): p. 905-9.

13. Crespo, J.L., et al., *The TOR-controlled transcription activators GLN3, RTG1, and RTG3 are regulated in response to intracellular levels of glutamine.* Proc Natl Acad Sci U S A, 2002. **99**(10): p. 6784-9.

14. Laxman, S. and B.P. Tu, *Multiple TORC1-associated proteins regulate nitrogen starvation-dependent cellular differentiation in Saccharomyces cerevisiae.* PLoS One, 2011. **6**(10): p. e26081.

15. Soulard, A., et al., *The rapamycin-sensitive phosphoproteome reveals that TOR controls protein kinase A toward some but not all substrates.* Mol Biol Cell, 2010. **21**(19): p. 3475-86.

16. Umekawa, M. and D.J. Klionsky, *Ksp1 kinase regulates autophagy via the target of rapamycin complex 1 (TORC1) pathway.* J Biol Chem, 2012. **287**(20): p. 16300-10.

17. Ong, S.E., et al., *Stable isotope labeling by amino acids in cell culture, SILAC, as a simple and accurate approach to expression proteomics.* Mol Cell Proteomics, 2002. **1**(5): p. 376-86.

18. Ashburner, M., et al., *Gene ontology: tool for the unification of biology. The Gene Ontology Consortium.* Nat Genet, 2000. **25**(1): p. 25-9.

19. Kedersha, N. and P. Anderson, *Stress granules: sites of mRNA triage that regulate mRNA stability and translatability.* Biochem Soc Trans, 2002. **30**(Pt 6): p. 963-9.

20. Buchan, J.R., J.H. Yoon, and R. Parker, *Stress-specific composition, assembly and kinetics of stress granules in Saccharomyces cerevisiae.* J Cell Sci, 2011. **124**(Pt 2): p. 228-39.

21. Buchan, J.R., D. Muhlrad, and R. Parker, *P bodies promote stress granule assembly in Saccharomyces cerevisiae.* J Cell Biol, 2008. **183**(3): p. 441-55.

22. Shah, K.H., et al., *Protein kinases are associated with multiple, distinct cytoplasmic granules in quiescent yeast cells.* Genetics, 2014. **198**(4): p. 1495-512.

23. Takahara, T. and T. Maeda, *Transient sequestration of TORC1 into stress granules during heat stress.* Mol Cell, 2012. **47**(2): p. 242-52.

24. Brengues, M. and R. Parker, *Accumulation of polyadenylated mRNA, Pab1p, eIF4E, and eIF4G with P-bodies in Saccharomyces cerevisiae.* Mol Biol Cell, 2007. **18**(7): p. 2592-602.

25. Hoyle, N.P., et al., *Stress-dependent relocalization of translationally primed mRNPs to cytoplasmic granules that are kinetically and spatially distinct from P-bodies.* J Cell Biol, 2007. **179**(1): p. 65-74.

26. Johnson, C., et al., *The yeast Sks1p kinase signaling network regulates pseudohyphal growth and glucose response.* PLoS Genet, 2014. **10**(3): p. e1004183.

27. Huh, W.K., et al., *Global analysis of protein localization in budding yeast.* Nature, 2003. **425**(6959): p. 686-91.

28. Amberg, D., Burke, DJ., Strathern, JN., ed. *Methods in Yeast Genetics: A Cold Spring Harbor Laboratory Course Manual*. 2005 ed. 2005, Cold Spring Harbor Laboratory Press: Cold Spring Harbor.

29. Shaner, N.C., et al., *Improved monomeric red, orange and yellow fluorescent proteins derived from Discosoma sp. red fluorescent protein.* Nat Biotechnol, 2004. **22**(12): p. 1567-72.

30. Brengues, M., D. Teixeira, and R. Parker, *Movement of eukaryotic mRNAs between polysomes and cytoplasmic processing bodies.* Science, 2005. **310**(5747): p. 486-9.

31. Longtine, M.S., et al., *Additional modules for versatile and economical PCR-based gene deletion and modification in Saccharomyces cerevisiae.* Yeast, 1998. **14**(10): p. 953-61.

32. Gray, M., M. Kupiec, and S.M. Honigberg, *Site-specific genomic (SSG) and random domain-localized (RDL) mutagenesis in yeast.* BMC Biotechnol, 2004. **4**: p. 7.

33. Aun, A., T. Tamm, and J. Sedman, *Dysfunctional mitochondria modulate cAMP-PKA signaling and filamentous and invasive growth of Saccharomyces cerevisiae.* Genetics, 2013. **193**(2): p. 467-81.

34. Dickinson, J.R., Schweizer, M., ed. *The Metabolism and Molecular Physiology of Saccharomyces cerevisiae*. 2nd ed. 2004, CRC Press: Philadelphia.

35. Galdieri, L., et al., *Transcriptional regulation in yeast during diauxic shift and stationary phase.* OMICS, 2010. **14**(6): p. 629-38.

36. Winzeler, E.A., et al., *Functional characterization of the S. cerevisiae genome by gene deletion and parallel analysis.* Science, 1999. **285**(5429): p. 901-6.

37. Sikorski, R.S. and P. Hieter, *A system of shuttle vectors and yeast host strains designed for efficient manipulation of DNA in Saccharomyces cerevisiae.* Genetics, 1989. **122**(1): p. 19-27.

38. Brodsky, A.S. and P.A. Silver, *Pre-mRNA processing factors are required for nuclear export.* Rna, 2000. **6**(12): p. 1737-49.

Chapter V
Future Directions

5.1. ProQ

Elucidation of the mechanism of action of ProQ will require three separate but complementary approaches: 1) Determination of the factors governing ProQ-ribosome association. 2) Compilation of a ProQ “regulatome”, and 3) Targeted probing of the circumstantial evidence linking RNase III and ProQ.

5.1.1. Exploring the ProQ-mRNA-Ribosome interaction

Data in Chapter II of this document presents evidence that the primary reason that ProQ is found in ribosomal fractions separated on sucrose gradients is because it binds to the mRNA being translated (Figure 2.3A and B). With that in mind, there also appears to be a small increase in ProQ cosedimentation with 30S subunits when translating ribosomes are dissociated (Figure 2.1B). Also, ProQ is found in detectable levels in fractions corresponding to mRNA-free ribosomal particles (Figure 2.3B). Together, this suggests that association with ribosomes is not strictly occurring via tethering by the mRNA. Therefore, it is necessary to firmly determine the interdependence of ProQ domains, mRNAs, and the ribosome on association. This will most likely require an *in vitro* approach, as mRNA must be removed from the system. In addition to working *in vitro*, discontinuation of the use of sucrose gradients must be considered. The forces and heat generated by long centrifugation times may cause

dissociation of weak interactions between ProQ and ribosomal particles. Potential replacement assays could include: far-western blotting of SDS-PAGE separated, or dot-blotted, ribosomes, or fluorescence anisotropy. The large size of the ribosome makes other methods more technically challenging. To proceed, ribosomal particles, as well as individual domain constructs of ProQ (Figure 2.2A) would need to be purified. This is trivial. It seems reasonable to continue to use *in vitro* transcribed *proP* mRNAs to assay the dependence upon mRNA for ribosomal interaction, but in light of the facts discussed in Chapter II, *rpoS* must be reconsidered as a negative control. Any other mRNA not controlled by a sRNA would be a better choice.

5.1.2. Identifying the ProQ regulatome

A key piece of information hindering the elucidation of the role of ProQ in translation is a *bona fide* target. The data showing changes in ProP protein levels in a *proQ* mutant strain are, for lack of a better word, underwhelming. It is clear that proline import is down in these strains, but the published change ProP expression levels is very subtle. The ProP-independent effect of ProQ on biofilm formation is a promising lead in finding a true target. In addition, the almost complete loss of FliC in a *proQ* mutant is striking. Though this loss of FliC was not successfully complemented (Figure 2.10) it cannot yet be dismissed. Personal communication with other labs studying ProQ has indicated FliC as a potential target as well.

Because of the advances in sequencing technology, the most reasonable way to move forward on finding more targets of ProQ regulation is to perform RNA-seq experiments. First, comparison of the relative abundance of individual RNAs between a

wild type strain and a Δ*proQ* strain would yield mRNAs and sRNAs which are (de)stabilized in the absence of ProQ. Since there are no current examples of ProQ functioning as an inhibitor of translation, I would expect that targets of ProQ would be found in lower abundance when ProQ is deleted, suggesting that they are not efficiently translated, and therefore degraded, or they are not protected from degradation by nucleases. A second, and more sophisticated, method would involve using either cross-linking immunoprecipitation followed by deep sequencing (CLIP-Seq) or ribosome immunoprecipitation followed by deep sequencing (RIP-Seq). The former would yield RNAs which are bound to ProQ both independently and dependently of the ribosome. The latter would show mRNAs which IP with ProQ-associated ribosome.

Once a list of putative targets is generated via one of the above methods, follow-up analysis would include *in vivo* experiments to verify differential RNA levels. Northern blots could also be performed on polysome fractionations to probe for changes in ribosome occupancy of target mRNAs. It would also be profitable to mine targets for sequence determinants, as this may yield mechanistic details, as well.

5.1.3. RNase III and ProQ

The recent publication, discussed in Chapter II of this document, showing that *proP* mRNA transcribed from the distal P1 promoter is degraded by RNase III, suggests a link between ProQ and RNase III. In addition, the increase in *fliC* mRNA levels in an RNase III mutant background reinforces the antagonistic relationship between ProQ and RNase III. The simplest hypothesis is that ProQ binds to RNAs targeted for degradation by RNase III and precludes the nuclease from cleaving. However, the homology of

ProQ to FinO and Hfq must not be dismissed. As both of these proteins mediate sRNA-RNA interactions, it seems likely that ProQ would behave in a similar manner. Similar to the DsrA/*rpoS* interaction described in Chapter I, ProQ may facilitate the binding between an sRNA and *proP*. This interaction may cause a change in the secondary structure of *proP*, dissolving the double-stranded RNase III cleavage site. In this way, *proP* mRNA would be stabilized and more efficiently translated. Testing of these hypotheses will again require discovery of true targets of ProQ-RNA binding.

5.2. Ksp1p

The continued study of Ksp1p will focus on several open questions. Not previously discussed is the fact that Ksp1p contains a prion-like domain which has been shown to be able to form aggregates *in vivo* [1]. Ksp1p also has a putative eIF4E binding domain [2]. It must be determined if these domains are important for Ksp1p regulation of pseudohyphal growth or mRNP granule formation. Next, direct targets of Ksp1p phosphorylation should be determined. The data presented in Chapter IV will guide these studies. Lastly, the recruitment of Ksp1p to stress granules may serve one of two purposes. It may be a mechanism to protect Ksp1p during stress, ensuring that once conditions are favorable, Ksp1p can again be active without delay, or it may serve to regulate Ksp1p kinase activity, either concentrating Ksp1p with its targets during stress, or similarly, sequestering it from targets.

5.2.1. Probing of Ksp1p structural domains

The putative eIF4E (4E) binding domain of Ksp1p resides between residues 246 and 252. I have already constructed a mutant which substitutes this entire region to 7 alanines, and this mutant can be stably expressed and seen by western-blot analysis. Attempts to coimmunoprecipitate a T7- and His-tagged 4E with a c-terminally HA tagged Ksp1p resulted in non-specific binding of 4E to the anti-HA resin. Eventually, determining if Ksp1p and 4E interact *in vivo* fell outside of the scope of this project. Moving forward, the changing of epitope tags is a trivial matter which can be addressed. If changing tags does not optimize the assay, other methods could be used, including far-western blotting or yeast two-hybrid assays. The former would require purified components. For these purposes I have already constructed plasmids for over expression and purification of full length Ksp1p, and a truncated version of Ksp1p covering the N-terminal domain where the kinase activity and putative 4E binding site reside.

Determining if Ksp1p forms functional prions *in vivo* is a more difficult question. The hallmark of prions is their non-Mendelian inheritance, and this can lead to highly variable results which make it difficult to draw solid conclusions. Formation of prions in yeast is dependent upon the activity of the chaperone Hsp104p [3]. Therefore, deletion of Hsp104p, or inhibition of its activity using chemical inhibitors such as guanidine hydrochloride (GuHCl), can cure yeast of prions [4]. Unfortunately, such a broad approach is unlikely to yield any useful data about Ksp1p. Any phenotypes seen in the presence of GuHCl or in an *hsp104* mutant would likely be indirect. The predicted prion-forming domain of Ksp1p lies between residues 400 and 625 [1]. Preliminary data, which again did not fall within the scope of this project, indicates that this region is not

necessary for Ksp1p to form cytoplasmic foci. However, examination of foci formation of GFP-tagged stress granule markers was altered in a *ksp1* background when the c-terminus was deleted after the 350th residue. The effects of this truncation on pseudohyphal growth were not studied, but they must be.

5.2.2. Finding direct targets of Ksp1p phosphorylation

The study presented in Chapter IV yielded 180 peptides with differential phosphorylation states in a *ksp1* kinase dead mutant. Of these 180 peptides, 137 of them show decreased phosphorylation. As increased phosphorylation at a particular residue eliminates it as a direct target of Ksp1p, the focus can shift to these remaining proteins. Further trimming of the list must be done by looking at the specific residues and mining the literature for available information. The best choices for narrowing down the list include an online database dedicated to compiling all known phosphorylation sites, their kinases, and their motifs, called phosphoGRID [5]. A second resource comes from a high-throughput study of *in vitro* phosphorylation by yeast kinases [6]. To guide the search for direct targets, any Ksp1p-dependent phosphorylation sites found in phosphoGRID, for which the kinase is already know can potentially be eliminated, though it is possible that there is redundancy in the kinome. It may also be possible to trim the list further by eliminating sites which contain a consensus motif for a different kinase. Comparison of the remaining candidates to the dataset from the high-throughput study may yield overlapping proteins. If necessary, the data could be filtered again for proteins whose phosphorylation states are dependent upon PKA signaling.

Once the list is narrowed, it will be necessary to verify that the phosphorylation state of the candidate changes *in vivo* in a Ksp1p-dependent manner. This would be accomplished by looking for changes in phosphorylation states in different *ksp1* mutant backgrounds. Also, phosphorylation will require a physical interaction, so immunoprecipitation would provide further evidence that a particular protein is a target of Ksp1p kinase activity. Lastly, it is necessary to show that phosphorylation of a target can happen in a purified system *in vitro*. This will require both proteins to be purified, but is fairly straight forward.

5.2.3. Understanding the purpose for Ksp1p granule localization

This final direction is one of great interest to the Kumar Lab, but it also the most difficult question to answer. As mentioned, the exact purpose for the formation of stress granules is not completely understood; though, there are many hypotheses. Similarly, it is not well understood why some proteins have evolved to localize to these aggregates during stress. Since the Kumar Lab is keenly interested in the kinase signaling networks which respond to stress, we would particularly like to understand why kinases localize to these mRNP granules. A favored hypothesis is that localization of a kinase to an aggregate of RNA and proteins may serve to concentrate the kinase and its targets, enhancing phosphorylation of the targets. This could also work in the opposite direction, as the kinase may be sequestered from its targets by aggregating while its targets remain free in the cytosol.

Any progress made on this front, with respect to Ksp1p, will only come after a direct target is found, and a particular residue is identified as a *bona fide* Ksp1p target,

to the exclusion of all other kinases. It will then be beneficial to obtain phospho-specific antibodies to this target residue. In this way, we could monitor phosphorylation state of a particular residue under specific conditions. We can then ask questions to test these hypotheses. Questions include: What is the phosphorylation state during vegetative growth? How does the phosphorylation state change when cells are shifted to stress conditions? Do the two proteins colocalize in granules? Does mutation of the residue perturb the localization pattern during normal growth or stress conditions? The exact parameters of each experiment will depend on the identity of the target and the conditions necessary for phenotypic analysis.

5.3. Conclusions

Our understanding of ProQ and Ksp1p is starting to increase, but the details of the mechanisms by which they function are still very hazy. Both proteins merit further study. Determining the targets and mechanism of ProQ regulation will expand the understanding of messenger specific translation regulation in bacteria. The current literature places most of the *onus* of sRNA and mRNA-specific regulation on Hfq. In ProQ we find a protein which, while related to Hfq structurally, seems to function in a slightly different manner, under different conditions, and with distinct targets.

For its part, Ksp1p plays a diverse, but seemingly non-essential, role in yeast. The dependency on Ksp1p during times of nutrient excess is likely minimal, but mutations of *ksp1* manifest as defects in response to stress. As life outside of the laboratory is more volatile (if not for graduate students, at least for microorganisms), the need to cope with changing conditions is exaggerated. In addition to a greater

understanding of how yeast respond to stress, the role of Ksp1p in mRNP granule regulation makes further study imperative. To restate, improper regulation of the formation and clearing of these cytoplasmic aggregates have many implications in disease. Any insight gained by the study of the highly tractable yeast system is likely to be applicable to humans.

References

1. Alberti, S., et al., *A systematic survey identifies prions and illuminates sequence features of prionogenic proteins.* Cell, 2009. **137**(1): p. 146-58.
2. Mader, S., et al., *The translation initiation factor eIF-4E binds to a common motif shared by the translation factor eIF-4 gamma and the translational repressors 4E-binding proteins.* Mol Cell Biol, 1995. **15**(9): p. 4990-7.
3. Kryndushkin, D.S., et al., *Molecular chaperone Hsp104 can promote yeast prion generation.* Genetics, 2011. **188**(2): p. 339-48.
4. Grimminger, V., et al., *The prion curing agent guanidinium chloride specifically inhibits ATP hydrolysis by Hsp104.* J Biol Chem, 2004. **279**(9): p. 7378-83.
5. Tyers, M., Sadowski, I., *phosphoGRID*. 2015.
6. Ptacek, J., et al., *Global analysis of protein phosphorylation in yeast.* Nature, 2005. **438**(7068): p. 679-84.